

2012

# A Magnetic Resonance Study of the GCPII+/- Mouse Model

Stephanie S. Huang

Wellesley College, [shuang@wellesley.edu](mailto:shuang@wellesley.edu)

Follow this and additional works at: <https://repository.wellesley.edu/thesiscollection>

---

## Recommended Citation

Huang, Stephanie S., "A Magnetic Resonance Study of the GCPII+/- Mouse Model" (2012). *Honors Thesis Collection*. 61.  
<https://repository.wellesley.edu/thesiscollection/61>

This Dissertation/Thesis is brought to you for free and open access by Wellesley College Digital Scholarship and Archive. It has been accepted for inclusion in Honors Thesis Collection by an authorized administrator of Wellesley College Digital Scholarship and Archive. For more information, please contact [ir@wellesley.edu](mailto:ir@wellesley.edu).

# A Magnetic Resonance Study of the GCPII<sup>+/-</sup> Mouse Model

**Stephanie S. Huang**

Advisor: Dr. Nancy H. Kolodny

Chemistry Department

Wellesley College

Submitted in Partial Fulfillment of the Prerequisite for Honors in the Department of Chemistry

May 2012

© 2012 Stephanie S. Huang



## Abstract

Schizophrenia is a devastating psychiatric condition marked by severe cognitive impairments, brain anatomy alterations, and abnormal neurotransmitter activity. This study examines whether the genetically modified GCPII<sup>+/-</sup> mouse model, which has reduced glutamate carboxypeptidase II (GCPII) enzyme activity to mimic the hypoglutamatergic pathways observed in schizophrenia, creates magnetic resonance-detectable alterations in morphology and/or neurochemistry that can be used for studies of potential treatments. The longitudinal portion of this study employs the non-invasive techniques of magnetic resonance imaging (MRI) and spectroscopy (MRS). Data were collected from 4 male and 7 female heterozygous GCPII<sup>+/-</sup> (HET) and 6 male and 7 female normal (wild-type; WT) mice on postnatal days (PND) 35/36, 49/50 and 63/64. MRI was used to examine the volumes of the brain structures affected by schizophrenia in humans. MRS was used to measure neurometabolite concentrations in the hippocampus, a brain structure known to function differently in schizophrenia. We hypothesized that the brain morphology and metabolite concentrations between HET and WT mice would differ and that HET mice would mirror characteristics found in human schizophrenia patients. If reduced GCPII function could replicate neurological symptoms of schizophrenia, then the GCPII<sup>+/-</sup> model would be a promising tool for treatment studies that target the glutamatergic pathways of schizophrenia.

MRI data revealed enlarged third, fourth, and lateral ventricles, and asymmetric hippocampi in HET mice compared to WT mice. These findings are characteristic of schizophrenia patients. MRS data showed apparent differences in (N-acetylaspartate + N-acetylaspartylglutamate)/ creatine (Cr) levels, but no significant effect of genotype on (N-acetylaspartate + N-acetylaspartylglutamate)/Cr, choline/Cr, taurine/Cr, or (glutamate + glutamine)/Cr ratios. Sex differences were found in cerebellum to WBV ratios of HET and WT mice, and hippocampus asymmetry and choline/Cr levels in HET mice. These data are consistent with findings on schizophrenia patients and suggest that the GCPII<sup>+/-</sup> mouse model may be a good mouse model for schizophrenia treatment development. However, more research must be conducted to increase the sample size of data and further characterize the GCPII<sup>+/-</sup> mouse model.



## Acknowledgements

I would like to thank my adviser, Nancy H. Kolodny, for her endless support and guidance these past four years. I've learned and experienced more than I could have ever anticipated when I joined her lab, and for that I am forever grateful. Her attention to detail and thoughtful suggestions made this thesis project possible.

I would also like to thank all those who helped me on this project: My thesis committee members – Professor Chris Arumainayagam, Professor Adele Wolfson, and Professor Martin Magid for not only their guidance, but also for their courage in agreeing to read my entire thesis; Pat Carey and Val LePage for taking excellent care of the mice; Jon Rose for instrument maintenance; Dr. Laura Schaevitz for her advice on this project; my labmate and sister, Laura Huang, for being my mentor when I was a first-year and teaching me how to image and trace mouse brains; and all previous and current labmates for their support, especially Weiya Mu, Palig Mouradian, and Heather Pearson for their contributions to this project and endless enthusiasm for tracing brains.

Finally, I would like to thank my friends and family who have kept me motivated – Rachel Magid and Phoebe Handler, for the edits, suggestions, and many hours spent in the science center together; Jenny Lu and Wendy Dickieson, for their support; my mother, father, and sisters, for their encouragement and love.

Financial support for this project was provided by the Staley Award for Cancer-Related Research and the Beck Senior Fellowship.



# Table of Contents

<b>Abstract</b> .....	iii
<b>Acknowledgements</b> .....	v
<b>Table of Contents</b> .....	vii
<b>1 Introduction</b> .....	1
<b>1.1 Dopamine Hypothesis</b> .....	2
<b>1.2 Glutamate Hypothesis</b> .....	4
<b>1.3 Animal Models</b> .....	5
<b>1.4 The GCPII Mouse Model</b> .....	7
<b>1.5 Magnetic Resonance Theory</b> .....	10
<b>1.6 Magnetic Resonance Imaging</b> .....	14
<b>1.7 Magnetic Resonance Spectroscopy</b> .....	17
<b>1.8 Metabolites of Interest</b> .....	21
<b>2 Materials and Methods</b> .....	26
<b>2.1 Subject and Subject Maintenance</b> .....	26
<b>2.2 <i>In vivo</i> Magnetic Resonance Imaging and Spectroscopy</b> .....	27
<b>2.3 Animal Preparation</b> .....	27
<b>2.4 Magnetic Resonance Imaging</b> .....	28
<b>2.5 Magnetic Resonance Spectroscopy</b> .....	29
<b>2.6 Data Analysis</b> .....	30
<i>MRI Data Analysis</i> .....	30
<i>MRS Data Analysis</i> .....	31
<i>Statistical Analysis</i> .....	32
<b>3 Results and Discussion</b> .....	33
<b>3.1 Magnetic Resonance Imaging</b> .....	33
<i>Sexual Dimorphism</i> .....	34
<i>Whole Brain</i> .....	39
<i>Cerebellum</i> .....	41
<i>Fourth Ventricle</i> .....	43
<i>Third Ventricle</i> .....	44
<i>Lateral Ventricles</i> .....	46
<i>Hippocampus</i> .....	49
<i>Individual Volume Trends</i> .....	53
<i>Summary of MRI Findings</i> .....	55



<b>3.2</b>	<b>Magnetic Resonance Spectroscopy</b> .....	56
	<i>Sexual Dimorphism</i> .....	56
	<i>N-acetylaspartate and N-acetylaspartylglutamate</i> .....	59
	<i>Taurine</i> .....	62
	<i>Choline</i> .....	63
	<i>Glutamate and Glutamine</i> .....	65
	<i>Individual Metabolite Level Trends</i> .....	67
	<i>Summary of MRS Findings</i> .....	70
<b>4</b>	<b>Conclusions and Future Work</b> .....	70
	<b>References</b> .....	72
	<b>Appendix A: Tracing Guide</b> .....	79
	<b>Appendix B: The R168X Mouse Model of Rett Syndrome and Viability</b> ...	85
	<b>Appendix C: Development of a “Green” MRI Phantom</b> .....	89

Schizophrenia is a severe mental disorder whose treatments are limited as they only partially relieve symptoms (Jones et al. 2011; Nasrallah et al., 2011; Trivedi and Jarbe, 2011). This thesis investigates a genetically modified mouse (GCPII<sup>+/-</sup>) that has reduced GCPII enzyme activity to replicate the hypoglutamatergic activity suspected in schizophrenia patients. The goal of this developmental study was to characterize the GCPII<sup>+/-</sup> mouse model and to investigate sex differences using magnetic resonance techniques. If the GCPII<sup>+/-</sup> mouse model replicates the pathophysiology and neurological symptoms of schizophrenia then the model would be a promising tool for treatment studies that target the glutamatergic pathways of schizophrenia.

# 1 Introduction

---

Schizophrenia is a disabling and chronic mental disorder that affects the most complex functions of the brain. The onset of schizophrenia occurs in young adulthood, but the disorder persists chronically and can cause a lifetime of suffering for the diagnosed individual and their family members. Women and men are affected equally, however women often exhibit symptoms later than men and in a milder form (Vorvick, 2010). Those with schizophrenia tend to have a shorter life expectancy by approximately 12-15 years as compared to the average population – a gap that has been increasing (van Os and Kapur, 2009). Physical causes are responsible for most deaths and result from decreased access to medical care and increased frequency of routine risk factors – such as a poor diet and smoking (van Os and Kapur, 2009). Though schizophrenia has a prevalence of about 1% in the world population, little is known about the disorder and current treatments are inadequate, as they can only partially relieve symptoms (Jones et al. 2011; Nasrallah et al., 2011; Trivedi and Jarbe, 2011).

Schizophrenia's multitude of symptoms makes diagnosis difficult because individual symptoms can be associated with other mental illnesses (van Os and Kapur, 2009). Symptoms of schizophrenia are categorized into three categories: positive, negative, and cognitive. Positive symptoms reflect an excess or distortion of normal functions and include characteristics commonly associated with schizophrenia, such as delusions and hallucinations. Negative symptoms refer to diminished characteristics of normal function and include depression, lack of emotion, and social withdrawal. Cognitive symptoms involve thought processes and include difficulties in memory, attention, and making sense of information (Andreason, 2000; Wilson and Terry, 2010). Current treatment options can only alleviate positive symptoms (Nasrallah et al., 2011).

Research on the etiology of schizophrenia suggests that genetic factors play a role as the offspring of those with schizophrenia have a higher likelihood of also being diagnosed compared to controls (van Os and Kapur, 2009). However, no single genetic alteration is responsible for schizophrenia (Jones et al., 2011). Certain environmental factors, such as prenatal exposures or social stress have also been linked to an increased risk of developing schizophrenia. These factors disrupt neural development, resulting in subtle changes of specific neurons and circuits, which may then lead to neurological malfunction (Lieberman et al., 2002). Altered levels of certain naturally occurring brain chemicals, including the neurotransmitters dopamine and glutamate, support the neurochemical basis of schizophrenia (Lieberman et al., 2002).

### 1.1 Dopamine Hypothesis

The first and most enduring neurochemically-based hypothesis suggests that the central pathophysiology of schizophrenia arises from dopamine dysfunction in the limbic system, an area in the brain associated with learning, memory, and emotional response (Figure 1-1). The

limbic system is known to be overactive in schizophrenia. Two major clinical observations provided evidence for the dopamine hypothesis – (1) schizophrenic-like symptoms occur in people who use amphetamine, a drug that causes excessive dopamine release and (2) dopamine antagonists resulted in alleviation of the positive symptoms of schizophrenia (Howes and Kapur, 2009; Konradi and Hecker, 2003). Though promising, this hypothesis is incomplete as patients who took dopamine antagonists still suffered from the disabling cognitive and motivational impairments of negative symptoms (van Os and Kapur, 2009). Thus researchers developed new hypotheses involving other neurotransmitters such as glutamate.

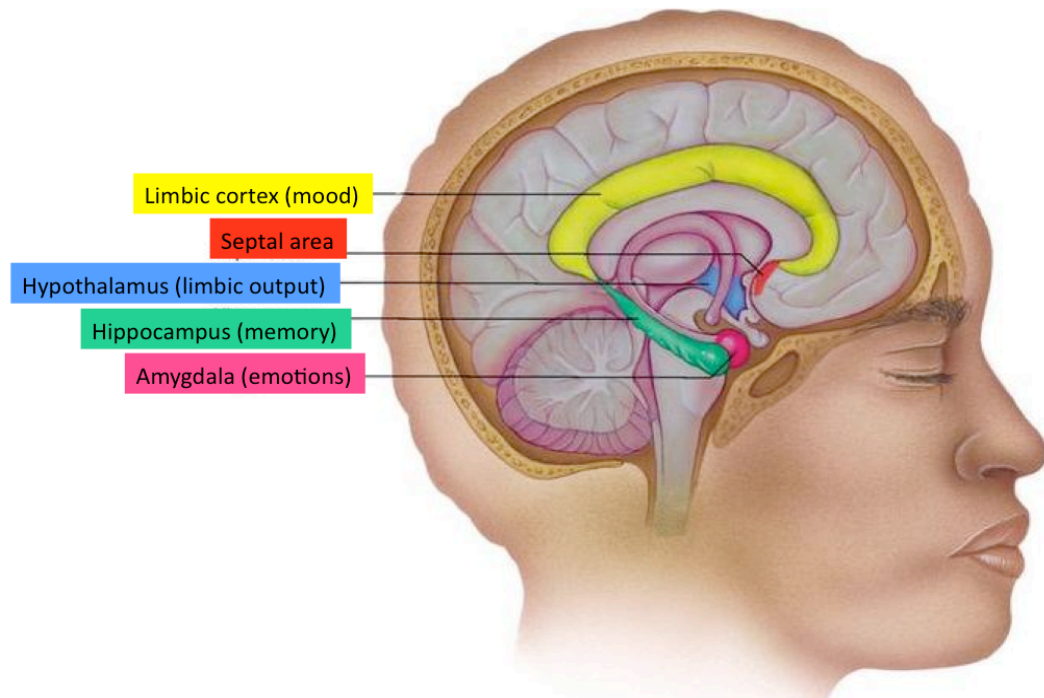


**Figure 1-1.** Cartoon of a human brain with the structures of the limbic system labeled by color. The main role of each structure is indicated in parentheses. Adapted from University of Colorado (2008).

## 1.2 Glutamate Hypothesis

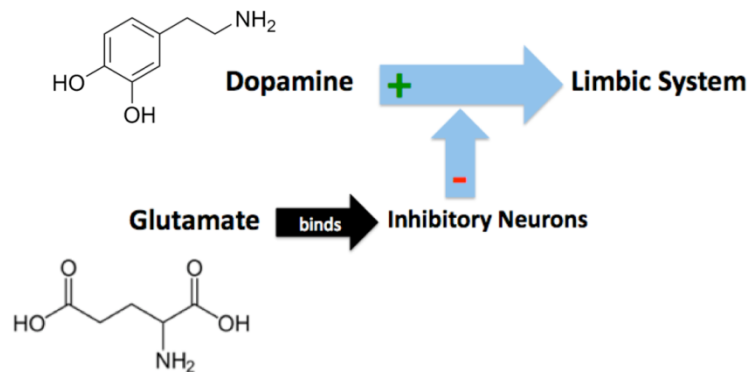


**Figure 1-2.** Interaction of dopamine and glutamate pathways. Dopamine activates the limbic system. Glutamate binds to inhibitory neurons, which inhibit limbic system activity. Chemical structures of dopamine and glutamate appear next to the name of each neurotransmitter.

Glutamate is the primary neurotransmitter in the mammalian brain and a key regulator of inhibition. When glutamate activates N-methyl-D-aspartate receptors (NMDAR) on inhibitory neurons, synaptic activity to the limbic system is inhibited (Figure 1-2; Olney et al., 1999). The glutamate hypothesis suggests that schizophrenia is caused by hypoactivity of glutamate due to hypofunction of NMDAR in the frontal lobe (Coyle, 2006; Han et al., 2009; Olney et al., 1999). If NMDAR function is reduced, then there would be increased limbic system activity, a characteristic of schizophrenia. This hypothesis was formulated when it was determined that hallucinogenic drugs that block signals in the brain and reduce the perception of pain, called dissociative anesthetics, such as phencyclidine (PCP) and ketamine induced positive, negative, and cognitive symptoms similar to those of schizophrenia (Moghaddam and Javitt, 2011). The discovery that these compounds function by blocking the NMDAR channel was key to the generation of the hypothesis that hypofunction of NMDAR, not hyperactivity of dopamine, may contribute to the pathophysiology of schizophrenia (Coyle, 2006; Olney et al., 1999). When NMDAR are blocked, there is an excessive release of glutamate and acetylcholine. Olney et al.

(1999) suggested that the abundant release of excitatory transmitters and consequent overstimulation of postsynaptic neurons may be the source of the cognitive and behavioral disturbances connected to NMDA receptor hypofunction. This theory aligns with the dopamine hypothesis as the glutamatergic system is normally responsible for inhibiting dopamine activity. A hypoglutamatergic system would disinhibit the dopaminergic system and cause hyperdopaminergic activity in the limbic system.

### 1.3 Animal Models

The etiology and pathophysiology of schizophrenia is poorly understood and is further complicated by a lack of appropriate animal models. Animal models of psychiatric disorders are crucial to our understanding of the neurobiological basis of schizophrenia and for the development of efficacious drugs (Jones et al., 2011). Animal models of human illnesses must meet the requirements of face, construct, and predictive validity (Figure 1-3). Face validity describes the degree of phenomenological similarity between the animal model and the symptoms of the human condition. While some symptoms, such as hyperactivity, have been modeled successfully, uniquely human symptoms, such as hallucinations, introduce difficulties, as there are currently no methods to quantify or investigate psychological processes in animals. Construct validity is the level of homology in pathological mechanisms. This requirement is also difficult to achieve for schizophrenia because the neurobiological basis of the symptoms has not been established. Predictive validity, the most critical feature, is the degree to which the model can be used to predict the efficacy of therapeutic agents in humans (Tordjman et al., 2007; Wilson and Terry, 2010).

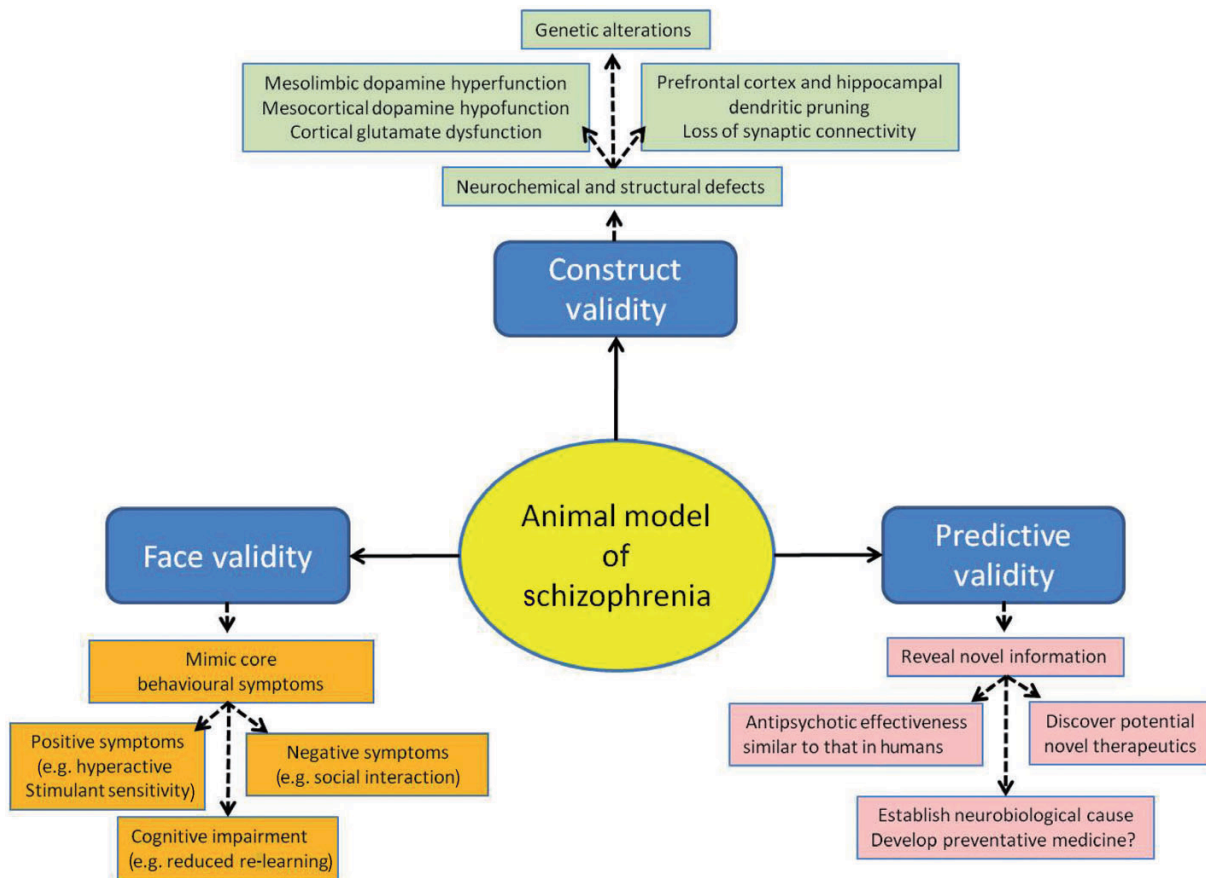


**Figure 1-3.** Schematic of the three main requirements for an animal model of schizophrenia and the behavioral, neurochemical and structural changes expected and relevant to each domain. (Jones et al., 2011)

Schizophrenia is a complex and heterogeneous disease, differing slightly for every individual (Wilson and Terry Jr., 2010). Thus, the likelihood of developing a single animal model that completely represents the range of symptoms associated with schizophrenia is unlikely. Focusing on specific symptoms, or specific neurobiological pathways, of the disorder may be the most logical approach to improving face and construct validity in animal models. Several animal models may then be useful for modeling various phenomenological and pathophysiological components of schizophrenia that could be targeted independently with separate molecules or multi-drug targets (Wilson and Terry Jr., 2010).

So far, over 20 different animal models of schizophrenia have been developed, each representing some aspect of the disorder. (See Jones et al. 2011 for a review on select models). Most models can be categorized under four different induction categories: developmental, drug-induced, lesion, or genetic manipulation (Jones et al. 2011). Animal models that exhibit pathophysiological features, such as neurochemical dysfunction, are valuable to learning more about what pathways play a role in schizophrenia. There is growing evidence that the pathways related to Glutamate Carboxypeptidase II (GCPII), an enzyme responsible for glutamate activity and NMDAR function, are viable therapeutic targets for intervention for schizophrenia and related psychiatric diseases (Guilarte et al., 2008; Han et al., 2009). In the present study we used a genetically modified mouse that has reduced GCPII enzyme activity to replicate glutamatergic activity that is suspected in schizophrenia patients.

#### 1.4 The GCPII Mouse Model

The GCPII<sup>+/-</sup> mouse model is unique as it involves the glutamatergic system, a highly implicated pathway in schizophrenia (Han et al., 2009). While dopamine antagonists can only alleviate positive symptoms, treatments that reverse hypofunction of NMDA receptors can potentially relieve positive, negative, and cognitive symptoms. Most pharmacological treatments for the disease are now focusing on a glutamate-modulating class because of the limitations of treatments that target dopamine receptors (Nasrallah et al., 2011).

GCPII regulates both folate absorption and activation of NMDAR (Goff et al., 2004). In the jejunum GCPII hydrolyzes folylpoly-gamma-glutamate and facilitates folate absorption (Sacha et al., 2007). When expressed in the brain, GCPII hydrolyzes N-acetylaspartylglutamate (NAAG) into glutamate and N-acetylaspartate (NAA; Figure 1-4).



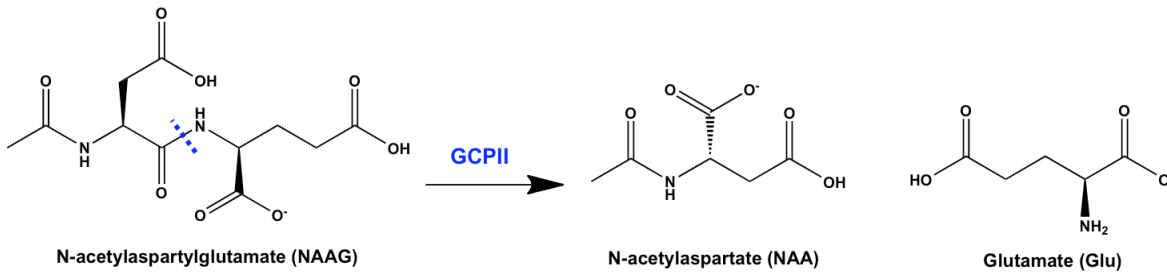


**Figure 1-4.** Function of the GCPII enzyme

GCPII regulates NMDAR activation via glutamate and NAAG. Glutamate activates NMDAR while NAAG is a neuropeptide that is a NMDAR antagonist and mGluR3 agonist, which downregulates glutamate release (Figure 1-5). There are discrepancies in the literature regarding the effect of NAAG at mGluR3 and NMDAR (Fricker et al., 2009). However, postmortem schizophrenia patients exhibited less GCPII activity in the prefrontal cortex, temporal cortex, and hippocampus compared to age matched controls, which supports the function of NAAG as stated above (Tsai et al., 1995). Further, these findings parallel the glutamate hypothesis and suggest that schizophrenia supports a hypoglutamatergic state (Coyle, 2006).

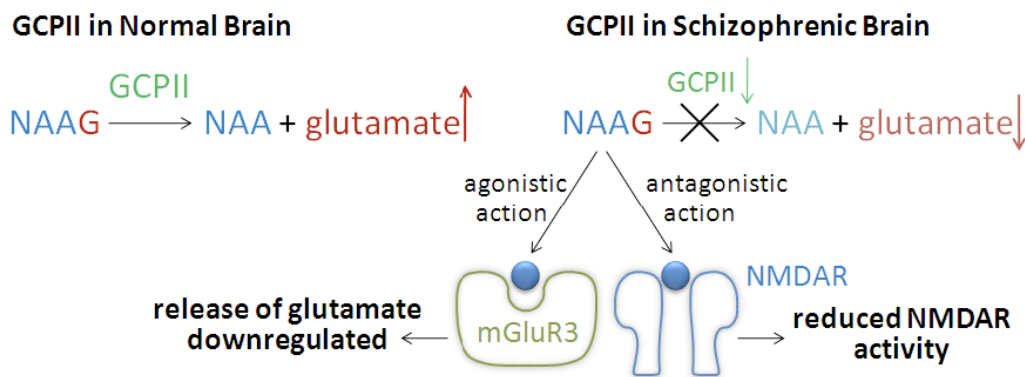


**Figure 1-5.** Pathways of GCPII in the normal and schizophrenic brain. (Chu, 2009)

Our study compares heterozygous GCPII<sup>+/-</sup> (HET) mice and mutation free wild-type (WT) mice. HET mice were generated using the Cre-*loxP* system. Exons 1 and 2 of the GCPII gene were flanked by *LoxP* sites then excised by crossing with a Cre-expressing mouse. Cre is a recombinase protein, which mediates excision of sites located between *loxP* sites. In the study that generated this mouse model, mouse brain tissues were removed to determine GCPII protein expression by chemiluminescence and radioenzymatic assays, which were performed to assess GCPII enzyme activity. (Han et al., 2009)

As a result of this mutation, HET mice have the GCPII gene knocked out, which causes a 50% decrease in levels and functioning of the enzyme GCPII (Han et al., 2009). Null GCPII<sup>+/-</sup> mice, or mice with the GCPII gene completely knocked out, were not used as they are not viable (Han et al., 2009). Diminished GCPII function leads to lower levels of NAA and glutamate and higher levels of NAAG, thereby suppressing NMDAR function.

If HET mice successfully model aspects of schizophrenia, they should be behaviorally and neurologically different from WT mice. The study that first explored the viability of this model performed a battery of behavioral tests that assessed locomotor, social, and cognitive behaviors and found that the HET mice exhibited increased locomotor activity, reduced social interaction, and impaired working memory compared to WT mice (Han et al., 2009). These differences reflect many, but not all, of the behavioral abnormalities observed in schizophrenia patients. These results were expected as the GCPII<sup>+/-</sup> model only reflects the GCPII pathway of schizophrenia; more pathways are likely implicated.

The goal of our developmental study was to use magnetic resonance techniques to further establish the face and construct validity of the GCPII<sup>+/-</sup> mouse model and to investigate sex differences. Male and female HET and WT mice were investigated on postnatal day (PND)

35/36, 49/50, and 63/64, where PND 63 corresponds to young adulthood in a mouse. If the GCPII<sup>+/-</sup> mouse model could replicate the pathophysiology and neurological symptoms of schizophrenia, then it would be expected that the longitudinal neuroanatomy and neurochemistry in HET mice would parallel symptoms seen in human schizophrenia.

### 1.5 Magnetic Resonance Theory (Hashemi, 2004)

The numerous definitive findings on brain abnormalities in schizophrenia have made brain scans increasingly important in their identification and determination of causes and function. Magnetic Resonance Imaging (MRI) and Spectroscopy (MRS) are non-invasive techniques used to investigate the longitudinal neuroanatomy and neurochemistry, respectively, of the GCPII<sup>+/-</sup> mouse model (Figure 1-6). This section discusses the theory behind these magnetic resonance techniques.

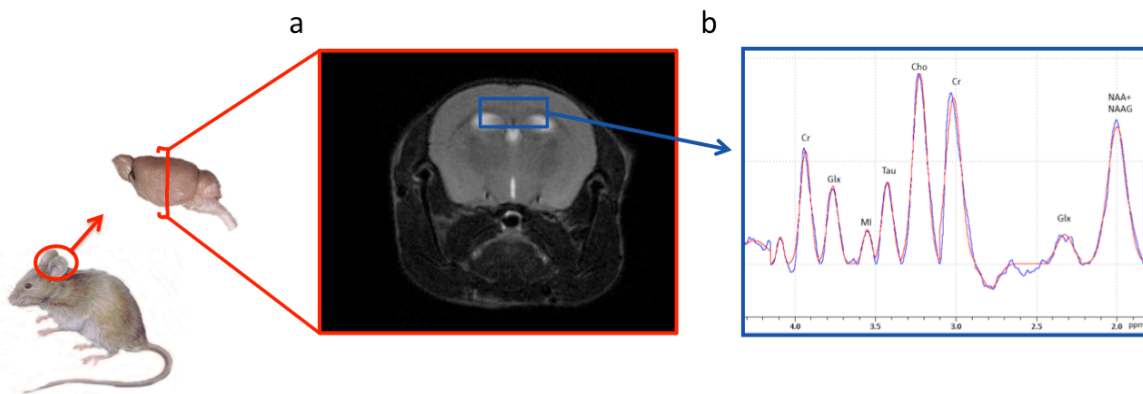


**Figure 1-6.** The brain of a mouse was imaged to produce an MR image (a). MR images were used to position a cuboid voxel in the hippocampus/cortex of the mouse brain from which an MR spectrum (b) was obtained.

Only nuclei with an odd number of protons and/or neutrons can be detected with magnetic resonance. These nuclei always have at least one proton or neutron that is unpaired, giving the nucleus a magnetic dipole moment, or spin magnetic moment, when in a magnetic field ( $B_0$ ). In biological systems, magnetic resonance techniques take advantage of the abundance

of hydrogen, mostly present in water and fat. As this study works with mice, hydrogen,  $^1\text{H}$ , will be the nucleus of focus, unless otherwise noted.

Each nucleus has specific energy levels related to the spin quantum number  $S$ . The number of energy states of a nucleus is determined as follows:

$$\# \text{ energy states} = 2S + 1$$

For the hydrogen nucleus,  $S = \frac{1}{2}$ , there are two energy states. In the absence of  $B_0$  the spin magnetic moments are randomly oriented so that no net magnetization is produced. When  $B_0$  is applied, the spin magnetic moments align parallel or antiparallel to  $B_0$ , which correspond to low and high energy states, respectively. A slight majority of spin magnetic moments will prefer the lower energy state over the higher energy state causing  $M_0$ , the net magnetization vector, to be in the direction of the  $B_0$  (Figure 1-7).

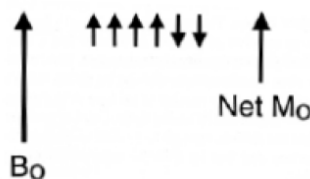


**Figure 1-7.** The net magnetization vector,  $M_0$ , aligns with the magnetic field  $B_0$  because the majority of spin magnetic moments align with  $B_0$  (Hashemi, 2004).

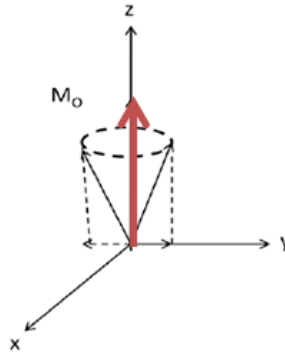
The spin magnetic moments spin about their own axes in addition to precessing, or wobbling, about the axis of  $B_0$ . The rate of the precession is given by the Larmor equation:

$$\omega_0 = \gamma B_0$$

where  $\omega_0$  is the Larmor precession frequency of the hydrogen nuclear magnetic moment and  $\gamma$  is gyromagnetic ratio, a constant.  $M_0$ , the net magnetization of the vector sum of all the individual

spins is denoted as the + z-axis in a three-dimensional coordinate system (Figure 1-8). There are no components along the x or y-axes because the individual spins are all out of phase.

**Figure 1-8.**  $M_0$ , the net magnetization (red), is along the z-axis. There is no x or y component because the spins are out of phase (Hashemi, 2004).



A radio frequency (RF) pulse is a type of electromagnetic wave. When an RF pulse is applied along the x-axis, perpendicularly to  $M_0$ , the magnetic component of the electromagnetic wave creates a new magnetic field,  $B_1$ , in the direction of the RF pulse (Figure 1-9). If the frequency of the RF pulse is at the same (Larmor) frequency as the precession of the protons, resonance occurs. Resonance allows energy to be added to the system and enables protons in the low energy state to move to a high energy state. Though the strength of  $B_1$  is much weaker than  $B_0$ , the protons respond to the new magnetic field and precess about the x-axis at a frequency of  $\omega_1 = \gamma_1 B_1$ . Consequently,  $M_0$  undergoes nutation, or a spiral motion, from the axis of  $B_0$  into the perpendicular x-y plane. This creates transverse magnetization. The angle to which  $M_0$  is rotated is determined by the gyromagnetic ratio and the strength and duration of the RF pulse.

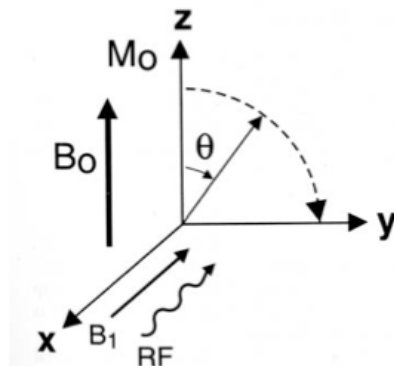


**Figure 1-9.** Application of a radiofrequency (RF) pulse along the x-axis creates  $B_1$ , a new magnetic field. This causes  $M_0$ , the net magnetization to flip into the x-y plane (Hashemi, 2004).

When the RF pulse is turned off, the spin magnetic moments must return to their original orientations, or their lowest energy states, along the z-axis. They undergo two processes of relaxation – longitudinal and transverse. T1 is the longitudinal, or spin-lattice, relaxation time. T1 describes the time it takes for 63% for the spin magnetic moments to realign along the z-axis or for the spin magnetic moments to release the energy gained from the RF pulse. The T2 time constant is for transverse relaxation, or spin-spin relaxation, and describes the time it takes for 63% of the  $M_{xy}$  component to decay. T2 primarily depends on the inherent dephasing caused by interaction between spins.  $T2^*$  accounts for spin-spin interactions, but differs from T2 in that it considers the effects of  $B_0$  inhomogeneities. During relaxation, the precession of magnetization in the xy plane forms a signal. This signal is called a free induction decay (FID) and contains information regarding the properties of the sampled nuclei. In MRI, spatial information is obtained to produce a two-dimensional image. In MRS, the signal undergoes Fourier Transformation to produce a spectrum. The next two sections discuss these techniques in greater detail.

## 1.6 Magnetic Resonance Imaging (MRI) (Hashemi, 2004)

In biological subjects, MRI uses the signals from protons in the form of water. Different tissues possess unique atomic compositions and can be used to provide image contrast. A pulse sequence is used to spatially encode these signals. In a pulse sequence, the RF pulse is applied multiple times, gradient coils are varied, and multiple FIDs are obtained. The information from these FIDs is then combined to create an image (Figure 1-10). This section gives an overview of these processes and how MR images are obtained.

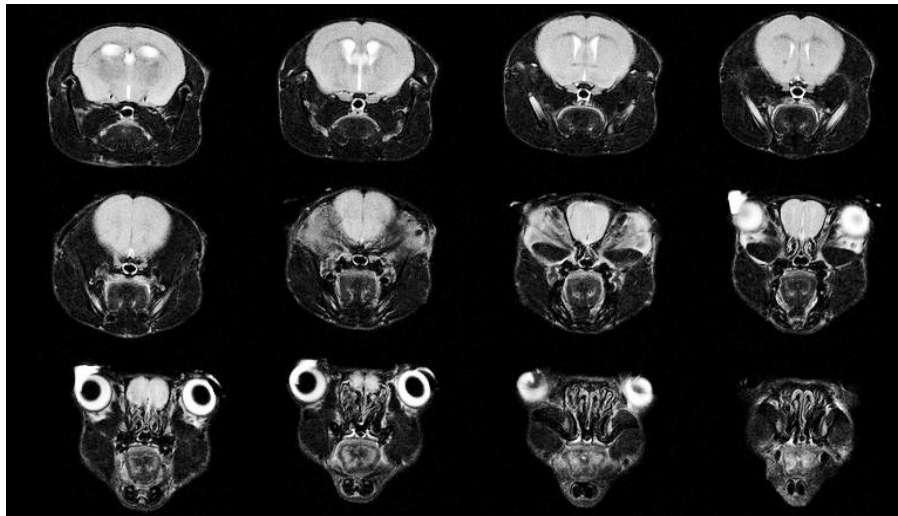


**Figure 1-10.** Contiguous T2-weighted magnetic resonance images of a mouse brain obtained *in vivo*.

A pulse sequence (Figure 1-11) uses the parameters of repetition time (TR) and echo time (TE) to obtain T1 and T2- weighted images.

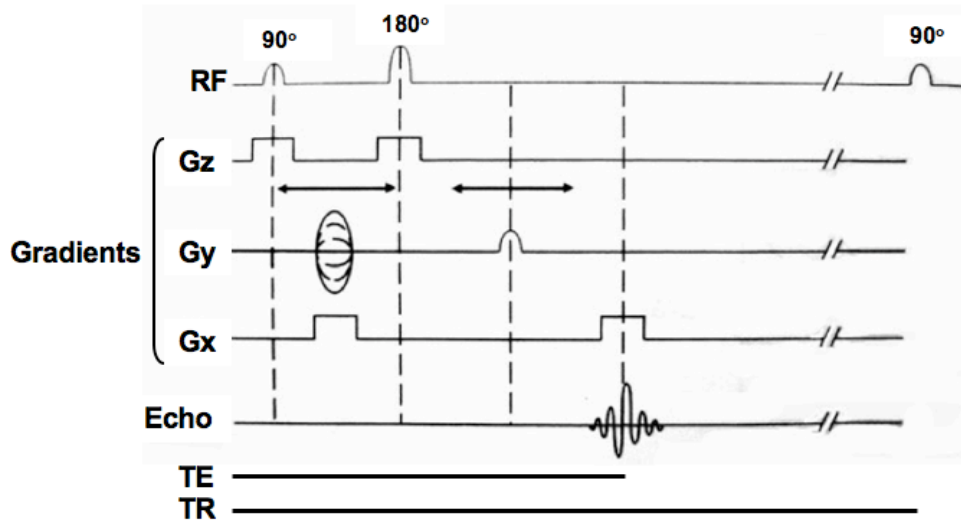
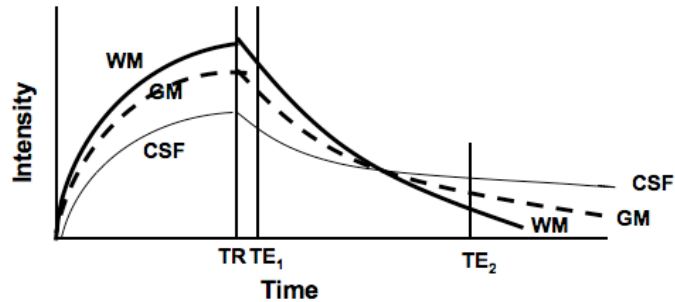


**Figure 1-11.** Spin-echo pulse sequence diagram. The 90° pulse flips the spin magnetic moments into the x-y plane. The 180° pulse is then applied to flip the spin magnetic moments 180° in the x-y plane. Thus, this second pulse causes a recovery of phase coherence so that maximum signal can be collected (Hashemi, 2004).

TR and TE are closely related to the previously mentioned relaxation constants T1 and T2, respectively. However, while T1 and T2 are inherent, TR and TE can be adjusted to provide optimal contrast. The time between each pair of 90° pulses is the repetition time (TR). The interval between the application of the RF pulse and the measurement of a signal is the echo time (TE). A short TR and TE are optimal for T1-weighted contrast where fat is bright and water is dark. Accordingly, a long TR and TE produces T2-weighted contrast where water is bright and fat is dark. These differences are based on the T1 and T2 relaxation times of protons in different environments. Cerebrospinal fluid (CSF) is mostly comprised of water and has a long T2 compared to white matter, which contains fat. Thus given time after an RF pulse, the magnetic moments in CSF will have dephased less than the protons in white matter and will have greater signal intensity (Figure 1-12).



**Figure 1-12.** T1 recovery (left) and T2 decay (right) curves of white matter (WM), grey matter (GM), and cerebrospinalfluid (CSF) (Hashemi, 2004).



In order to create spatially organized two-dimensional MR images, gradient coils are used. A gradient coil is an electrical device composed of loops of wire that perturb  $B_0$  to create a magnetic field gradient. The three gradients, slice-select ( $G_z$ ), phase-encoding ( $G_y$ ), and frequency-encoding ( $G_x$ ), each serve a unique function. During the pulse sequence, each gradient is applied at a specific point in the sequence (Figure 1-11).  $G_z$  is applied during pulse application and varies  $B_0$  linearly along the z-axis.  $G_z$  enables a slice to be selected based on a frequency range in the RF pulse that corresponds to the slice location and thickness. In order to differentiate points within the slice,  $G_x$  is applied between pulses and during readout.  $G_x$  distinguishes proton frequencies along the x-axis.  $G_y$  is then applied between pulses or before readout in the y-axis and distinguishes protons by their phase. These latter two gradients can differentiate pixel-specific properties in the x-y plane. Each time  $G_y$  with a different value is applied, one line is added to k-space, a digitized space for data from each slice. The data in k-space then undergo Fourier Transformation and are converted from the time domain to the frequency domain to produce an MR image.

MRI is useful for structural studies because the technique can non-invasively visualize and create contrast among anatomical structures based on the unique characteristics of protons in tissue. This is relevant to schizophrenia as schizophrenia patients exhibit structural brain abnormalities. Human studies on schizophrenia have found an enlargement of ventricles,

asymmetrical lateral ventricles, asymmetric hippocampi, and a reduced hippocampus (Shenton et al. 2001, Tsai, 2002). Previous work with the GCPII<sup>+/-</sup> mouse model found that the hippocampus was reduced and asymmetric, lateral ventricles were asymmetric, and third ventricle was enlarged in GCPII<sup>+/-</sup> compared to WT (Mu, 2011). Through this study we hope to replicate these findings with statistical significance and validate the GCPII<sup>+/-</sup> mouse model.

### 1.7 Magnetic Resonance Spectroscopy (Hornak, 2011)

Following an MRI experiment, the MR images are used to specify a voxel, or volume of tissue in the brain, to perform *in-vivo* <sup>1</sup>H-MR spectroscopy (MRS), which uses the signal from hydrogen protons to non-invasively investigate the concentration of brain metabolites.

Brain metabolites are differentiated in MRS by their chemical properties. The electrons surrounding a nucleus can create a small magnetic field that opposes or enhances B<sub>0</sub>. This new magnetic field causes the effective magnetic field, B<sub>eff</sub>, at the nucleus to be greater or less than B<sub>0</sub>:

$$B_{\text{eff}} = B_0 (1 - \sigma)$$

The value of  $\sigma$  depends on the electron density of protons, which are unique for each molecule and depends on the type of nuclei and bonds. When a signal is collected and Fourier Transformed, a spectrum is created in which protons in molecules can be identified as unique peaks along the x-axis labeled in parts per million (ppm; Figure 1-13). A proton with an electron density that enhances B<sub>0</sub> will appear downfield in a spectrum. Conversely, a proton with an electron density that opposes B<sub>0</sub> will appear upfield. Each peak can represent one or more molecule(s) and the area under the peak is proportional to the concentration of the molecule(s). The location of each molecule on the x-axis is determined by its chemical shift,  $\delta$ , and compared

relative to a reference frequency. In this study, we use the (NAA+NAAG) peak as a reference as it has a unique shape and is easy to distinguish in spectra of the mouse brain.

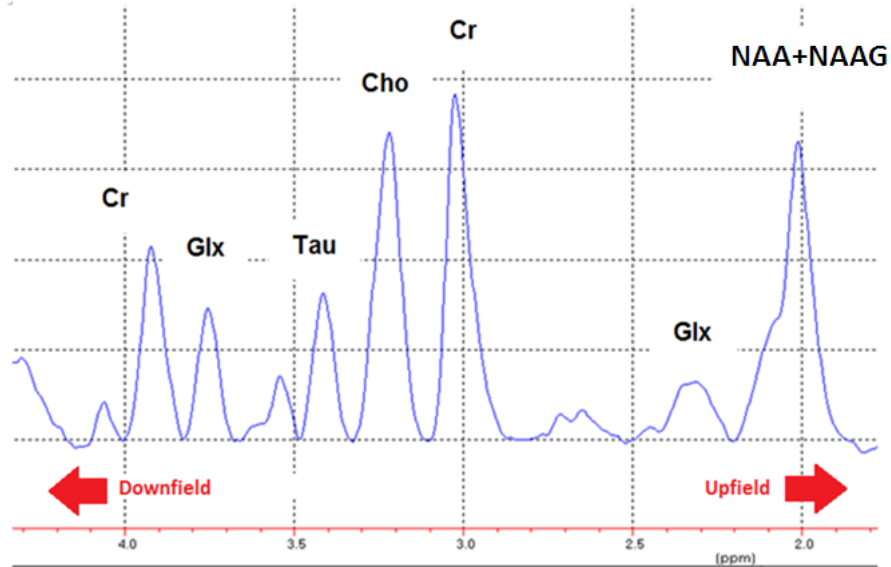


**Figure 1-13.**  $^1\text{H}$ -MR spectrum of a mouse brain. Metabolites are labeled above their respective peaks.

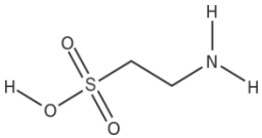
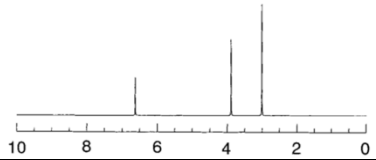
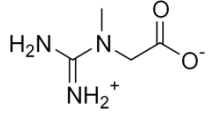
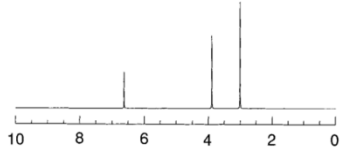
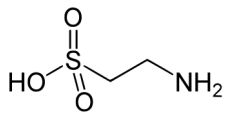
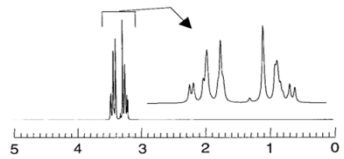
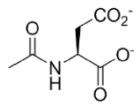
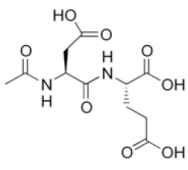
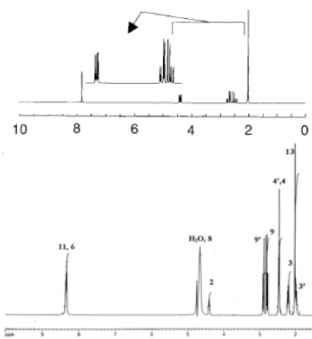
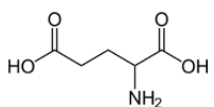
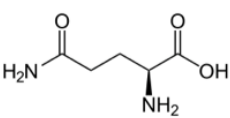
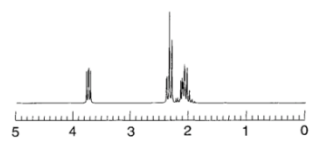
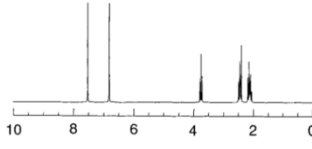
In order to perform MRS, the magnetic field must be made homogenous. This is achieved by shimming, which is an automated or manual process that homogenizes the magnetic field by adjusting shim coils (Gujar et al., 2005). In this study, shimming is accomplished with a FASTMAP pulse sequence that automatically adjusts first and second order shims.

MRS investigates neurometabolites, whose concentrations are much smaller than that of water. Thus it is necessary to suppress the water signal so that it does not overwhelm the metabolite signals (Gujar et al., 2005). This is achieved by exciting the water protons with an RF pulse, then dephasing the water protons with a crusher, or spoiler, gradient. This results in a smaller water peak in the spectrum. Outer volume suppression is also necessary to suppress signals surrounding the voxel.

In this study, a **Point-RESolved Spectroscopy (PRESS)** pulse sequence was used for volume selection. In this pulse sequence, three separate pulses are applied, in the x-, y-, and z-axes, and with 90°, 180°, and 90° flip angles, respectively. The intersection of these pulses results in a volume of interest, or voxel, from which a spectrum is obtained.

Metabolites were analyzed from a cuboid voxel positioned primarily in the hippocampus and cortex. This region was selected because the hippocampus is linked to the limbic system and is known to function differently in schizophrenia patients (Harrison, 2003; Hecker 2001; Shenton et al., 2001) With our current spectroscopy parameters, the metabolites that can be resolved are Choline (Cho), Creatine (Cr), Taurine (Tau), N-acetylaspartate + N-acetylaspartylglutamate (NAA + NAAG), and Glutamate + Glutamine (Glu and Gln; Glx) (Table 1-1).

**Table 1-1.** Metabolite structure, predicted chemical shifts and experimental spectra analyzed in this study (Govindaraju, 2000).

Metabolite	Structure	Predicted Chemical Shifts for $^1\text{H}$ -MRS (ppm)	Spectrum
<b>Cho</b>		<b>3.1850, 4.0540, 3.5010</b>	
<b>Cr</b>		<b>3.0270, 3.9130, 6.6490</b>	
<b>Tau</b>		<b>3.4206, 3.2459</b>	
<b>(NAA+NAAG)</b>	<b>NAA</b>  <b>NAAG</b> 	<b>2.0080, 4.3817, 2.6727, 2.4863, 7.8205</b>	
<b>Glx</b>	<b>Glu</b>  <b>Gln</b> 	<b>3.7433, 2.0375, 2.1200, 2.3378, 2.3520</b>  <b>2.1290, 2.1090, 2.3378, 2.4320, 2.4540, 3.7530, 6.8160, 7.5290</b>	 

## 1.8 Metabolites of Interest

### ***Choline***

The Cho peak in MR spectra is a combination of several choline-containing compounds including glycerophosphocholine, phosphatidylcholine, and phosphocholine (Govindaraju et al., 2000). Cho is a precursor for cytidine diphosphate choline, a mononucleotide involved in the synthesis of phospholipid structural components of cell membranes. Changes in Cho levels are indicative of changes in neuronal membrane composition (Bracken et al., 2011, Govindaraju, 2000). Increased Cho is thought to signal either an increase in the amount of cell membrane per unit volume or an increase in the release of Cho during the breakdown of myelin as in the case in neurodegenerative disorders (Bracken et al., 2011). Reductions in Cho levels have been found in the left hippocampus of schizophrenia patients compared to controls (Maier et al., 1995).

### ***Creatine***

Cr, including phosphocreatine (PCr), is a non-essential nutrient and a marker for brain energy metabolism. It plays a role in energy metabolism, especially in neurons where energy requirements are high and fluctuate (Andres et al., 2008). In MRS studies, the magnitude of Cr has largely been used as an internal reference (Ongur et al., 2009). In this study, metabolite levels are reported as ratios in comparison to Cr. There is some concern regarding this practice because patients with schizophrenia have lower Cr levels than controls. However, this should not be a problem if Cr levels are shown to be normal in the study population (Ongur et al., 2008). In this study, Cr levels have been used as an internal reference based on previous work that determined sufficient controls (Mu, 2011).

## ***Taurine***

Tau is a semi-essential amino acid. In mammals, Tau is the most abundant amino acid in the heart, retina, skeletal muscle, brain, and leukocytes (Schuller-Levis and Park, 2003). Tau is thought to protect cell membranes from toxins and act as a neuroprotectant by increasing neural acetylcholine levels, helping neuronal growth and survival (Schuller-Levis and Park, 2003). Tau uptake and release may also represent a form of communication between neurons and glial cell (Sturman, 1988). Elevated levels of Tau were found in the prefrontal cortex of schizophrenia patients, suggesting a response to increased oxidative stress due to metabolic abnormalities in schizophrenia (Shirayama et al., 2009). Previous work with the GCPII<sup>+/-</sup> mouse model also found increased Tau levels in GCPII<sup>+/-</sup> mice compared to WT (Chen, 2010; Mu, 2011).

## ***N-acetylaspartate and N-acetylaspartylglutamate***

NAA is a metabolite of NAAG. NAA is synthesized by neuronal mitochondria and is abundantly located in neurons throughout the brain. NAA is known to be a marker of neuronal integrity as levels of NAA are altered in a wide range of disorders. However, the biological role of NAA in the brain is unclear (Coyle, 2006). Changes in NAA levels may be indicative of spine/synapse number, neuron size, neuron density, or some combination of these (Bracken et al., 2011).

In schizophrenia patients, *in-vivo* levels of NAA have been found to be reduced in several regions of the brain including the hippocampus (Bertolino et al., 1997; Deicken et al., 1998; Miyaoka et al., 2004; Nasrallah et al., 1994; Steen et al., 2005) and cortical gray matter (Bustillo et al., 2011; Tayoshi et al., 2011). This is consistent with a reduction in GCPII activity and with the process of early dendritic retraction. Correlation was also discovered between NAA levels and social functioning in schizophrenia patients suggesting that NAA may also be an indicator of

disease severity (Sigmundsson et al., 2003).

NAAG is a neuroactive peptide and is localized to subpopulations of glutamatergic, cholinergic, GABAergic, and noradrenergic neuronal systems (Coyle, 1997). As previously mentioned, NAAG is an agonist at mGluR3 receptors and an antagonist at NMDA receptors. NAAG is hydrolyzed to N-acetylaspartate and glutamate by GCPII, which is expressed on the extracellular surface of astrocytes. The levels of NAAG and the activity of GCPII are altered in a regionally specific fashion in several neuropsychiatric disorders (Coyle, 1997). Postmortem studies of NAAG levels in schizophrenia patients have found increases of NAAG in the hippocampus (Tsai et al., 1995).

Based on the glutamate hypothesis, we expect to find reduced levels of NAA and increased levels of NAAG in GCPII<sup>+/-</sup> mice compared to WT mice. NAA and NAAG contribute to the same chemical peak in the <sup>1</sup>H-MRS spectrum and are not distinguishable. If the only factor were the conversion between NAA and NAAG, we would expect this peak, referred to as (NAA+NAAG), to remain the same between GCPII<sup>+/-</sup> and WT mice. However, other problems that account for the viability of cells may result in reductions of NAA (Steen, 2005). Accordingly we expect the (NAA+NAAG) peak to be reduced in GCPII<sup>+/-</sup> compared to WT mice.

### ***Glutamate and Glutamine***

Glu and Gln are both non-essential amino acids. Glu is the primary excitatory neurotransmitter in the brain, while Gln is its precursor and byproduct. In Glu-Gln cycle, Glu and Gln are interconverted into each other (Figure 1-14).



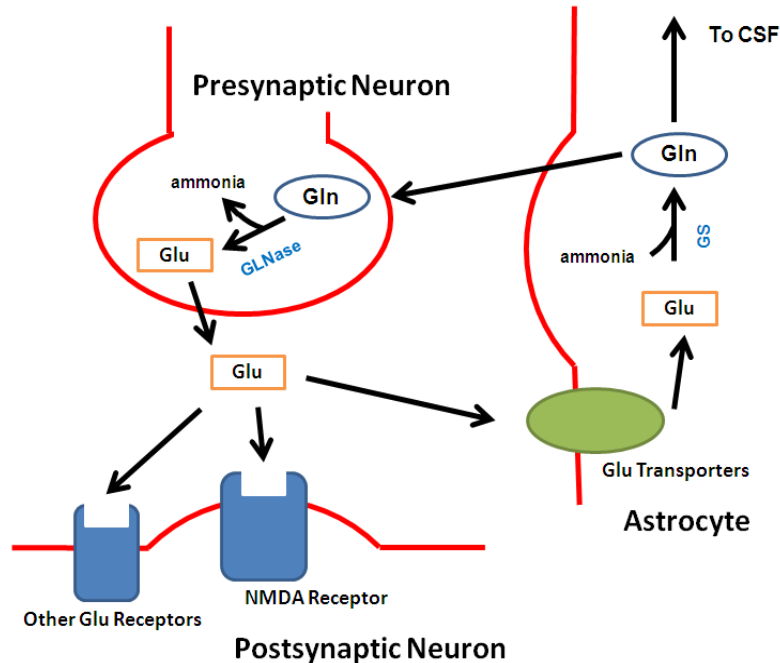


**Figure 1-14.** The glutamate–glutamine (Glu-Gln) cycle. Glu is released from the presynaptic neuron into the synaptic cleft where it acts on postsynaptic receptors, such as NMDA and other Glu receptors. Glu is further removed from the synaptic cleft by glutamate transporters (EAAT1 and EAAT2) which are mainly located on astrocytes. Within the astrocyte, ammonia and Glu combine to form Gln via glutamine synthetase (GS), an astrocyte-specific enzyme. In order to replenish stores of Glu, Gln is released from astrocytes and enters the presynaptic neuron. Once inside the neuron, neuron phosphate-activated glutaminase (GLNase) splits Gln into Glu and ammonia. The cycle then repeats. (Adapted from Rodrigo and Felipo, 2007).

In glial cells, or non-neuronal cells such as astrocytes, Glu is converted into Gln while in the central nervous system Gln is either used for other neuronal processes or converted back to Glu and stored for future use (Rothman et al., 1999). Glu can also be produced *de novo* from tricyclic intermediates in the presynaptic neuron. The rate that Glu is released and processes that follow are controlled by neuronal and metabolic activity through stimulation of extrasynaptic glutamate receptors, such as mGlu3 (Yuksel and Ongur, 2005). Glu and Gln appear at similar chemical shifts and are indistinguishable using *in-vivo* MRS. Thus these metabolites are quantified together as Glx.

The glutamate hypothesis predicts that schizophrenia will function in a hypoglutamatergic state. Accordingly, decreased levels of Glu have been found in schizophrenia patients (Tsai et al., 1995; Tayoshi et al. 2008; Guilarte et al., 2008). In schizophrenia, Glx levels were found to be a marker of cognitive function where levels of Glx were positively correlated with overall cognitive performance (Bustillo et al., 2011). These findings confirm a change in the glutamatergic system and suggest an involvement in the pathophysiology of schizophrenia. However, it must be noted that an increase, lack of change, and decrease of Glx or Glx/Cr in schizophrenia patients have also been found in various studies (Tayoshi et al., 2009). This is likely due to regional differences or time of sampling as Glu concentrations are thought to be higher in the acute stage, but lower in chronic stage (Tayoshi et al., 2009). Our study focuses on the hippocampus with the stage, acute or chronic, unknown. As GCPII activity is prominent in the hippocampus related to levels of Glu, we expect our findings to parallel MRS studies of the hippocampus, which reported decreased levels of Glu (Tayoshi et al., 2009; Tsai et al., 1995).

## 2 Materials and Methods

---

### 2.1 Subjects and Subject Maintenance

All experiments were conducted on GCPII<sup>+/-</sup> (HET) mice or C57BL/6 (WT) mice, which descended from the founding colony at McLean hospital (Belmont, MA). HET mice contain a knockout of the GCPII gene and exhibit reduced GCPII enzyme function (Han et al., 2009), while WT mice have no genetic modification and serve as controls. HET mice were bred on a WT mice background for over 9 generations with procedures approved by the Wellesley College Institutional Animal Care and Use Committee and conform to the standards set forth in the National Institute of Health Guide for the Care and Use of Laboratory Animals. HET dams were mated with WT male mice and the day after birth was considered postnatal day (PND) 1.

WT and HET mice were weaned on PND 21 and separated by sex into standard sized mouse cages that contained at least 2 mice and held a maximum of 4 mice. There were four types of mice used: HET males (n = 4), WT males (n = 6), HET females (n = 7), and WT females (n = 7), and. Mice were exposed to a 12:12 light-dark cycle and temperatures of  $21 \pm 1$  °C with food and water available *ad libitum*. Markings were periodically drawn on mice tails for identification. For genotyping, mice ears were clipped and ear samples were sent to Mouse Genotype (Carlsbad, CA) for analysis. Subsequently, observations of ear clippings were used to identify mice.

## 2.2 *In vivo* Magnetic Resonance Imaging and Spectroscopy

Brain MR images of each mouse were obtained on PND 35/36, 49/50, 63/64 on a 9.4 T Bruker Avance DRX 400 MHz vertical bore NMR spectrometer equipped with a MicroMouse 2.5 imaging accessory (Bruker Biospin, Billerica, MA). Bruker ParaVision 4.0 and Bruker Topspin 1.5 software (Ettlingen, Germany) were used to acquire images and analyze spectra, respectively, on a Linux system. After imaging, all data were analyzed using a genotype-blind protocol with Analyze 10.0 image analysis software (Mayo Clinic, Rochester, MN).

## 2.3 Animal Preparation

Mice were anesthetized with 1-1.5% isoflurane in oxygen, at a flow rate of 0.2 L/min in a plexiglass chamber (Braintree Scientific, Inc., Braintree, MA). Once a mouse was anesthetized, approximately 10 minutes after exposure to isoflurane/O<sub>2</sub>, the isoflurane/O<sub>2</sub> flow was directed into the nose cone of a mouse bed (Wellesley College, Wellesley, MA), which has an opening for the exhaust tube and is located inside the micro-imaging probe (Figure 2-1). The exhaust tube was connected to a F/AIR Scavenger activated charcoal filter (Paragonmed, Coral Springs, FL) to prevent airborne contaminants from entering the environment. The mouse was then transferred to the mouse bed where it was positioned using a bite bar and secured using 3M Micropore™ tape (St. Paul, MN). Once taped into the mouse bed, the breath rate of the mouse was monitored with a respiration sensor pad (SA Instrument, Inc., Stony Brook, NY) configured with BioTrig Builder 1.01 Software (Bruker Biospin, Billerica, MA) on a PC system. The breathing rate was maintained between 30 and 100 breaths per minute by adjusting the isoflurane level with a VIP Veterinary Vaporizer (Colonial Medical Supply, Co., Franconia, NH).

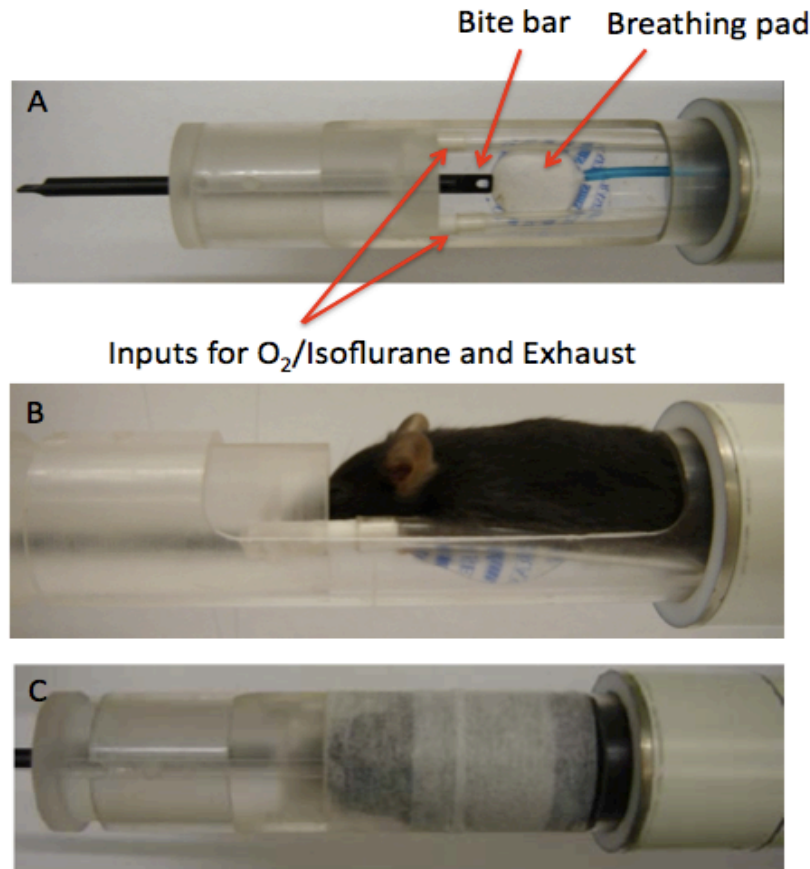


**Figure 2-1.** Mousebed (A; top view). Arrows, as labelled, indicate location of bite bar, respiration sensorpad, and air inputs. Mousebed with mouse positioned inside (B; side view). Mousebed with mouse secured (C; topview).

Once the mouse was secured in the mouse bed and inserted into the probe, the probe was positioned in the spectrometer to center the brain in the magnet and gradient coils. Throughout the experiment, a water circulation unit was used to maintain the temperature of the coils surrounding the mouse at 32 °C to help the mouse maintain a body temperature.

## 2.4 Magnetic Resonance Imaging

The probe was tuned and matched before imaging or acquiring spectra. A RARE\_tripilot sequence was used to visualize the mouse's position in three orthogonal slices (TE = 12.500 ms, TR = 2000.000 ms, rare factor = 8, matrix size = 128x128, number of averages = 1). The

RARE\_tripilot images were then used to position the field-of-view (FOV) on the entire mouse brain (Figure 2-2). If the brain was not centered in the gradients, the mouse was removed, repositioned, and the RARE\_tripilot scan was repeated. Next, 24 contiguous coronal MR images of 0.7 mm thick slices were acquired with a RARE\_8\_bas T2 weighted pulse sequence (TE = 15 ms, TR = 3109 ms, Tx0 ~ 15 dB, Tx1 ~ 5.2 dB, FOV = 2.6 cm<sup>2</sup>, averages =16). A pre-scan macro was used to automatically adjust the attenuators, receiver gain, and shim settings.

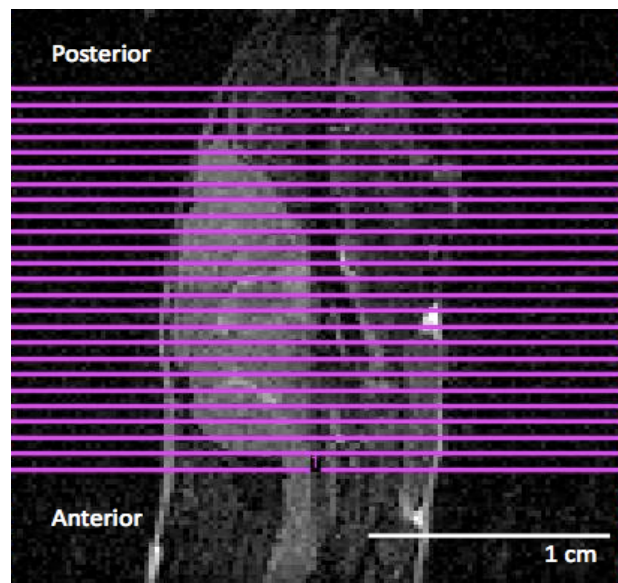


**Figure 2-2.** Selection of 24 contiguous slices on a sagittal RARE\_tripilot image of a mouse brain.

## 2.5 Magnetic Resonance Spectroscopy

Following the imaging portion of the experiment, with the mouse still in the magnet, a spectrum of the hippocampus region was obtained. With the Geometry Editor tool, a 4x4x4 mm<sup>3</sup> (64  $\mu$ L) voxel was positioned to include the hippocampus using the RARE\_8\_bas images as a reference. A fastmap\_4mm scan automatically adjusted first and second order shims over the cubic region. The voxel was reduced to a 4x2x3 mm<sup>3</sup> (24  $\mu$ L) cube focused on the hippocampus

(Figure 2-3). The PRESS\_waterline pulse sequence was used to obtain a water peak (TE = 20 ms, TR = 2000 ms, averages = 8). This sequence included Outer Volume Suppression (OVS) but not water suppression. The spectrum obtained from PRESS\_waterline was analyzed with Bruker TopSpin 1.5 software to determine the linewidth of the water peak. If the width was larger than 25 Hz, the spectrum could not be obtained and fastmap\_4mm was repeated to further homogenize the magnetic field. With a satisfactory water peak, the final metabolite spectrum was obtained using the Press-1H pulse sequence with VAPOR water suppression and outer volume suppression (OVS) (TE= 20 ms, TR = 2000 ms, Tx0~ 150, Tx1~ 9.4, averages = 800).

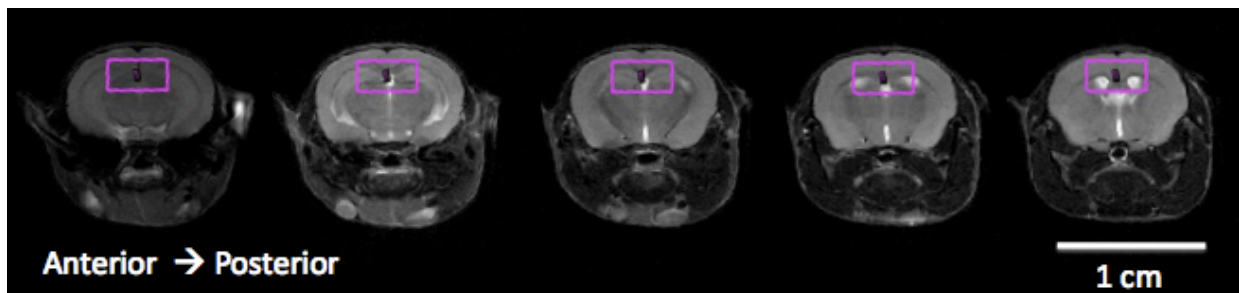


**Figure 2-3.** A 4x2x3 mm<sup>3</sup> cuboid voxel positioned on the hippocampus in 5 slices, which were contiguous and each had a thickness of .7 mm.

After the spectrum was acquired, the mouse was removed from the probe and was monitored on a heating pad until it recovered full consciousness.

## 2.6 Data Analysis

### *MRI Data Analysis*

After imaging, all data were analyzed using a genotype-blind protocol with Analyze 10.0 image analysis software (Mayo Clinic, Rochester, MN). Whole brain, cerebellum, fourth ventricle, third ventricle, left and right hippocampus, and left and right lateral ventricles were traced as separate objects with the Region of Interest Tool and Wacom Cintiq 12WX tablet

display (Wacom Co., Ltd., Tokyo, Japan). A stereotaxic atlas was used as a reference to determine regional borders of structures and structural markers (Paxinos and Franklin, 2004). Three laboratory members, including the author, traced the brains in order to minimize the total amount of tracing for each person and maximize tracing consistency for each brain structure. Each person traced specific structures in every brain; one traced the whole brain, another the cerebellum, and the final traced all other structures (See Appendix-A for tracing guide). The final traces were then combined and the Sample Images tool on Analyze 10.0 was used to determine the volume of each structure. The combined area of each traced region was multiplied by the summed thickness of the slices for the relevant brain region.

### ***MRS Data Analysis***

The spectral peaks were analyzed with Bruker TopSpin 1.5 to determine relative metabolite concentrations. Line broadening, or exponential multiplication, of 10 Hz was applied to the FID to improve the signal to noise ratio of the spectrum. The reduction of noise made the spectrum lines smoother and easier to read. The spectra were then phased and calibrated, where the distinguishable (NAA+NAAG) peak was set to 2.01 ppm. The troughs between each pair of peaks were marked as baseline points. The deconvolution tool was then used to fit Gaussian curves under each peak and provide the calculated area under the Gaussian peaks. Each peak of the spectrum represents the unique properties of equivalent protons in the neurometabolites. The Gaussian peak area could then be used to represent the levels of a specific neurometabolite. The metabolites Cr, Tau, Cho, Glx, and (NAA+NAAG) were resolved and compared to Cr (3.0 ppm), an internal standard (Recall Figure 1-13).



### ***Statistical Analysis***

All data were analyzed by genotype and PND with males and females grouped separately. Independent unpaired two-tailed t-tests assuming unequal variances were used to detect differences between genotypes at a single time point. Paired t-tests were used to detect developmental differences within a genotype between two time points. Bar graphs were created to represent mean volume or ratio of brain structures or metabolites with error bars representing standard deviation. All analyses were performed using Microsoft Excel where a  $p < 0.05$  was considered significant. Q-tests were performed to detect outliers, but outliers were not removed given the small sample size of data.

# 3 Results and Discussion

---

## 3.1 Magnetic Resonance Imaging

MRI data were collected from the same HET males (n = 4), WT males (n = 6), HET females (n = 7), and WT females (n = 7) on PND 35/36, 49/50, and 63/64. The effect of sex differences on MRI data were first examined in HET and WT mice. Because sex differences were found between male and female mice, all data from males and females were analyzed separately. The volume or volume ratio of each structure was averaged at each time point for all mice in each of the four groups. Brain structures volumes were normalized to the whole brain volume (WBV) to account for size differences among mice. WBV, cerebellum to WBV ratio (C/WB), fourth ventricle to WBV ratio (4V/WB), third ventricle to WBV ratio (3V/WB), lateral ventricle to WBV ratio (LV/WB), left to right lateral ventricle volume ratio (Left/Right LV), hippocampus to WBV ratio (HP/WB), and left to right hippocampus volume ratio (Left/Right HP) were examined for all mice. The individual volume trends of four mice, one mouse of each genotype and sex from the same litter, were also examined.

### ***Sexual Dimorphism***

Phenotypic differences between male and female mice (sexual dimorphisms) were examined in HET and WT mouse brain structures. Male HET mice had significantly larger cerebellum to WBV ratios than females on PND 63 ( $t(9) = 1.833, p < .01$ ; Figure 3-1B). At all time points, male HET mice exhibited a greater left to right hippocampus ratio than female HET mice and was significantly different on PND 49 ( $t(9) = 1.833, p = 0.01$ ; Figure 3-1H). Female WT mice had larger cerebellum to WBV ratios than male WT mice at all time points and trended towards significance on PND 63 ( $t(11) = 1.796, p = 0.050$ ; Figure 3-2B). At all time points, male WT mice had larger whole brain volumes compared to female WT mice and male HET mice had smaller whole brain volumes compared to female HET mice (Figure 3-1A and 3-2A). No significant volume differences were found between male and female WT mice at any time point. Longitudinal differences within a brain region are discussed later in each structure's respective section.

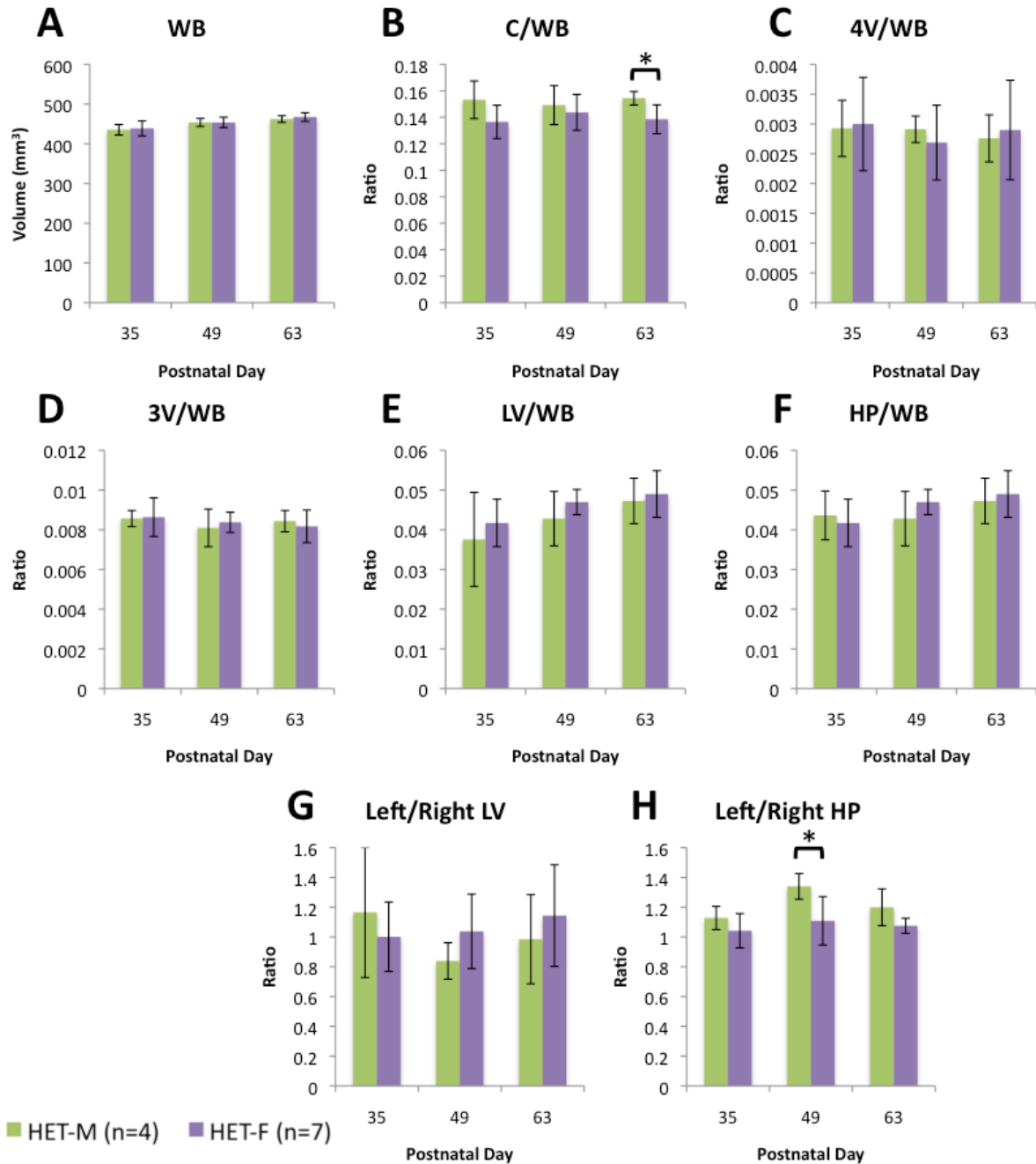


**Figure 3-1.** Mean brain structure volume or ratio  $\pm$  SD between GCPII<sup>+/-</sup> heterozygous (HET) males (M) and females (F) from postnatal day 35 to 63. Regions analyzed were A. Whole brain (WB), B. Cerebellum (C) to WB ratio, C. Fourth ventricle (4V) to WB ratio, D. Third ventricle (3V) to WB ratio, E. Lateral ventricle (LV) to WB ratio, F. Hippocampus (HP) to WB ratio, G. Left LV to right LV ratio, H. Left HP to right HP ratio. Key on the bottom left indicates sex and genotype. Data from the same mice were collected over time. Regions were manually traced and volume was calculated using the Region of Interest tool on Analyze 10.0. \* indicates a significant difference ( $p < 0.05$ ) between genotypes at a single time point as determined with unpaired two-tailed t-tests assuming unequal variances.

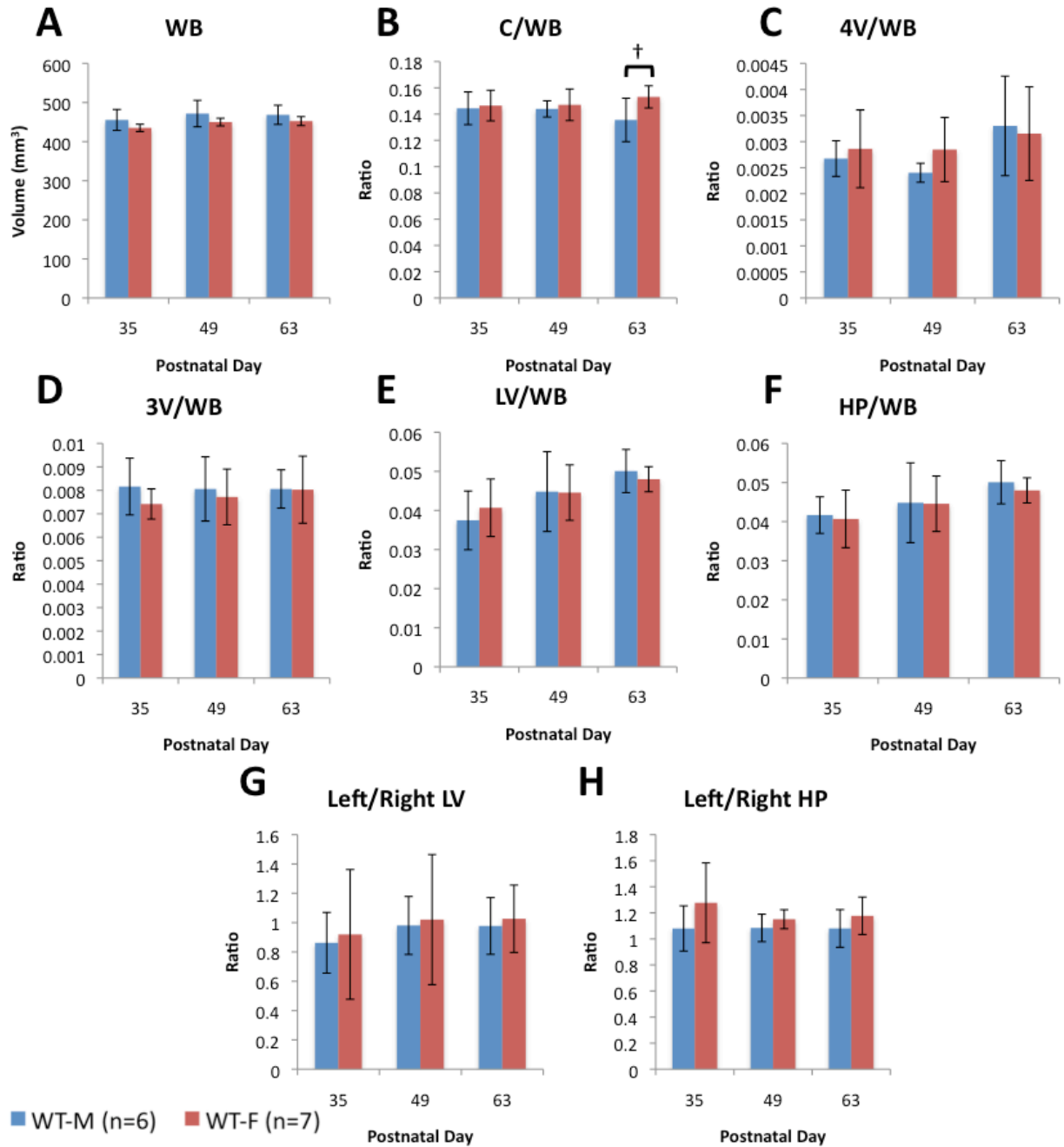


**Figure 3-2.** Mean brain structure volume or ratio  $\pm$  SD between wild-type (WT) males (M) and females (F) from postnatal day 35 to 63. Regions analyzed were A. Whole brain (WB), B. Cerebellum (C) to WB ratio, C. Fourth ventricle (4V) to WB ratio, D. Third ventricle (3V) to WB ratio, E. Lateral ventricle (LV) to WB ratio, F. Hippocampus (HP) to WB ratio, G. Left LV to right LV ratio, H. Left HP to right HP ratio. Key on the bottom left indicates sex and genotype. Data from the same mice were collected over time. Regions were manually traced and volume was calculated using the Region of Interest tool on Analyze 10.0. † indicates a trend towards a significant difference between genotypes ( $0.05 < p < 0.07$ ).

Sexually dimorphic characteristics have been found in both human and mouse brains, but the etiology of these differences is not well understood (Goldstein et al., 2001; Spring et al., 2007). Our finding that the male WT whole brain is larger than the female WT whole brain agrees with a 3D MRI study that examined the same WT (C57BL/6) mice (Spring et al., 2007). Volume studies on humans report similar results (Chance et al., 2003; Goldstein et al., 2001). Differences in whole brain size may stem from the release of different sex hormones (Cooke et al., 1999; Goldstein et al., 2001). Cooke et al. (1999) found that adult hormone manipulation can completely reverse sexual dimorphism in the postdorsal component of the medial amygdala of rats. However, hormone manipulation could not reverse all sexually dimorphic neural volumes. This suggests that non-biological factors, such as behavior and environment, may also play a role in the development of sexually dimorphic characteristics.

Brain metabolic (Tayoshi et al., 2009), morphologic (Springer et al., 2007; Takayanagi et al., 2009), behavioral (Seeman et al., 1997), and hormonal (Seeman et al., 1997) sex differences have been observed in schizophrenia patients. Males experience an earlier onset and a more severe form of schizophrenia than females, as males experience more negative symptoms and exhibit greater brain abnormalities (Seeman et al., 1997). These findings may relate to morphological changes, which are more prominent in male subjects as compared to females (Tayoshi et al.; 2009). Reduced WBV is a characteristic of male and female schizophrenia patients (Nakamura et al., 2004; Steen et al., 2006). While we do not see significantly reduced WBVs in our mouse model, we found that male HET mice had smaller WBVs than female HET mice. This suggests that male HET mice exhibit greater morphological changes than female HET mice, as male WT WBVs are normally greater than WT female volumes. Hippocampus

asymmetry is also a characteristic of schizophrenia patients (Harrison, 2003; Heckers, 2001; Petty, 1999). Our finding that male HET mice exhibit greater asymmetry, or a larger left to right hippocampus ratio than female HET mice, further confirms that HET males are more affected than females. Cerebellum to WBV sex differences were apparent in WT mice and significant in HET mice. However, each genotype exhibited opposite trends – female WT mice had larger C/WB ratios than male WT mice and vice versa for HET mice. These differences are, once again, likely related to male HET mice exhibiting greater morphological changes than female HET mice as an enlarged cerebellum is a characteristic of schizophrenia patients (Levitt et al., 1999). Other reasons for observed differences in brain structures are discussed later in each region's respective section (See Cerebellum finding, p. 45).

Collectively, these findings suggest volumetric differences between male and female brains in both WT and GCPII<sup>+/-</sup> mice. In order to control for sex differences, all volume analyses between WT and HET mice were grouped by sex (Table 3-1).

**Table 3-1.** MRI brain volume data for male WT, male HET, female WT, and female HET mice. A. \* indicates a significant difference between WT and HET mice at that time point ( $p < 0.05$ ). † indicates a trend towards significance between WT and HET mice ( $0.05 < p < 0.07$ ). B. \* indicates a significant developmental difference between indicated time points within a genotype and sex ( $p < 0.05$ ). † indicates a trend towards a significant developmental difference between time points ( $0.05 < p < 0.07$ ).

A. Comparisons between WT and HET at each of the sampled time points (independent t-tests)							
	PND 35/36		PND 49/50		PND 63/64		
	M	F	M	F	M	F	
Whole brain volume (mm <sup>3</sup> )							* 0.0275
Cerebellum/WB							* 0.0377 * 0.0176
4th Ventricle/WB							* 0.0100
3rd Ventricle/WB							* 0.0216
Lateral Ventricles/WB							* 0.0122
Hippocampus/WB							
L/R Lateral Ventricle							
L/R Hippocampus							* 0.0034

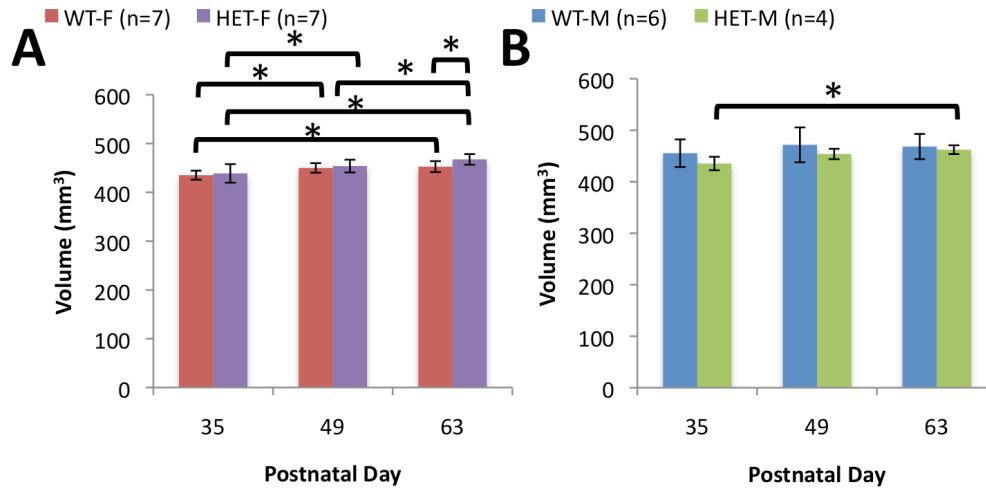
  

B. Comparisons among particular time points within each genotype (paired t-test)												
	PND 35/36 vs 49/50				PND 49/50 vs 63/64				PND 35/36 vs 63/64			
	WT-M	HET-M	WT-F	HET-F	WT-M	HET-M	WT-F	HET-F	WT-M	HET-M	WT-F	HET-F
Whole brain volume (mm <sup>3</sup> )												
Cerebellum/WB												
4th Ventricle/WB												
3rd Ventricle/WB												
Lateral Ventricles/WB												
Hippocampus/WB												
L/R Lateral Ventricle												
L/R Hippocampus												

### Whole Brain Volume Results

WBV was significantly greater for HET female mice than for WT female mice on PND 63 ( $t(12) = 1.782, p = 0.03$ ; Figure 3-3A). WBV significantly increased from PND 35 to 63 for female WT ( $t(12) = 1.782, p = 0.02$ ), female HET ( $t(12) = 1.782, p < .01$ ) and male HET mice ( $t(6) = 1.943, p = 0.04$ ; Figure 3-3). WBV significantly increased from PND 35 to 49 for female HET ( $t(12) = 1.782, p < .01$ ) and female WT mice ( $t(12) = 1.782, p = 0.03$ ; Figure 3-3A). Only female HET mice showed a significant increase in WBV from PND 49 to 63 ( $t(12) = 1.782, p < 0.01$ ; Figure 3-3A). At all time points, male WT mice had larger WBVs than male HET mice (Figure 3-3B).





**Figure 3-3.** Mean whole brain volume  $\pm$  SD of A. wild-type (WT) and GCPII<sup>+/-</sup> heterozygous (HET) females and B. WT and HET males from postnatal day 35 to 63. Keys above graphs indicate sex and genotype. Data from the same mice were collected over time. Regions were manually traced and volume was calculated using the Region of Interest tool on Analyze 10.0. \* indicates a significant difference ( $p < 0.05$ ) between genotypes at a single time point as determined with unpaired two-tailed student t-tests assuming unequal variances or a significant developmental difference within a genotype and between two time points as determined with paired two-tailed t-tests.

### ***Whole Brain Volume Development***

Structural studies have found reduced WBVs in schizophrenia patients compared to controls (Nakamura et al., 2004; Steen et al., 2006). Our result that male HET WBVs appear smaller than male WT WBVs at all time points agrees with these findings. A meta-analysis of *in vivo* MRI studies on the brain volume of schizophrenia patients suggests that the whole brain of schizophrenia patients may not exhibit progressive deficits (Steen et al., 2006). In other words, the whole brain in schizophrenia patients is growing at the same rate as a healthy person. Steen et al. (2006) hypothesized that abnormalities in brain development, which begin after birth or after the onset of symptoms, are what cause the brain to be smaller than healthy controls. If abnormal brain development begins later for the GCPII<sup>+/-</sup> mouse model, it is possible that male and female HET mice would exhibit significantly smaller WBVs compared to, respectively, male and female WT mice at later time points. WBV growth from PND 35 to 63 for male and female HET mice

was expected, as WBV of both healthy and schizophrenic individuals is known to increase over time. WBV growth from PND 35 to 63 for male WT mice would likely reach significance with a larger sample size as this pattern was observed in all other mice.

### ***Cerebellum to Whole Brain Volume Ratio Results***

female HET mice had significantly lower cerebellum to WBV ratios on PND 63 compared to female WT mice ( $t(12) = 1.782, p = 0.02$ ; Figure 3-4A), whereas male HET mice had significantly higher cerebellum to WBV ratios on PND 63 compared to male WT mice ( $t(8) = 1.860, p = 0.04$ ; Figure 3-4B). At all time points, male HET mice had higher cerebellum to WBV ratios than male WT mice. Female mice exhibited the opposite pattern; female HET mice had lower cerebellum to WBV ratios compared to female WT mice.

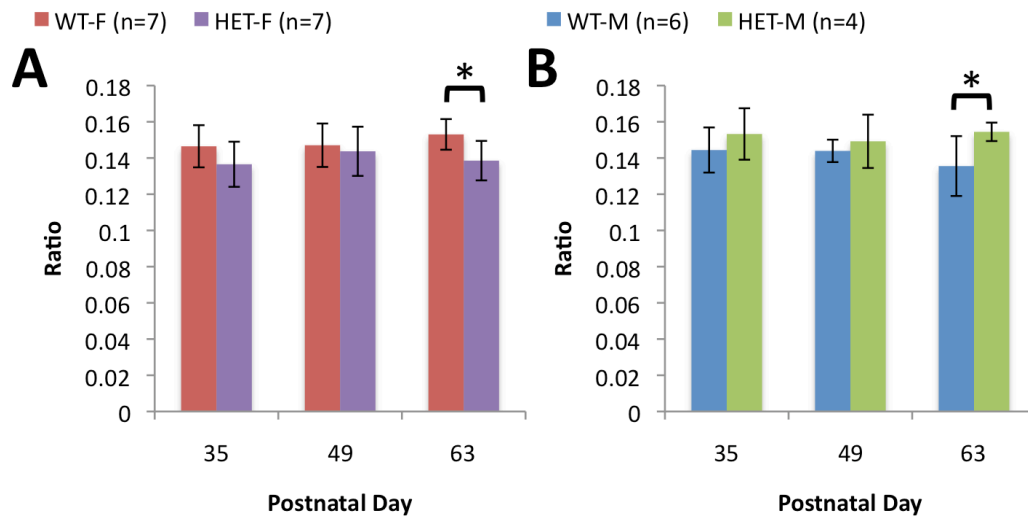


**Figure 3-4.** Mean cerebellum to whole brain volume ratio  $\pm$  SD of A. wild-type (WT) and GCPII $\pm$  heterozygous (HET) females and B. WT and HET males from postnatal day 35 to 63. Keys above graphs indicate sex and genotype. Data from the same mice were collected over time. Regions were manually traced and volume was calculated using the Region of Interest tool on Analyze 10.0. \* indicates a significant difference ( $p < 0.05$ ) between genotypes at a single time point as determined with unpaired two-tailed student t-tests assuming unequal variances.

### ***Cerebellum Findings on PND 63 May be Linked to Sexual Dimorphism***

Few studies have examined the role of the cerebellum in schizophrenia patients, as schizophrenia is known to primarily affect structures associated with the cerebrum and limbic system. While the cerebellum is primarily associated with motor function, there is evidence that the cerebellum may play a role in higher cognitive function (Andreason and Pierson, 2008; Shenton et al., 2001; Yeganeh-Doost et al., 2011). This was partially confirmed by Levitt et al. (1999) in a study that investigated the vermis, a structure in the cerebellum, and found greater vermis white matter volume is correlated to positive symptoms and thought disorder in schizophrenia. Further, they found that the vermis is enlarged in schizophrenia patients compared to controls (Levitt et al., 1999). Our findings that male HET mice had significantly larger cerebellum to WBV ratios on PND 63 and non-significantly larger ratios on PND 35 and 49 agree with this study. Conversely, other studies found that cerebellum volume is reduced (Martin and Albers, 1995) or remains unchanged (Steen et al., 2006) in schizophrenia patients compared to controls. The former study agrees with our finding that WT female mice have larger cerebellums than HET female mice on PND 63. While previous work in our lab found no difference in cerebellum to WBV ratio between HET and WT mice, male and female data were combined in the analysis (Mu, 2011). Our data suggest sexual dimorphism could account for the observed differences, but a larger sample size or data from later time points are needed to make our results more conclusive. If it was determined that female and male HET mice show significantly smaller and larger cerebellum to WBV ratios compared to WT mice, respectively, at multiple time points, then there would be strong indication of sexual dimorphism in the cerebellum.

### Fourth Ventricle to Whole Brain Volume Ratio Results

The fourth ventricle to WBV ratios of male HET mice were significantly higher than those of male WT mice on PND 49 ( $t(8) = 1.860, p = 0.01$ ; Figure 3-5B). There was a trend toward significance where fourth ventricle to WBV ratio increased from PND 49 to 63 for male HET mice ( $t(6) = 1.943, p = 0.048$ ; Figure 3-5B). There were no fourth ventricle to WBV ratio trends observed for female HET and WT at any time point or between time points for each genotype (Figure 3-5A).

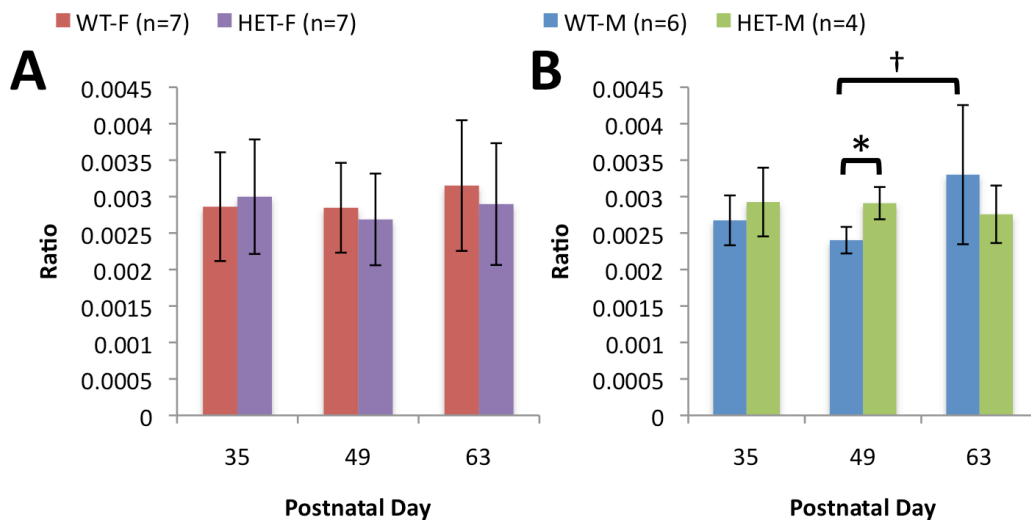


**Figure 3-5.** Mean fourth ventricle to whole brain volume ratio  $\pm$  SD of A. wild-type (WT) and GCPII<sup>+/-</sup> heterozygous (HET) females and B. WT and HET males from postnatal day 35 to 63. Keys above graphs indicate sex and genotype. Data from the same mice were collected over time. Regions were manually traced and volume was calculated using the Region of Interest tool on Analyze 10.0. \* indicates a significant difference ( $p < 0.05$ ) between genotypes at a single time point as determined with unpaired two-tailed student t-tests assuming unequal variances. † indicates a trend towards a significant developmental difference between time points ( $0.05 < p < 0.07$ ).

### Fourth Ventricle Enlargement in Male HET Mice

Increased ventricular volume is a common characteristic of schizophrenia (Shenton et al., 2001). However, there is dispute regarding fourth ventricle character in schizophrenia. Out of the five *in vivo* MRI studies reviewed in a meta-analysis, four found no difference in fourth ventricle volume between schizophrenia patients and controls (Shenton et al., 2001). The one study with

positive findings, by Keshavan et al. (1998), found that the fourth ventricle was enlarged in the superior temporal gyrus of schizophrenia patients compared to controls. Our findings that male HET mice exhibit significantly larger fourth ventricle to whole brain volume ratios than male WT mice support these results. However, our findings were only significant at the one time point, PND 49. As we only found differences between genotypes in males, it is possible that there is an effect of sexual dimorphism on fourth ventricle development. A greater sample size is needed to see if these differences also occur on PND 35 and 63 in male mice or at any time point in female mice.

We found that male WT mice exhibited an increase in fourth ventricle to WBV ratio from PND 49 to 63 and trended towards significance. However, it is difficult to analyze or compare our findings, as there were no studies that related developmental trends of the fourth ventricle in humans to mice. It would be interesting to see if a larger sample size would reveal this pattern in other groups of mice, as it would suggest that an increase in fourth ventricle to WBV ratio from PND 49 to PND 63 is a part of normal brain growth.

### ***Third Ventricle to Whole Brain Volume Ratio Results***

Female HET mice had significantly higher third ventricle to WBV ratios compared to female WT mice on PND 35 ( $t(12) = 1.782, p = 0.0332$ ; Figure 3-6A). There were no third ventricle to WBV ratio trends observed for male HET and WT at any time point or between time points for each genotype (Figure 3-6B)

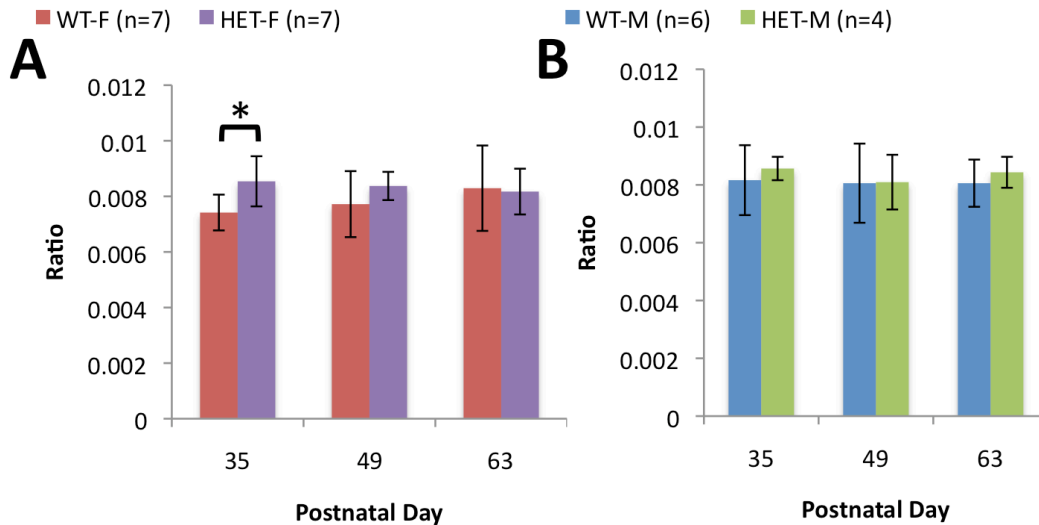


**Figure 3-6.** Mean third ventricle to whole brain volume ratio  $\pm$  SD of A. wild-type (WT) and GCPII $\pm$  heterozygous (HET) females and B. WT and HET males from postnatal day 35 to 63. Keys above graphs indicate sex and genotype. Data from the same mice were collected over time. Regions were manually traced and volume was calculated using the Region of Interest tool on Analyze 10.0. \* indicates a significant difference ( $p < 0.05$ ) between genotypes at a single time point as determined with unpaired two-tailed student t-tests assuming unequal variances.

### *Third Ventricle Enlargement in Female HET Mice*

Structural studies have found enlargement of the third ventricle in schizophrenia patients compared to controls (Nakamura et al., 2004; Shenton et al., 2001; Tsai et al., 2002). Previous work in our lab found the third ventricle to WBV ratio to be increased in male and female HET mice compared to controls on PND 77. Our findings that female HET mice exhibit significantly larger third ventricles than female WT mice on PND 35 agree with these studies. Shenton et al. (2001) hypothesizes that increased fluid in the third ventricle observed in schizophrenia patients may be related to reduced volume of the thalamus— a limbic system structure adjacent to the hypothalamus. Thus, an enlarged third ventricle may be linked to abnormal thalamus development. Additional differences between genotypes would likely reach significance on PND 49 as differences are apparent, but not yet significant.

### Lateral Ventricle to Whole Brain Volume Ratio Results

Female HET mice exhibited significantly higher lateral ventricle to WBV ratios compared to female WT mice on PND 35 ( $t(12) = 1.782, p = 0.01$ ; Figure 3-9A). Female WT lateral ventricle to WBV ratio showed a significant increase from PND 35 to 63 ( $t(12) = 1.782, p = 0.02$ ; Figure 3-9A). Female WT lateral ventricle to WBV ratios on PND 49 were higher than on PND 35 and trended towards significance ( $t(12) = 1.782, p = 0.047$ ; Figure 3-9A). For male HET and WT mice there were no differences in lateral ventricle to WBV ratio at a single time point or between time points for each genotype (Figure 3-9B). For male WT, female HET, and female WT mice, lateral ventricle to WBV ratio increased over time (Figure 3-9). Female HET mice had higher lateral ventricle to WBV ratios than female WT mice at all time points (Figure 3-9A). Male HET mice demonstrated lateral ventricle to WBV ratio growth from PND 35 to 49, with a subsequent decline on PND 63 (Figure 3-9B).

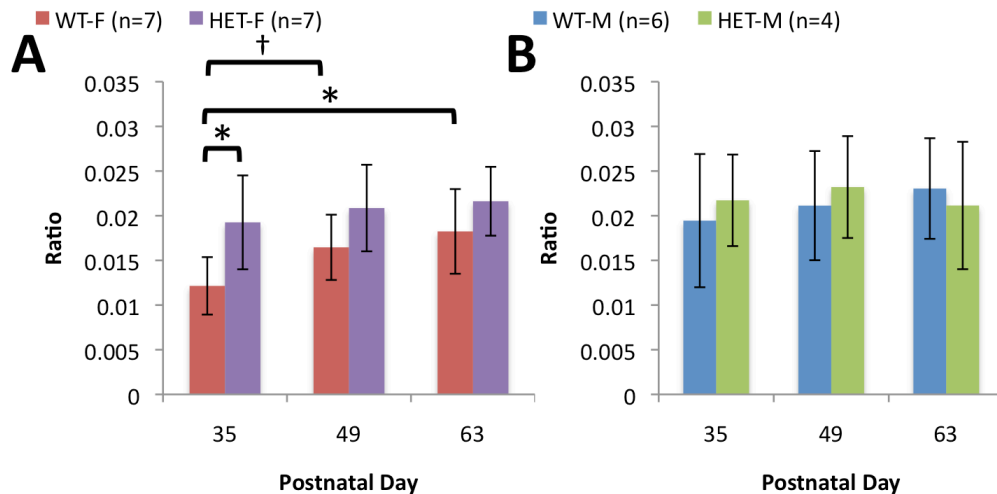


**Figure 3-9.** Mean lateral ventricle to whole brain volume ratio  $\pm$  SD of A. WT and GCPII $\pm$ -heterozygous (HET) females and B. WT and GCPII $\pm$ -heterozygous (HET) males from postnatal day 35 to 63. Key above each group indicates sex and genotype. Data from the same mice were collected over time. Regions were manually traced and volume was calculated using the Region of Interest tool on Analyze 10.0. \* indicates a significant differences ( $p < 0.05$ ) between genotypes at a single time point as determined with unpaired two-tailed student t-tests assuming unequal variances or a significant developmental difference within a genotype and between two time points as determined with paired two-tailed t-tests. † indicates a trend towards significant developmental difference between time points ( $0.05 < p < 0.07$ ).

### ***Lateral Ventricle Development***

*In vivo* and post-mortem structural imaging studies have found lateral ventricle enlargement in schizophrenia patients compared to controls (Chance et al., 2003; Kempton et al., 2010; Meduri et al., 2010). Ventricle enlargement was found to be greater in female than male schizophrenia patients (Chance et al., 2003). Our findings that female HET mice have significantly higher lateral ventricles to WBV ratios than female WT mice on PND 35 agree with these findings. Female HET mice also appear to have higher lateral ventricles to WBV ratios on PND 49 and 63, but these differences are not significant. Results at these time points require a large sample size to reach statistical significance.

The connection between ventricle enlargement and the biochemical processes in schizophrenia remain unclear. Studies suggest that lateral ventricle enlargement occurs either from abnormal brain development starting at birth or during the prodromal phase of schizophrenia, the period of time from when symptoms manifest to the full development of the schizophrenia (Kempton et al., 2010). Ventricular enlargement has been associated with smaller cortical and subcortical grey matter volumes (cerebral cortex and neural tissue that comprises the outer layer of the cerebrum; Meduri et al., 2010). There is also a possibility that genetic factors, such as heritability, can influence lateral ventricular volume (Reveley et al., 1984).

Our findings that female WT mice showed significant lateral ventricle to whole brain volume ratio growth and that female HET and male WT mice showed non-significant growth were expected as the lateral ventricles in healthy individuals and schizophrenia patients are expected to grow over time (Kempton et al., 2010). Female HET, male WT mice would likely show significant lateral ventricle to WBV ratio growth with a larger sample size as differences between time points were apparent but did not reach statistical significance.



### ***Lateral Ventricle Asymmetry Results***

Lateral ventricle asymmetry was measured by determining the ratio between left and right lateral ventricle volumes. Values that deviated from 1 indicated asymmetry where one ventricle was larger than the other. For male and female groups, HET and WT mice showed no significant difference in lateral ventricle symmetry at a single time point or between time points for each genotype (Figure 3-10). For female HET mice, asymmetry increased over time (Figure 3-10A). It should be noted that the standard deviations were very large for most groups of mice at all time points, so that differences that were apparent were not statistically significant.

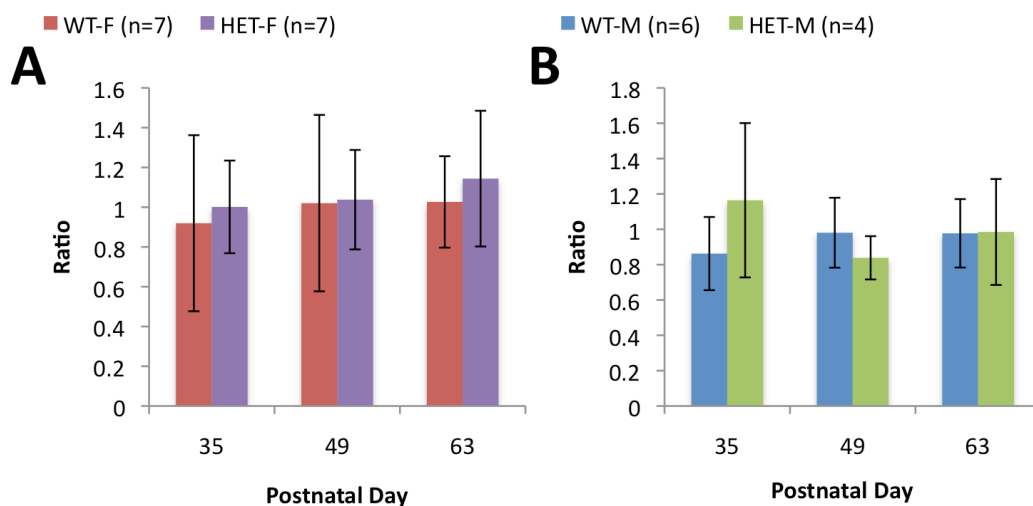


**Figure 3-10.** Mean left to right lateral ventricle volume ratio ± SD of A. wild-type (WT) and GCPII<sup>+/-</sup> heterozygous (HET) females and B. WT and HET males from postnatal day 35 to 63. Key above each group indicates sex and genotype. Data from the same mice were collected over time. Regions were manually traced and volume was calculated using the Region of Interest tool on Analyze 10.0. Asterisks indicate significant differences ( $p < 0.05$ ) as determined with unpaired two-tailed student t-tests assuming unequal variances. No asterisks indicate a lack of significant findings.

### ***Lateral Ventricle Asymmetry***

Schizophrenia patients are known to exhibit lateral ventricle asymmetry where the left lateral ventricle is larger than the right (Chance et al., 2002; Petty, 1999). However, the opposite

has also been found in schizophrenia patients, where the right lateral ventricle is larger than the left (Meduri et al., 2010). Previous work in our lab found no difference in lateral ventricle asymmetry in male and female HET mice compared to controls (Mu, 2011). While we similarly found no difference in lateral ventricle symmetry between HET and WT mice, female HET mice exhibit a trend where the left lateral ventricle was larger than the right lateral ventricle. A greater sample size is needed to reach statistical significance, as these trends were only apparent and not significant.

### ***Hippocampus to Whole Brain Volume Ratio Results***

Male WT ( $t(10) = 1.812, p = 0.02$ ) and female HET ( $t(12) = 1.782, p = 0.02$ ) mice showed significant increase in hippocampus to WBV ratio from PND 35 to PND 63 (Figure 3-7). There was a trend towards significance where female WT mice showed an increase in hippocampus to WBV ratio from PND 35 to PND 63 ( $t(12) = 1.782, p = 0.053$ ; Figure 3-7A). For male WT, female WT, and female HET mice, hippocampus to WBV ratio increased over time.

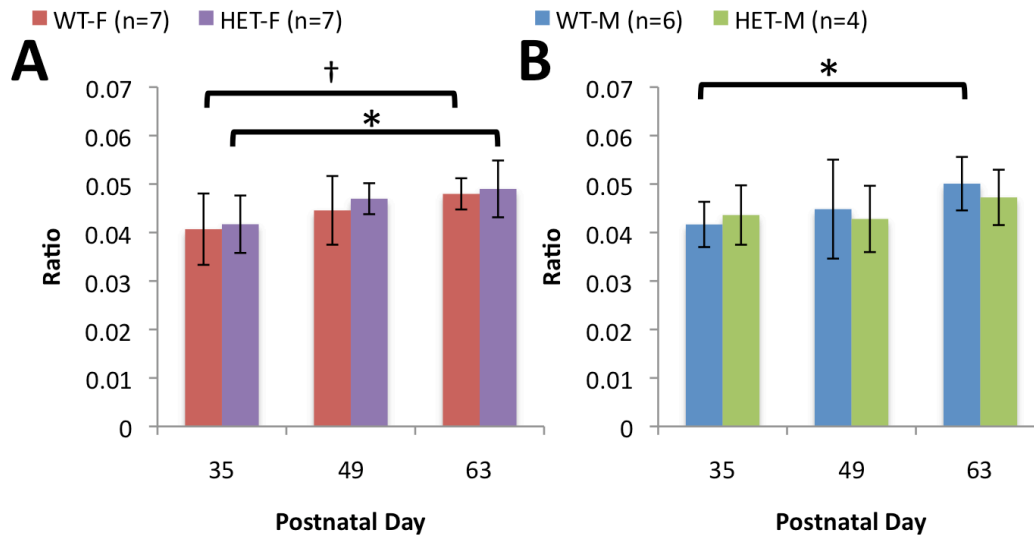


**Figure 3-7.** Mean hippocampus to whole brain volume ratio  $\pm$  SD of A. wild-type (WT) and GCPII $\pm$  heterozygous (HET) females and B. WT and HET males from postnatal day 35 to 63. Key above each group indicates sex and genotype. Data from the same mice were collected over time. Regions were manually traced and volume was calculated using the Region of Interest tool on Analyze 10.0. \* indicates significant developmental difference ( $p < 0.05$ ) within a genotype and between two time points as determined with paired two-tailed t-tests. † indicates a trend towards significant developmental difference between time points ( $0.05 < p < 0.07$ ).

### *Hippocampal Asymmetry*

Hippocampal asymmetry was measured by determining the ratio between left and right hippocampus volumes (Figure 3-8). Values that deviated from 1 indicated asymmetry, where one side of the hippocampus was larger than the other. Male HET mice had significantly greater asymmetry in hippocampi compared to male WT mice on PND 49 ( $t(8) = 1.860, p < .01$ ; Figure 3-8B). For all time points, male HET mice show greater hippocampi asymmetry than male WT mice (Figure 3-8B). Conversely, female WT mice showed greater hippocampi asymmetry than female HET mice at all time points (Figure 3-8A).

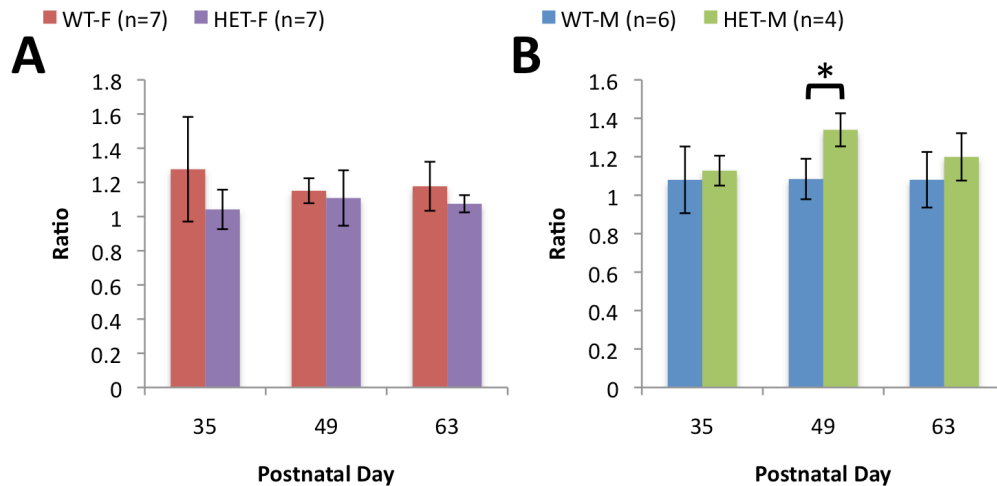


**Figure 3-8.** Mean left to right hippocampus volume ratio  $\pm$  SD of A. wild-type (WT) and GCPII $^{+/-}$  heterozygous (HET) females and B. WT and HET males from postnatal day 35 to 63. Key above each group indicates sex and genotype. Data from the same mice were collected over time. Regions were manually traced and volume was calculated using the Region of Interest tool on Analyze 10.0. \* indicates a significant difference ( $p < 0.05$ ) between genotypes at a single time point as determined with unpaired two-tailed t-tests assuming unequal variances.

### *Hippocampus Development and Asymmetry*

The hippocampus is known to exhibit abnormal function and structure in schizophrenia patients. Altered synaptic wiring from the hippocampus to extrinsic connections is hypothesized to alter glutamatergic pathways (Harrison, 2003). Further, hippocampal abnormalities have been linked to neuropsychological impairments (Harrison, 2003; Heckers, 2001). For example, small hippocampal size is correlated to poor premorbid adjustment, a rating scale that evaluates the degree of achievement of developmental goals at several points of a subject's life before the onset of schizophrenia (Smith et al., 2003).

Hippocampus to WBV ratios significantly increased from PND 35 to 63 for male WT, and female HET mice, and trended toward significance for female WT mice. This was expected and considered an effect of normal brain growth. Male HET mice, the one group that did not show a significant increase from PND 35 to 63, would likely reveal significant differences with a

larger sample size as the growth is apparent but not significant. Studies have found reduced hippocampal volume in schizophrenia patients compared to controls (Chance et al., 2001; Harrison, 2003; Heckers, 2001; Tsai et al., 2002). Previous work in our lab also found hippocampus to WBV ratio to be decreased at PND 77 in male and female HET mice compared to controls (Mu, 2011). Our results that HET males had non-significantly smaller hippocampus to WBV ratios than WT males on PND 49 and 63 agree with these findings. However, these results require a large sample size to reach statistical significance.

Hippocampal asymmetry is hypothesized to develop from asymmetric neural development (Harrison, 2003). Structural imaging studies have found hippocampal asymmetry where the left hippocampus is smaller than the right hippocampus in schizophrenia patients compared to controls (Harrison, 2003; Heckers, 2001). Previous works in our lab have found the left to right hippocampus ratio in male and female HET mice to be higher than controls (Mu, 2011). We found that male HET mice had significantly greater left to right hippocampus ratios compared to male WT mice on PND 49 and non-significantly greater ratios compared to WT mice on PND 35 and 63. Our findings agree with the previous studies in terms of identifying asymmetry. However, we found the opposite asymmetry than human studies. More studies on how the left and right hemispheres of a mouse brain correspond to the left and right side of a human brain would help elucidate our results.

The significant increase in asymmetry from PND 35 to 49 for male HET mice could be indicative of disease progression. Interestingly, results from the female group differ from those in males, where female WT mice exhibited a trend of greater asymmetry than female HET mice at all time points. These trends are apparent at PND 35 and 49 for female mice and on PND 49 and 63 for male mice, but are not significant. Our results on hippocampal asymmetry would be

more conclusive if consistent significance differences could be identified at multiple time points. Data from a larger sample size or later time points may reveal these differences.

### ***Individual Volume Trends***

Volume trends for one mouse of each genotype and sex from the same litter were examined to determine individual volume trends. Mouse 459 (WT-M), 458 (HET-M), 463 (WT-F), 462 (HET-F) from Litter 77 were used for this analysis (Figure 3-11). Third ventricle volume was different for HET and WT genotypes (Figure 3-11E). At all time points, male and female HET mice in this litter had larger third ventricle volumes than male and female WT mice (Figure 3-11E). An enlarged third ventricle is a known characteristic of schizophrenia patients compared to controls (Nakamura et al., 2004; Shenton et al., 2001; Tsai et al., 2002). These differences were not apparent at all time points when data from several mice were combined, which suggest there may be a litter effect. This is possible, as the volume of certain brain structures, such as the ventricles (Reveley et al., 1984) and whole brain (Bartley et al., 1997), are determined by genetic factors.

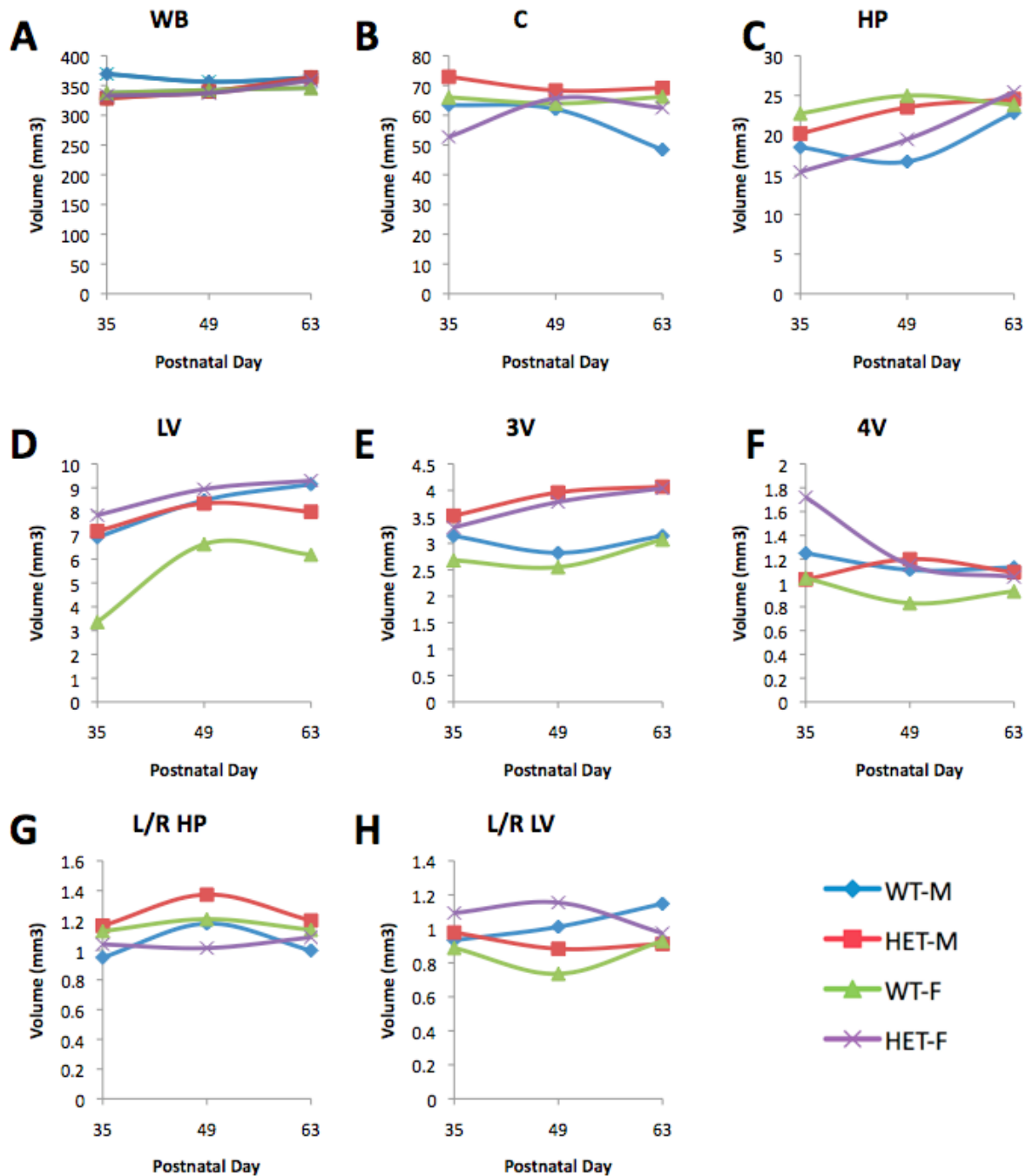


**Figure 3-11.** Volume of brain structures for a wild-type (WT)-male (M), GCPII<sup>+/-</sup> heterozygous (HET)-M, WT-F, and HET-F mouse (459, 458, 463, 462) from PND 35 to 63. All mice were from the same litter (77). Regions analyzed were A. Whole brain (WB) B. Cerebellum (C) C. Hippocampus (HP) D. Lateral ventricles (LV) E. third ventricle (3V) F. fourth ventricle (4V) G. Left to right hippocampus ratio (L/R HP) H. Left to right lateral ventricle ratio (L/R LV). Key on the bottom right indicates genotype and sex of each mouse. Regions were manually traced and volume was calculated using the Region of Interest tool on Analyze 10.0.

### ***Summary of MRI Findings***

- \* Sex differences were found in cerebellum/WB for HET and WT mice and hippocampi asymmetry for HET mice
- HET and WT mice exhibited similar development in WBV and hippocampus to WBV ratio
- WBV was significantly greater for female HET mice compared to female WT mice at PND 63.
- Cerebellum to WBV ratio was significantly higher in male HET mice than male WT at all time points, but was only significant on PND 63. Cerebellum to WBV was significantly higher in female WT mice compared to female HET mice, but was only significant on PND 63.
- \* Fourth ventricle to WBV ratio was significantly higher in male HET mice than male WT mice on PND 49
- \* Third ventricle to WBV ratio was significantly higher in female HET mice than female WT mice on PND 35
- \* Lateral ventricle to WBV ratio was greater in female HET mice than female WT mice at all time points, but was only significant on PND 35
- \* Hippocampi asymmetry was greater in male HET mice than male WT mice at all time points, but only significant on PND 49

An \* indicates findings that were consistent with literature results for schizophrenia patients compared to controls.



## 3.2 Magnetic Resonance Spectroscopy

MRS data were collected from a  $4 \times 3 \times 2 \text{ mm}^3$  (24  $\mu\text{L}$ ) voxel positioned on the hippocampus in same HET males ( $n = 2$ ), WT males ( $n = 6$ ), HET females ( $n = 7$ ), and WT females ( $n = 7$ ) on PND 35/36, 49/50, and 63/64. Two of the HET males used for MRI data could not be used for MRS data due to instrument difficulties that occurred at one time point. Metabolite peak areas were divided by the area of Cr (3.0 ppm), an internal standard, and averaged for each time point. The metabolite ratios of (NAA+NAAG)/Cr, Tau/Cr, Cho/Cr, and Glx/Cr were analyzed (Table 3-2).

### ***Sexual Dimorphism***

Metabolite differences between male and female mice were examined in HET and WT brain structures (Figure 3-12 and 3-13). Cho/Cr ratios were lower in HET males than females on PND 49 ( $t(7) = 1.895$ ,  $p = 0.02$ ; Figure 3-12C). This contrasts with a study by Buckley et al. (1994) that found male schizophrenic patients have less NAA and more Cho in the frontal cortex compared to male controls and female schizophrenia patients, but this study looked at a different brain structure. No differences were found between male and female WT mice (Figure 3-13). These findings agree with a study by Charles et al. (1994) that found no differences in Cho or NAA levels between males or females in grey or white matter. No studies report differences in Tau and Glx metabolite levels between male and female humans or mice.

Our MRS findings, in conjunction with volume data, are supportive of sex differences between male and female mice. In order to control for sex differences, all MRS analyses were grouped by sex.

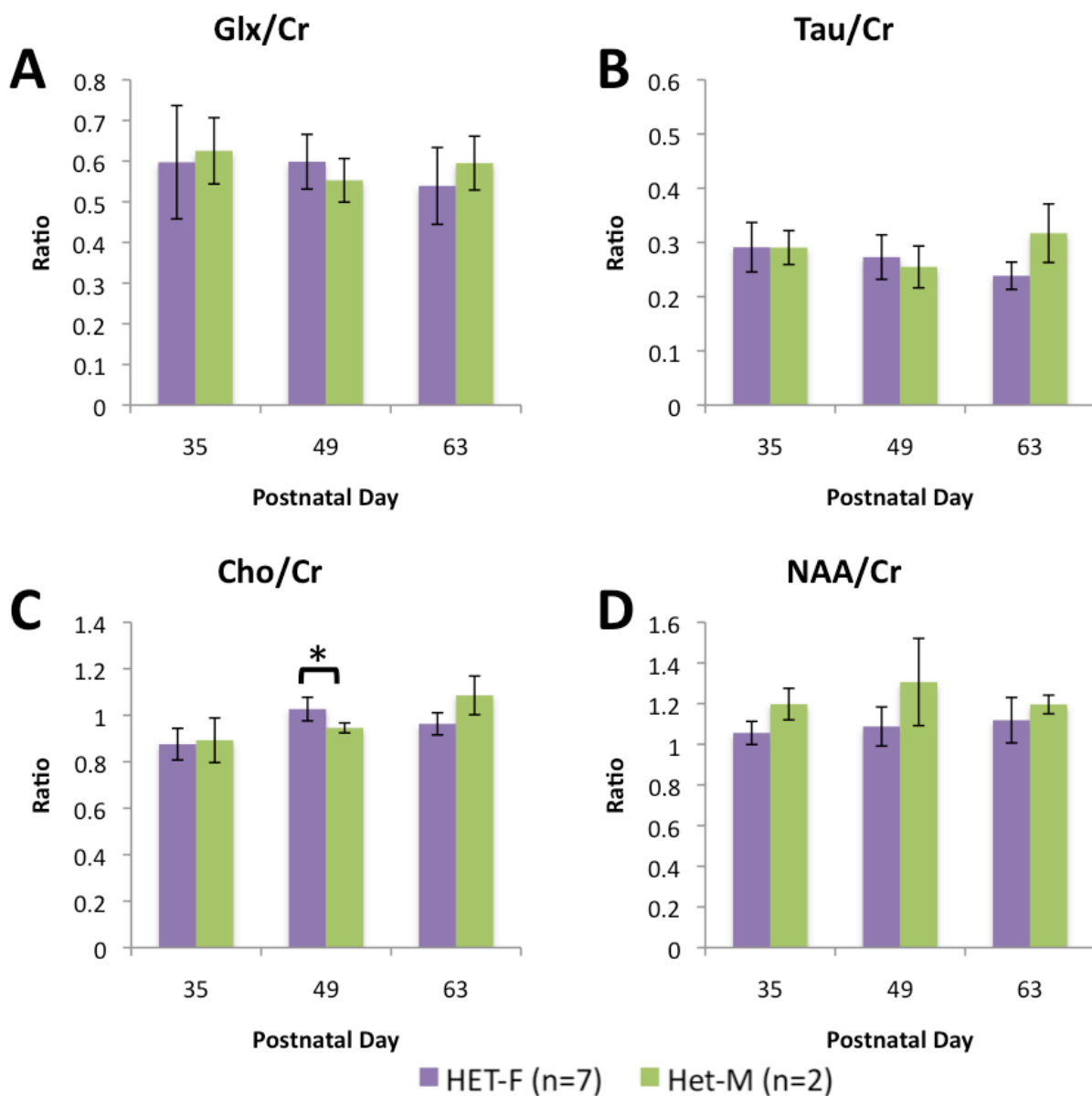


**Figure 3-12.** Mean metabolite concentration ratio  $\pm$  SD between GCPII<sup>+/-</sup> heterozygous (HET) males (M) and females (F) from postnatal day 35 to 63. A. Glutamate and Glutamine/Creatine concentration ratio (Glx/Cr), B. Taurine/Cr concentration ratio (Tau/Cr), C. Choline/Cr concentration ratio (Cho/Cr), D. N-acetylaspartate and N-acetylaspartylglutamate/Cr (NAA+NAAG/Cr). Key on the bottom indicates sex and genotype. Data from the same mice were collected over time. Bruker Topspin 1.5 was used to fit a Gaussian peak underneath each metabolite peak and quantify metabolite concentration. \* indicates a significant difference ( $p < 0.05$ ) as determined with unpaired two-tailed student t-tests assuming unequal variances.

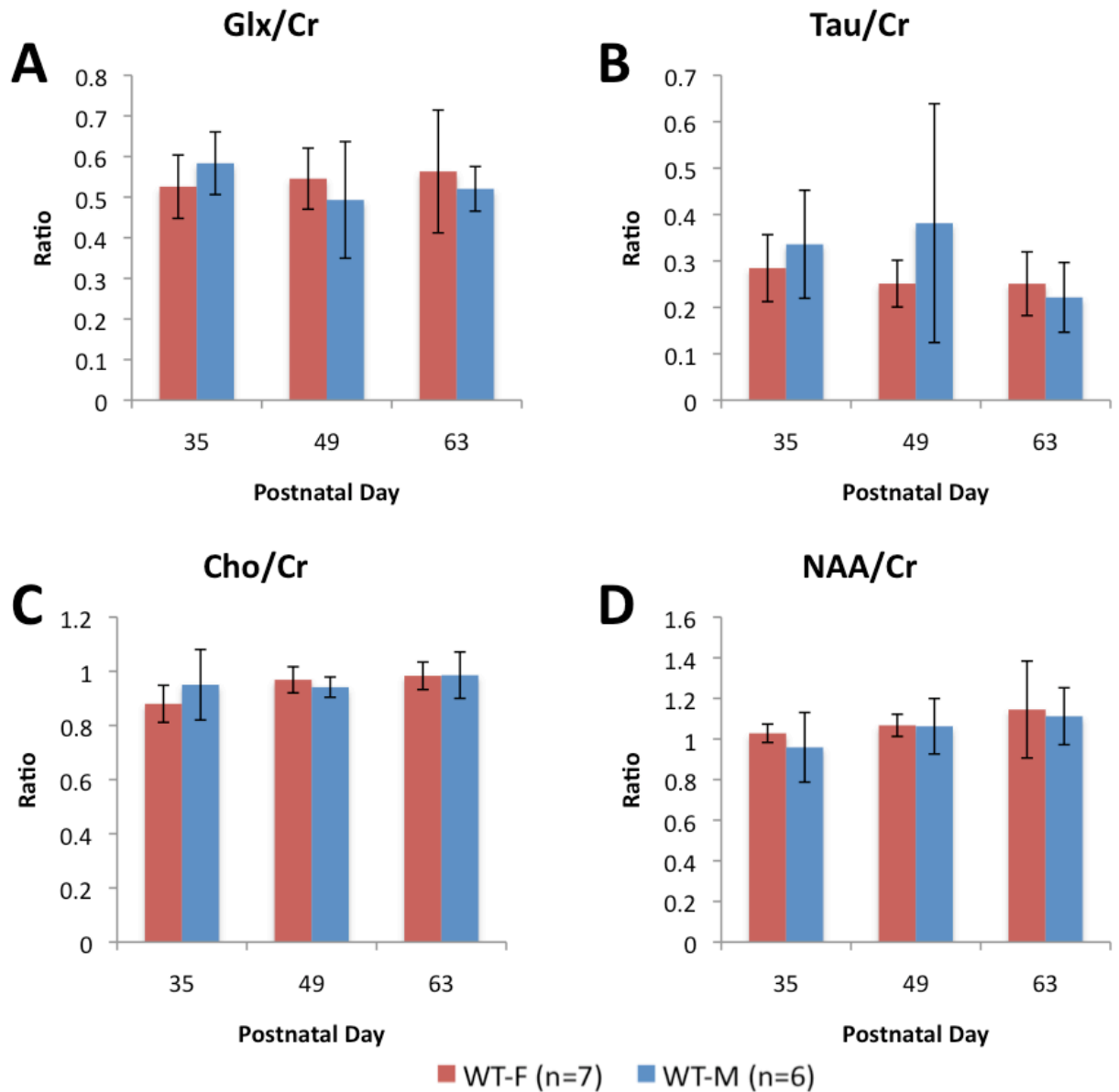


**Figure 3-13.** Mean metabolite concentration ratio  $\pm$  SD between GCPII<sup>-/-</sup> wild-type (WT) males (M) and females (F) from postnatal day 35 to 63. A. Glutamate and Glutamine/Creatine concentration ratio (Glx/Cr), B. Taurine/Cr concentration ratio (Tau/Cr), C. Choline/Cr concentration ratio (Cho/Cr), D. N-acetylaspartate and N-acetylaspartylglutamate/Cr (NAA+NAAG/Cr). Key on the bottom indicates sex and genotype. Data from the same mice were collected over time. Bruker Topspin 1.5 was used to fit a Gaussian peak underneath each metabolite peak and quantify metabolite concentration. \* indicates a significant difference ( $p < 0.05$ ) as determined with unpaired two-tailed student t-tests assuming unequal variances. No \* indicates no significant differences.

Our MRS findings, in conjunction with volume data, are supportive of sex differences between male and female mice. In order to control for sex differences, all MRS analyses were grouped by sex (Table 3-2).

**Table 3-2.** MRS metabolite data for male WT, male HET, female WT, and female HET mice. A. \* indicates a significant difference between WT and HET mice at that time point ( $p < 0.05$ ). † indicates a trend towards significance between WT and HET mice ( $0.05 < p < 0.07$ ). B. \* indicates a significant developmental difference between indicated time points within a genotype and sex ( $p < 0.05$ ). † indicates a trend towards significant developmental difference between time points ( $0.05 < p < 0.07$ ).

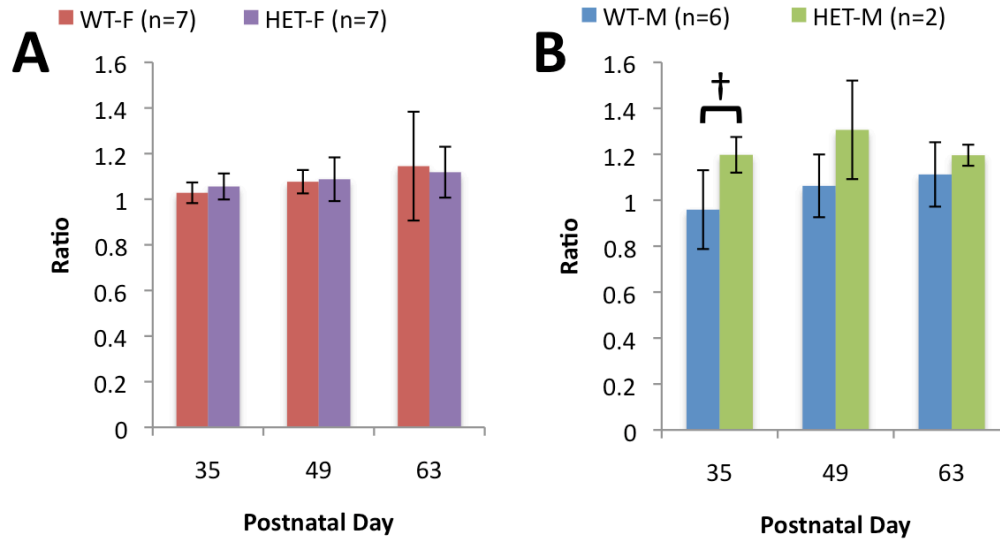
A. Comparisons between WT and HET at each of the sampled time points (independent t-tests)												
	PND 35/36		PND 49/50		PND 63/64							
	M	F	M	F	M	F						
Glx/Cr												
Tau/Cr												
(NAA+NAAG)/Cr												† 0.0484
Cho/Cr												

B. Comparisons among particular time points within each genotype (paired t-test)												
	PND 35/36 vs 49/50				PND 49/50 vs 63/64				PND 35/36 vs 63/64			
	WT-M	HET-M	WT-F	HET-F	WT-M	HET-M	WT-F	HET-F	WT-M	HET-M	WT-F	HET-F
Glx/Cr												
Tau/Cr												* 0.0337
(NAA+NAAG)/Cr												
Cho/Cr												

### *N-acetylaspartate and N-acetylaspartylglutamate to Creatine Results*

(NAA+NAAG)/Cr ratios in the hippocampus of male HET mice were higher than for male WT mice on PND 35 and trended towards significance ( $t(6) = 1.943, p = 0.048$ ; Figure 3-14B). At all time points, male HET mice had higher ratios of (NAA+NAAG)/Cr compared to male WT mice but they were not significant at later time points. Female WT, female HET, and male WT mice exhibited non-significant increases in (NAA+NAAG)/Cr ratios over time (Figure 3-14). For female mice, no significant differences were found at any time point or between time points for either genotype (Figure 3-14A).



**Figure 3-14.** Mean N-acetylaspartate and N-acetylaspartylglutamate/creatinine (NAA+NAAG/Cr) concentration ratio  $\pm$  SD between A. wild-type (WT) and GCPII<sup>+/-</sup> heterozygous (HET) females and B. WT and HET males from postnatal day 35 to 63. Keys above graphs indicate sex and genotype. Data from the same mice were collected over time. Bruker Topspin 1.5 was used to fit a Gaussian peak underneath each metabolite peak and quantify metabolite concentration. \* indicates a significant difference ( $p < 0.05$ ) as determined with unpaired two-tailed student t-tests assuming unequal variances.

### ***NAA and NAAG levels in HET mice compared to Schizophrenia Patients***

Studies on NAA in schizophrenia patients have found reduced levels in the hippocampus (Bertolino et al., 1997; Deicken et al., 1998; Nasrallah et al., 1994; Pegues et al., 2000; Steen et al., 2005) and reduced ratios of NAA/Cr in the left hippocampus (Deicken et al., 1998; Miyaoka et al., 2004). The opposite has also been found, where NAA levels were found to be higher in the hippocampus of schizophrenia patients compared to controls (Lutkenhoff et al., 2010). Previous work in our lab also found no differences in (NAA+NAAG)/Cr ratios in the hippocampus of male and female HET mice compared to controls (Mu, 2011). These results disagree with our findings, but this is not surprising as males and female data were analyzed separately in this study. Few studies have examined the combined ratio NAA and NAAG to Cr in the hippocampus. Our study that analyzed *ex vivo* metabolite levels in the cortex of the same mouse model (GCPII<sup>+/-</sup> HET) found no effect of genotype on (NAA+NAAG)/Cr compared to controls

(Schaevitz et al., 2011). Another study by Tsai et al. (1995) reported increased levels of NAAG in the hippocampus, but no significant changes of NAA in schizophrenia patients compared to controls. Additionally, Kegeles et al. (2000) and Sigmundsson et al. (2003) found no abnormal NAA levels in the hippocampus of schizophrenia patients compared to controls.

We found that male HET mice had higher ratios of (NAA+NAAG)/Cr that trended towards significance on PND 35 and non-significantly higher ratios of (NAA+NAAG)/Cr on PND 49 and 63 compared to male WT mice. These findings strongly support studies that report increased levels of NAA (Lutkenhoff et al., 2010) or increased levels of NAAG (Tsai et al., 1995) with slightly decreased (Bertolino et al., 1997; Deicken et al., 1998; Nasrallah et al., 1994; Miyaoka et al., 2004) or no changes (Kegeles et al., 2000; Sigmundsson et al. (2003); Tsai et al., 1995) in levels of NAA in the hippocampus of schizophrenia patients compared to controls. Increased levels of NAAG and proportionally smaller decreased levels of NAA in male HET mice compared to controls are most consistent with reduced GCPII enzyme function as GCPII is responsible for cleaving NAAG into NAA and Glu. We could not confirm or reject other combinations of increased, decreased, or lack of change in levels of NAA and NAAG as these metabolites could not be separately resolved in our spectra.

NMDAR hypofunction, the basis of the glutamate hypothesis, arises from a combination of reduced glutamate release and increased NMDAR antagonism by NAAG. Elevated levels of NAAG would suggest increased NMDAR inhibition and decreased levels of NAA may reflect decreased neuronal density or hypometabolism in schizophrenia patients compared to controls (Bracken et al., 2011). Thus our findings are consistent with the glutamate hypothesis if increased ratios of (NAAG+NAA)/Cr in the hippocampus correspond to increased levels of NAAG and decreased levels of NAA. These results were unexpected as we hypothesized that

HET mice would exhibit increased levels of NAAG, with an even greater reduction in levels of NAA such that (NAA+NAAG)/Cr would be reduced.

Our findings are interesting as they contribute to findings of NAA abnormalities in schizophrenia patients compared to controls. Differences in (NAA+NAAG)/Cr levels between male HET and WT mice on PND 35, 49, and 63 were apparent, yet not significant. A larger sample size would be needed to attain statistical significance. Further, the ability to resolve NAA and NAAG separately would also make our results more conclusive.

### ***Taurine to Creatine Results***

Tau/Cr ratios significantly decreased from PND 35 to 63 for female HET mice ( $t(12) = 1.782, p = 0.0248$ ; Figure 3-15A). For male mice, no significant differences were found at any time point or between time points for either genotype (Figure 3-15B).

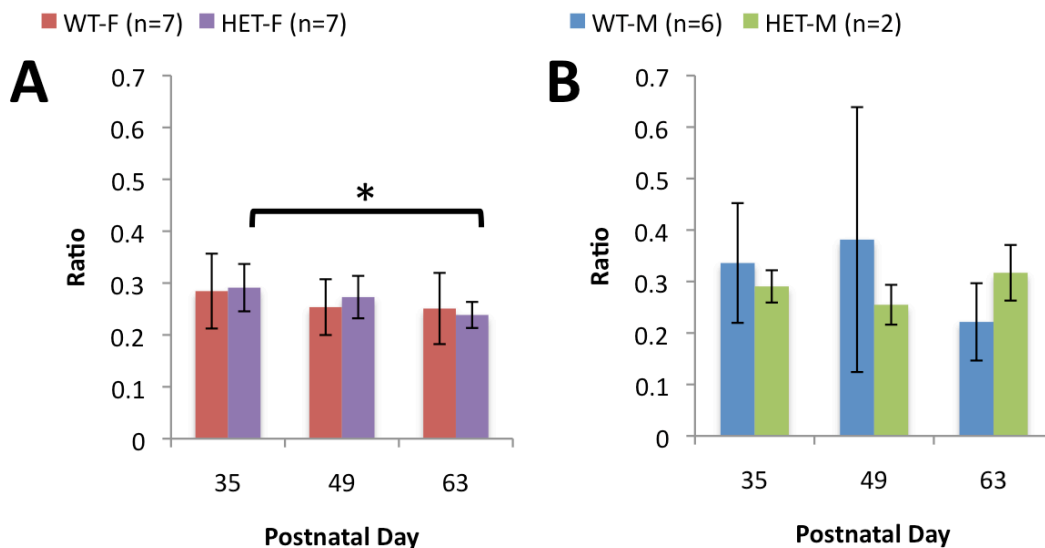


**Figure 3-15.** Mean taurine/creatine (Tau/Cr) concentration ratio  $\pm$  SD between A. wild-type (WT) and GCPII<sup>+/-</sup> heterozygous (HET) females and B. WT and HET males from postnatal day 35 to 63. Keys above graph indicate sex and genotype. Data from the same mice were collected over time. Bruker Topspin 1.5 was used to fit a Gaussian peak underneath each metabolite peak and quantify metabolite concentration. \* indicates a significant difference ( $p < 0.05$ ) as determined with unpaired two-tailed student t-tests assuming unequal variances.

### ***Developmental Changes in Tau***

Few studies have reported abnormalities in Tau levels in the hippocampus of schizophrenia patients. One study that examined metabolite levels in the medial prefrontal cortex found increased levels of Tau in schizophrenia patients compared to controls (Shirayama et al., 2010). Interestingly, we found that Tau levels in male HET mice significantly decreased from PND 35 to 63. A similar result was previously found in our lab, where male and female WT mice exhibited a significant decrease in Tau levels from PND 35 to PND 63 (Mu, 2011). A larger sample size would likely reveal similar findings for the WT mice in this study. These results suggest that HET mice reflect behavior of WT mice and that Tau/Cr ratios may not be a useful indicator of schizophrenia. Alternatively, Tau abnormalities in schizophrenia patients may exist, but our results are limited by our ability to resolve the Tau peak.

### ***Choline to Creatine Results***

Female HET and WT mice exhibited significant changes in Cho/Cr ratios over time (Figure 3-16A). Female HET mice showed a significant increase in Cho/Cr ratios from PND 35 to 63 ( $t(12) = 1.782, p = 0.0183$ ) and PND 35 to 49 ( $t(12) = 1.782, p = 0.0006$ ), and a significant decrease from PND 49 to 63 ( $t(12) = 1.782, p = 0.0323$ ; Figure 3-16A). Female WT mice showed an increase in Cho/Cr ratios from PND 35 to 63 ( $t(12) = 1.782, p = 0.0076$ ) and 35 to 49 ( $t(12) = 1.782, p = 0.0086$ ; Figure 3-16A). Male HET mice exhibited a trend of increased Cho/Cr ratios over time (Figure 3-16B).



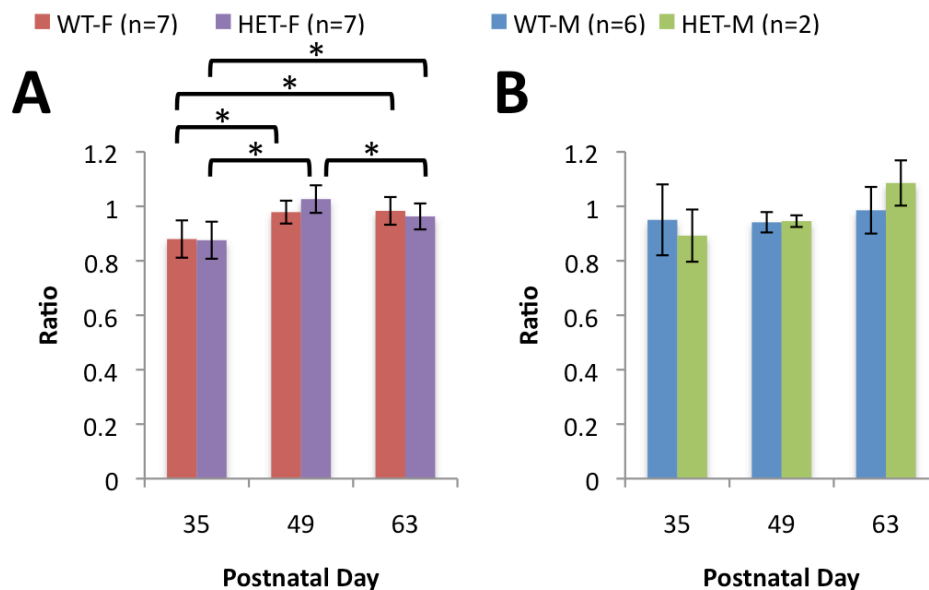


**Figure 3-16.** Mean choline/creatine (Cho/Cr) concentration ratio  $\pm$  SD between A. wild-type (WT) and GCPII<sup>+/-</sup> heterozygous (HET) females and B. WT and HET males from postnatal day 35 to 63. Data from the same mice were collected over time. Bruker Topspin 1.5 was used to fit a Gaussian peak underneath each metabolite peak and quantify metabolite concentration. \* indicates a significant difference ( $p < 0.05$ ) as determined with unpaired two-tailed student t-tests assuming unequal variances. † indicates a trend towards a significant difference between genotypes at a single time point ( $0.05 < p < 0.07$ ).

### *Developmental Changes in Cho*

Studies disagree on how Cho levels are affected in the hippocampus of schizophrenia patients. Reduced (Maier et al., 1995), increased (Lutkenhoff et al., 2010), and unchanged (Deicken et al., 1998; Delamillieure et al., 2002) levels of Cho have been found in the hippocampus of schizophrenia patients compared to controls. Our finding that there are no differences between HET and WT mice agrees with studies that propose no Cho abnormalities in the hippocampus of schizophrenia patients compared to controls. This is further confirmed by our finding that female WT and HET mice exhibit similar development trends from PND 35 to 49 and PND 35 to 63. Few studies have conducted longitudinal assessment of metabolite levels in schizophrenia over time. Previous work in our lab found an increase in Cho/Cr levels from PND 35 to 49 in male and female WT mice (Mu, 2011). However, the implications of this

change are unclear (Mu, 2011). The changes in Cho levels observed in females could reflect specific changes in the development of neural membrane composition. The lack of difference between HET and WT mice shows that phospholipid membrane turnover is not changed in schizophrenia. This confirms that schizophrenia is a neurodevelopmental, not neurodegenerative, disorder. Based on our findings, Cho/Cr ratios are not a good indicator of schizophrenia.

### ***Glutamate and Glutamine to Creatine Results***

There were no significant differences found for Glx/Cr ratios at any time point or between time points for either sex or genotype (Figure 3-17).

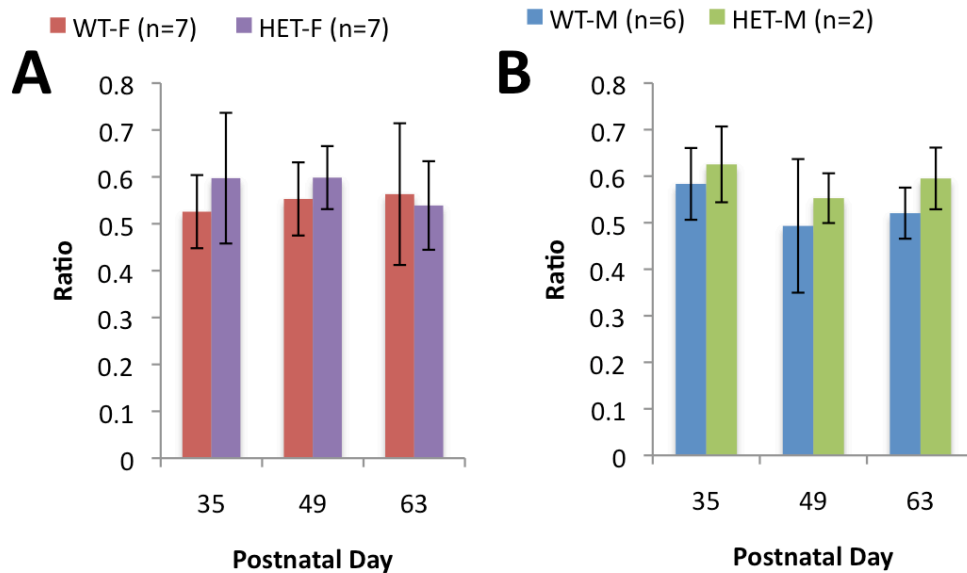


**Figure 3-17.** Mean glutamate and glutamine/creatine (Glx/Cr) concentration ratio  $\pm$  SD between A. wild-type (WT) and GCPII $\pm$  heterozygous (HET) females and B. WT and HET males from postnatal day 35 to 63. Keys above graphs indicate sex and genotype. Data from the same mice were collected over time. Bruker Topspin 1.5 was used to fit a Gaussian peak underneath each metabolite peak and quantify metabolite concentration. \* indicates a significant difference ( $p < 0.05$ ) as determined with unpaired two-tailed student t-tests assuming unequal variances. No asterisks indicate the lack of significant findings.

### ***Glx and Relevance to the Glutamate Hypothesis***

Glx or Glx/Cr ratios were found to be increased (Chang et al. 2007), decreased (Ohrmann et al., 2007), and the same (Bustillo et al., 2001, Wood et al., 2008) in various brain structures (white matter, prefrontal cortex, broad brain region, and hippocampus) of schizophrenia patients compared to controls. Previous work that combined male and female data found complex trends in Glx/Cr ratios where HET mice had higher Glx/Cr ratios than WT mice on PND 63 and Glx/Cr levels significantly increased from PND 49 to 63 for HET mice (Mu, 2011). Our finding, that there were no differences in Glx/Cr ratios between HET and WT mice, contrasts with previous work, yet supports studies that found no differences in Glx/Cr ratios between schizophrenia patients and controls. Our study that analyzed *ex vivo* metabolite levels in the cortex of the same mouse model (GCP11<sup>+/-</sup> HET) similarly found no effect of genotype on Glx/Cr ratios (Schaevitz et al., 2011).

The glutamate hypothesis is based on NMDAR hypofunction, which is caused by reduced Glu and increased NMDAR antagonism by NAAG. We expected Glx/Cr ratios to be reduced in HET mice compared to controls to reflect decreased levels of Glu, as Tsai et al. (1995) found Glu levels were reduced in the hippocampus of schizophrenia patients compared to controls. However, we found Glx/Cr ratios to remain unchanged between genotypes. These results were not surprising as Glu and Gln are separately affected in schizophrenia. Glx is a combined measurement of the metabolites of Glu and Gln and reflects the total glutamatergic pool available for synaptic–metabolic activity while separate levels of Glu and Gln reflect their respective distribution in neuronal and glial cells (Yuksel and Ongur, 2005). Though Glx/Cr ratios remained the same, it was possible that the proportions of Glu to Gln were different between genotypes.

Schaevitz et al. (2011) found the Glu to Gln ratio was significantly increased by 15% in the cortex of HET mice compared to controls, but determined no difference in Glu/Cr or Gln/Cr levels. The increased Glu to Gln ratio was hypothesized to occur from a decrease in glutamine levels rather than a change in glutamate levels (Schaevitz et al., 2011). An increased Glu/Gln ratio reflects reduced glutamatergic neurotransmission, as Gln is a precursor to Glu (Yuksel and Ongur, 2005). Glutamate-glutamine cycles that reflect this imbalance have been found in rodents given NMDAR antagonists (Schaevitz et al., 2011). This is promising as GCPII regulates NMDAR function and NMDAR antagonists in normal individuals mimic the biochemical pathways of schizophrenia.

Few studies have specifically examined Glu and Gln in the hippocampus, which makes it difficult to compare our results. Further, there is a wide range of possibilities for the Glu to Gln ratio in HET mice compared to controls. Given what previous studies have found, our results support an increased Glu/Gln ratio, which aligns with reduced GCPII function. The ability to separately resolve Glu and Gln would likely make our results more conclusive as changes in these metabolite levels are an indirect way of determining NMDAR function.

### ***Individual Metabolite Level Trends***

Metabolite/Cr trends for four mice, one mouse of each genotype and sex, from the same litter were examined (Figure 3-18). Mouse 459 (WT-M), 458 (HET-M), 463 (WT-F), 462 (HET-F) from Litter 77 were used for this analysis. These were the same mice used to investigate individual volume trends.

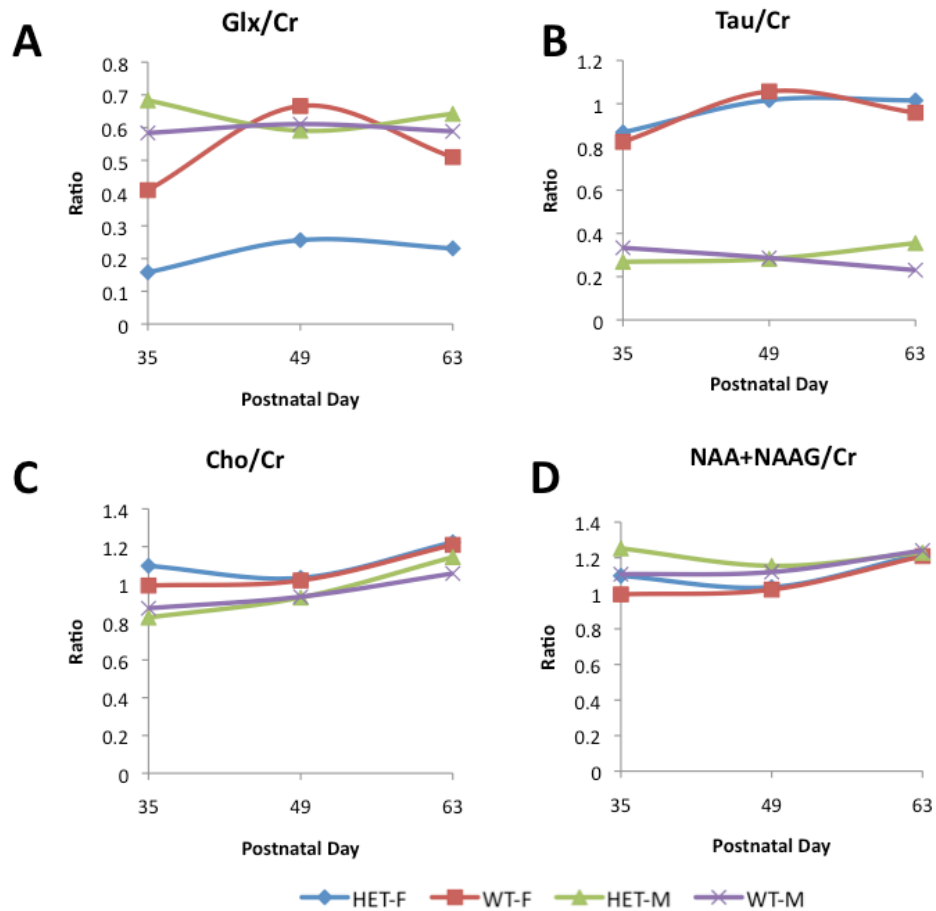


**Figure 3-18.** Metabolite/creatinine (Cr; 3.0 ppm) levels in the hippocampus of a wild-type (WT)-male (M), GCPII<sup>+/-</sup> heterozygous (HET)-M, WT-F, and HET-F mouse (459, 458, 463,462) from PND 35 to 63. All mice were from the same litter (77). Metabolites analyzed were A. Glutamine and Glutamate (Glx)/Cr B. Taurine (Tau)/Cr C. Choline (Cho)/Cr D. Key on the bottom indicates genotype and sex of each mouse. Bruker Topspin 1.5 was used to fit a Gaussian peak underneath each metabolite peak and quantify metabolite concentration.

Female HET and WT mice had higher Tau/Cr levels than male HET and WT mice at all time points (Figure 3-18B), suggesting a sex difference. No studies could be found that reported sex differences in Tau or Tau/Cr levels in humans or mice. Tau acts as a neuroprotectant and levels of Tau are hypothesized to elevate in response to increased oxidative stress. The release of different sex hormones may result in synaptic wiring that alters stress responses, thereby affecting Tau levels.

Female HET and WT mice had higher Cho/Cr levels than HET and WT males at all time points (Figure 3-18C). These findings agree with a study by Buckley et al. (1994) that found male schizophrenic patients had less NAA and more Cho in frontal cortex compared to female patients.

Male HET and WT (NAA+NAAG)/Cr levels were slightly greater than those of female HET and WT mice on PND 49 (Figure 3-18D). This contrasts with a study by Charles et al. (1994) that found no differences in NAA levels between males and females, and a study by Buckley et al. (1994) that found male schizophrenic patients had less NAA in frontal cortex compared to female patients. However, it is difficult to align our results with these findings as we examined a different brain region and could not resolve NAA and NAAG separately.

Glx/Cr trends were the least clear. The female HET mouse appeared to have a much lower Glx/Cr than all other mice at all time points (Figure 3-18A). This was interesting, as no studies have reported differences in Glx metabolite levels between male and female humans or mice.

All observed differences were not apparent when data from several mice were combined, suggesting a litter effect. With a larger sample size, it would be possible to see if characteristics of schizophrenia are affected by litter differences.

### *Summary of MRS Findings*

- Sex differences were found in Cho/Cr ratios for HET mice
- There were no significant differences between HET and WT mice in NAA/Cr, Cho/Cr, Tau/Cr or Glx/Cr ratios at any time point
- HET and WT mice exhibited similar development in Cho/Cr ratios
- Tau/Cr levels significantly decreased from PND 35 to 63 for female HET mice.
- (NAA+NAAG)/Cr ratios were greater for male HET mice than male WT mice at all time points and trended towards significance on PND 35.

While MRS findings did not reveal significant differences between genotypes, we found interesting developing trends that may be attributed to reduced GCPII function.

## 4 General Conclusions and Future Work

In this study, we found distinct morphological, neurochemical and sex differences in HET mice compared to WT mice. Volume data showed HET mice to exhibit asymmetric hippocampi and enlarged ventricle (fourth, third, and lateral) to WBV ratios. Metabolite data showed apparent differences in (NAA+NAAG)/Cr levels, but no significant effect of genotype on (NAA+NAAG)/Cr, Cho/Cr, Tau/Cr, or Glx/Cr ratios. Sex differences were found in cerebellum to WBV ratios of HET and WT mice, and hippocampus asymmetry and Cho/Cr levels in HET mice. Future work should increase the sample size such that differences between genotypes are significant at multiple time points. Later time points may also reveal distinct differences between genotypes. This is especially true for volume data, as certain brain structures may exhibit progressive growth or delayed, abnormal growth in schizophrenia patients. It is also possible that the mutation in this mouse model does not reflect all morphological and neurochemical characteristics of schizophrenia in humans.

There are other factors that may have contributed to fewer than expected significant differences. Difficulties in tracing may have caused large standard deviations in the volume data, as certain structures, such as the hippocampus and lateral ventricles, were difficult to trace if the outline of the structure was not apparent. For metabolite data, the Glx and (NAA+NAAG) peak each represented two metabolites, Glu and Gln and NAA and NAAG, respectively. The ability to separately resolve Glu, Gln, NAA, and NAAG would allow us to determine the exact concentration of each metabolite and make our results more conclusive. In the future, *ex vivo* studies could compare metabolite levels in the hippocampus of HET mice compared to controls. It would also be interesting to see how *ex vivo* data from the hippocampus compare to *in vivo* results from the cortex and *ex vivo* data from the cortex (Schaevtiz et al., 2011).

Results from individual volume and metabolite ratio trends indicated the possibility of litter effects. Future work should investigate these effects by quantifying individual brain volume or metabolite ratios of mice in the same litter with the same sex and genotype for each time point. Additionally, it would also be interesting to see if the litter effects are related to weight, as mice in the same litter tend to be in the same weight range.

Our findings from this study are exciting, as they show that the GCPII<sup>+/-</sup> mouse model mimics several of the characteristics of schizophrenia and that reduced GCPII function replicates certain aspects of the biochemical pathways in schizophrenia. This study has widened our understanding of the morphological and neurochemical abnormalities that may arise from reduced GCPII function in schizophrenia. With a greater sample size, this mouse model has the potential to test treatments that focus on the glutamatergic pathways of schizophrenia, offering help to those affected by this debilitating psychiatric disorder.



## References

- Andreasen, N. (2000) Schizophrenia: the fundamental questions, *Brain Research Reviews*31, 106–112.
- Andreasen, N. C., and Pierson, R. (2008) The role of the cerebellum in schizophrenia, *Biological Psychiatry*64, 81–88.
- Andres, R. H., Ducraya, A. D., Schlattner, U., Wallimann, T., and Widmer, H. R. (2008) Functions and effects of creatine in the central nervous system, *Brain Research Bulletin*76, 329–343.
- Bartley, A. (1997) Genetic variability of human brain size and cortical gyral patterns, *Brain*120, 257–269.
- Bertolino, A., Callicott, J. H., Elman, I., Mattay, V. S., Tedeschi, G., Frank, J. A., Breier, A., and Weinberger, D. R. (1998) Regionally Specific Neuronal Pathology in Untreated Patients with Schizophrenia: A Proton Magnetic Resonance Spectroscopic Imaging Study, *Biological Psychiatry*43, 641–648.
- Bogaert, E., d' Ydewalle, C., and Van Den Bosch, L. (2010) Amyotrophic Lateral Sclerosis and Excitotoxicity: From Pathological Mechanism to Therapeutic Target, *Cns & Neurological Disorders-Drug Targets*9, 297–304.
- Bracken, B. K., Jensen, J. E., Prescott, A. P., Cohen, B. M., Renshaw, P. F., and Ongur, D. (2011) Brain metabolite concentrations across cortical regions in healthy adults, *Brain Research*1369, 89–94.
- Bustillo, J. R., Chen, H. J., Gasparovic, C., Mullins, P., Caprihan, A., Qualls, C., Apfeldorf, W., Lauriello, J., and Posse, S. (2011) Glutamate as a Marker of Cognitive Function in Schizophrenia: A Proton Spectroscopic Imaging Study at 4 Tesla, *Biological Psychiatry*69, 19–27.
- Chance, S. A., Esiri, M. M., and Crow, T. J. (2003) Ventricular enlargement in schizophrenia: a primary change in the temporal lobe?, *Schizophrenia Research*62, 123–131.
- Chang, L., Friedman, J., Ernst, T., Zhong, K., Tsopelas, N. D., and Davis, K. (2007) Brain metabolite abnormalities in the white matter of elderly schizophrenic subjects: implication for glial dysfunction, *Biol. Psychiatry*62, 1396–1404.
- Charles, H. C., Lazeyras, F., Krishnan, K. R. R., Boyko, O. B., Patterson, L. J., Doraiswamy, P. M., and McDonald, W. M. (1994) Proton spectroscopy of human brain: Effects of age and sex, *Progress in Neuro-Psychopharmacology and Biological Psychiatry*18, 995–1004.
- Chu, H.C. (2009) Folate Deficiency in GCPII<sup>+/-</sup> Mice, A Mouse Model of Schizophrenia. Honors Thesis. Wellesley College, Wellesley, MA.
- Cooke, B. M. (1999) A brain sexual dimorphism controlled by adult circulating androgens, *Proceedings of the National Academy of Sciences*96, 7538–7540.
- Coyle, J. T. (1997) The nagging question of the function of N-acetylaspartylglutamate, *Neurobiology of Disease*4, 231–238.
- Coyle, J. T. (2006) A brief overview of N-acetylaspartate and N-acetylaspartylglutamate, *N-Acetylaspartate: A Unique Neuronal Molecule in the Central Nervous System*576, 1–6.
- Coyle, J. T. (2006) Glutamate and schizophrenia: beyond the dopamine hypothesis, *Cell. Mol. Neurobiol.*26, 365–384.

- Deicken, R. F., Zhou, L., Schuff, N., Fein, G., and Weiner, M. W. (1998) Hippocampal neuronal dysfunction in schizophrenia as measured by proton magnetic resonance spectroscopy, *Biol. Psychiatry*43, 483–488.
- Delamillieure, P., Constans, J. M., Fernandez, J., Brazo, P., Benali, K., Courtheoux, P., Thibant, F., Petit, M., and Dollfus, S. (2002) Proton magnetic resonance spectroscopy (H-1 MRS) in schizophrenia: Investigation of the right and left hippocampus, thalamus, and prefrontal cortex, *Schizophrenia Bulletin*28, 329–339.
- Fricker, A. C., Mok, M. H. S., de la Flor, R., Shah, A. J., Woolley, M., Dawson, L. A., and Kew, J. N. C. (2009) Effects of N-acetylaspartylglutamate (NAAG) at group II mGluRs and NMDAR, *Neuropharmacology*56, 1060–1067.
- Goldstein, J. M. (2001) Normal Sexual Dimorphism of the Adult Human Brain Assessed by In Vivo Magnetic Resonance Imaging, *Cerebral Cortex*11, 490–497.
- Govindaraju, V., Young, K., and Maudsley, A. A. (2000) Proton NMR chemical shifts and coupling constants for brain metabolites, *NMR Biomed.*13, 129–153.
- Guilarte, T. R., Hammoud, D. A., McGlothlan, J. L., Caffo, B. S., Foss, C. A., Kozikowski, A. P., and Pomper, M. G. (2008) Dysregulation of glutamate carboxypeptidase II in psychiatric disease, *Schizophrenia Research*99, 324–332.
- Han, L. Q., Picker, J. D., Schaevitz, L. R., Tsai, G. C., Feng, J. M., Jiang, Z. C., Chu, H. C., Basu, A. C., Berger-Sweeney, J., and Coyle, J. T. (2009) Phenotypic Characterization of Mice Heterozygous for a Null Mutation of Glutamate Carboxypeptidase II, *Synapse*63, 625–635.
- Harrison, P. J. (2004) The hippocampus in schizophrenia: a review of the neuropathological evidence and its pathophysiological implications, *Psychopharmacology*174, 151–162.
- Hashemi, R. H.; Bradley, W. G. Jr.; Lisanti, C. J. *MRI: The Basics*, 2nd ed.; Lippincott Williams & Wilkins: New York, 2004.
- Heckers, S. (2001) Neuroimaging studies of the hippocampus in schizophrenia, *Hippocampus*11, 520–528.
- Hornak, J. (2011). The Basics of NMR. <http://www.cis.rit.edu/htbooks/mri/> (accessed Jan 2012).
- Howes, O. D., and Kapur, S. (2009) The Dopamine Hypothesis of Schizophrenia: Version III--The Final Common Pathway, *Schizophrenia Bulletin*35, 549–562.
- Jones, C. A., Watson, D. J. G., and Fone, K. C. F. (2011) Animal models of schizophrenia, *British Journal of Pharmacology*164, 1162–1194.
- Kegeles, L. S., Shungu, D. C., Anjilvel, S., Chan, S., Ellis, S. P., Xanthopoulos, E., Malaspina, D., Gorman, J. M., Mann, J. J., Laruelle, M., and Kaufmann, C. A. (2000) Hippocampal pathology in schizophrenia: magnetic resonance imaging and spectroscopy studies, *Psychiatry Research: Neuroimaging*98, 163–175.
- Kempton, M. J., Stahl, D., Williams, S. C. R., and DeLisi, L. E. (2010) Progressive lateral ventricular enlargement in schizophrenia: A meta-analysis of longitudinal MRI studies, *Schizophrenia Research*120, 54–62.

- Keshavan, M. S., Haas, G. L., Kahn, C. E., Eduardo Aguilar, Dick, E. L., Schooler, N. R., Sweeney, J. A., and Pettegrew, J. W. (1998) Superior temporal gyrus and the course of early schizophrenia: Progressive, static, or reversible?, *Journal of Psychiatric Research*32, 161–167.
- Konradi, C., and Heckers, S. (2003) Molecular aspects of glutamate dysregulation: implications for schizophrenia and its treatment, *Pharmacology & Therapeutics*97, 153–179.
- Levitt, J. J., McCarley, R. W., Nestor, P. G., Petrescu, C., Donnino, R., Hirayasu, Y., Kikinis, R., Jolesz, F. A., and Shenton, M. E. (1999) Quantitative volumetric MRI study of the cerebellum and vermis in schizophrenia: clinical and cognitive correlates, *Am J Psychiatry*156, 1105–1107.
- Lieberman, J. A., Perkins, D., Belger, A., Chakos, M., Jarskog, F., Boteva, K., and Gilmore, J. (2001) The early stages of schizophrenia: speculations on pathogenesis, pathophysiology, and therapeutic approaches, *Biological Psychiatry*50, 884–897.
- Lutkenhoff, E. S., van Erp, T. G., Thomas, M. A., Therman, S., Manninen, M., Huttunen, M. O., Kaprio, J., Lonnqvist, J., O'Neill, J., and Cannon, T. D. (2008) Proton MRS in twin pairs discordant for schizophrenia, *Mol Psychiatry*15, 308–318.
- Maier, M., Ron, M. A., Barker, G. J., and Tofts, P. S. (1995) Proton magnetic resonance spectroscopy: an in vivo method of estimating hippocampal neuronal depletion in schizophrenia, *Psychol. Med.*25, 1201.
- Martin, P., and Albers, M. (1995) Cerebellum and schizophrenia: a selective review, *Schizophr Bull*21, 241–250.
- Meduri, M., Bramanti, P., Ielitto, G., Favaloro, A., Milardi, D., Cutroneo, G., Muscatello, M. R. A., Bruno, A., Mico, U., Pandolfo, G., La Torre, D., Vaccarino, G., and Anastasi, G. (2010) Morphometrical and morphological analysis of lateral ventricles in schizophrenia patients versus healthy controls, *Psychiatry Research-Neuroimaging*183, 52–58.
- Miyaoka, T., Yasukawa, R., Mizuno, S., Sukegawa, T., Inagaki, T., Horiguchi, J., Seno, H., Oda, K., and Kitagaki, H. (2004) Proton magnetic resonance spectroscopy (1H-MRS) of hippocampus, basal ganglia, and vermis of cerebellum in schizophrenia associated with idiopathic unconjugated hyperbilirubinemia (Gilbert's syndrome), *Journal of Psychiatric Research*39, 29–34.
- Moghaddam, B., and Javitt, D. (2011) From Revolution to Evolution: The Glutamate Hypothesis of Schizophrenia and its Implication for Treatment, *Neuropsychopharmacology*37, 4–15.
- Mu, W. (2011) Assessment of the Neuroanatomy and Neurochemistry GCPII<sup>+/-</sup> Mouse Model with Magnetic Resonance Imaging and Spectroscopy. Honors Thesis, Wellesley College, Wellesley, MA.
- Nakamura, K., Kawasaki, Y., Suzuki, M., Hagino, H., Kurokawa, K., Takahashi, T., Niu, L., Matsui, M., Seto, H., and Kurachi, M. (2004) Multiple structural brain measures obtained by three-dimensional magnetic resonance imaging to distinguish between schizophrenia patients and normal subjects, *Schizophrenia Bulletin*30, 393–404.
- Nasrallah, H., Tandon, R., and Keshavan, M. (2011) Beyond the facts in schizophrenia: closing the gaps in diagnosis, pathophysiology, and treatment, *Epidemiol Psychiatr Sci*20, 317–327.

- Nasrallah, H. A., Skinner, T. E., Schmalbrock, P., and Robitaille, P. M. (1994) Proton magnetic resonance spectroscopy (1H MRS) of the hippocampal formation in schizophrenia: a pilot study, *The British Journal of Psychiatry*165, 481–485.
- Ohrmann, P., Siegmund, A., Suslow, T., Pedersen, A., Spitzberg, K., Kersting, A., Rothermundt, M., Arolt, V., Heindel, W., and Pfleiderer, B. (2007) Cognitive impairment and in vivo metabolites in first-episode neuroleptic-naive and chronic medicated schizophrenic patients: A proton magnetic resonance spectroscopy study, *Journal of Psychiatric Research*41, 625–634.
- Olney, J. W., Newcomer, J. W., and Farber, N. B. (1999) NMDA receptor hypofunction model of schizophrenia, *Journal of Psychiatric Research*33, 523–533.
- Omori, M., Pearce, J., Komoroski, R. A., Griffin, W. S. T., Mrak, R. E., Husain, M. M., and Karson, C. N. (1997) In vitro H-1-magnetic resonance spectroscopy of postmortem brains with schizophrenia, *Biological Psychiatry*42, 359–366.
- Ongur, D., Prescott, A. P., Jensen, J. E., Cohen, B. M., and Renshaw, P. F. (2009) Creatine abnormalities in schizophrenia and bipolar disorder, *Psychiatry Research-Neuroimaging*172, 44–48.
- Paxinos, G., Franklin, G.B.J. (2004) *The Mouse Brain in Stereotaxic Coordinates*. Elsevier, San Diego.
- Pegues, M., Eliaz, Y., Chosiad, L., Schuff, N., Amend, D., and Deicken, R. F. (2000) Tissue volume corrected hippocampal NAA is reduced in schizophrenia, *Biological Psychiatry*47, 107s–107s.
- Petty, R. G. (1999) Structural asymmetries of the human brain and their disturbance in schizophrenia, *Schizophrenia Bulletin*25, 121–139.
- Reveley, A. M., Reveley, M. A., Chitkara, B., and Clifford, C. (1984) The genetic basis of cerebral ventricular volume, *Psychiatry Research*13, 261–266.
- Rodrigo, R., and Felipo, V. (2007) Control of brain glutamine synthesis by NMDA receptors, *Front. Biosci.*12, 883–890.
- Rothman, D. L., Sibson, N. R., Hyder, F., Shen, J., Behar, K. L., and Shulman, R. G. (1999) In vivo nuclear magnetic resonance spectroscopy studies of the relationship between the glutamate--glutamine neurotransmitter cycle and functional neuroenergetics, *Philosophical Transactions of the Royal Society B: Biological Sciences*354, 1165–1177.
- Šácha, P., Zámečník, J., Bařinka, C., Hlouchová, K., Vřcha, A., Mlřochová, P., Hilgert, I., Eckschlager, T., and Konvalinka, J. (2007) Expression of glutamate carboxypeptidase II in human brain, *Neuroscience*144, 1361–1372.
- Schaevitz, L., Picker, J., Rana, J., Kolodny, N., Shane, B., Berger-Sweeney, J., and Coyle, J. (2011) Glutamate carboxypeptidase II and folate deficiencies result in reciprocal protection against cognitive and social deficits in mice: Implications for neurodevelopmental disorders, *Developmental Neurobiology* n/a–n/a.
- Schuller-Levis, G. B., and Park, E. (2003) Taurine: new implications for an old amino acid, *Fems Microbiology Letters*226, 195–202.
- Seeman, M. *Psychopathology in Women and Men: Focus on Female Hormones*.
- Shenton, M. E., Dickey, C. C., Frumin, M., and McCarley, R. W. (2001) A review of MRI findings in schizophrenia, *Schizophrenia Research*49, 1–52.

- Shirayama, Y., Obata, T., Matsuzawa, D., Nonaka, H., Kanazawa, Y., Yoshitome, E., Ikehira, H., Hashimoto, K., and Iyo, M. (2010) Specific metabolites in the medial prefrontal cortex are associated with the neurocognitive deficits in schizophrenia: A preliminary study, *Neuroimage*49, 2783–2790.
- Sigmundsson, T., Maier, M., Toone, B. K., Williams, S. C. R., Simmons, A., Greenwood, K., and Ron, M. A. (2003) Frontal lobe N-acetylaspartate correlates with psychopathology in schizophrenia: a proton magnetic resonance spectroscopy study, *Schizophrenia Research*64, 63–71.
- Smith, G. N., Lang, D. J., Kopala, L. C., Lapointe, J. S., Falkai, P., and Honer, W. G. (2003) Developmental abnormalities of the hippocampus in first-episode schizophrenia, *Biological Psychiatry*53, 555–561.
- Spring, S., Lerch, J. P., and Henkelman, R. M. (2007) Sexual dimorphism revealed in the structure of the mouse brain using three-dimensional magnetic resonance imaging, *NeuroImage*35, 1424–1433.
- Steen, R. G., Hamer, R. M., and Lieberman, J. A. (2005) Measurement of Brain Metabolites by <sup>1</sup>H Magnetic Resonance Spectroscopy in Patients with Schizophrenia: A Systematic Review and Meta-Analysis, *Neuropsychopharmacology*30, 1949–1962.
- Steen, R. G., Mull, C., McClure, R., Hamer, R. M., and Lieberman, J. A. (2006) Brain volume in first-episode schizophrenia - Systematic review and meta-analysis of magnetic resonance imaging studies, *British Journal of Psychiatry*188, 510–518.
- Sturman, J. A. (1988) Taurine in Development, *Journal of Nutrition*118, 1169–1176.
- Tayoshi, S., Sumitani, S., Taniguchi, K., Shibuya-Tayoshi, S., Numata, S., Iga, J., Nakataki, M., Ueno, S., Harada, M., and Ohmori, T. (2009) Metabolite changes and gender differences in schizophrenia using 3-Tesla proton magnetic resonance spectroscopy ((<sup>1</sup>H)-MRS), *Schizophrenia Research*108, 69–77.
- Theberge, J. (2002) Glutamate and Glutamine Measured With 4.0 T Proton MRS in Never-Treated Patients With Schizophrenia and Healthy Volunteers, *American Journal of Psychiatry*159, 1944–1946.
- Tordjman, S., Drapier, D., Bonnot, O., Graignic, R., Fortes, S., Cohen, D., Millet, B., Laurent, C., and Roubertoux, P. L. (2006) Animal Models Relevant to Schizophrenia and Autism: Validity and Limitations, *Behavior Genetics*37, 61–78.
- Trivedi, M. S., and Jarbe, T. (2011) A brief review on recent developments in animal models of schizophrenia, *Indian Journal of Pharmacology*43, 375–380.
- Tsai, G., Passani, L. A., Slusher, B. S., Carter, R., Baer, L., Kleinman, J. E., and Coyle, J. T. (1995) Abnormal Excitatory Neurotransmitter Metabolism in Schizophrenic Brains, *Arch Gen Psychiatry*52, 829–836.
- University of Colorado. (2008) Central Nervous System. <http://www.colorado.edu/intphys/Class/IPHY3430-200/007cns.htm> (accessed Jan 2012).
- van Os, J., and Kapur, S. (2009) Schizophrenia, *Lancet*374, 635–645.
- Vorvick, L.J. (2010) Schizophrenia. <http://www.ncbi.nlm.nih.gov/pubmedhealth/PMH0001925/> (accessed Jan 2012).

- Wilson, C., and Terry, A. V. (2010) Neurodevelopmental Animal Models of Schizophrenia: Role in Novel Drug Discovery and Development, *Clinical Schizophrenia & Related Psychoses*4, 124–137.
- Wood, S. J., Yücel, M., Wellard, R. M., Harrison, B. J., Clarke, K., Fornito, A., Velakoulis, D., and Pantelis, C. (2007) Evidence for neuronal dysfunction in the anterior cingulate of patients with schizophrenia: A proton magnetic resonance spectroscopy study at 3 T, *Schizophrenia Research*94, 328–331.
- Yeganeh-Doost, P., Gruber, O., Falkai, P., and Schmitt, A. (2011) The role of the cerebellum in schizophrenia: from cognition to molecular pathways, *Clinics*66, 71–77.
- Yüksel, C., and Öngür, D. (2010) Magnetic Resonance Spectroscopy Studies of Glutamate-Related Abnormalities in Mood Disorders, *Biological Psychiatry*68, 785–794.



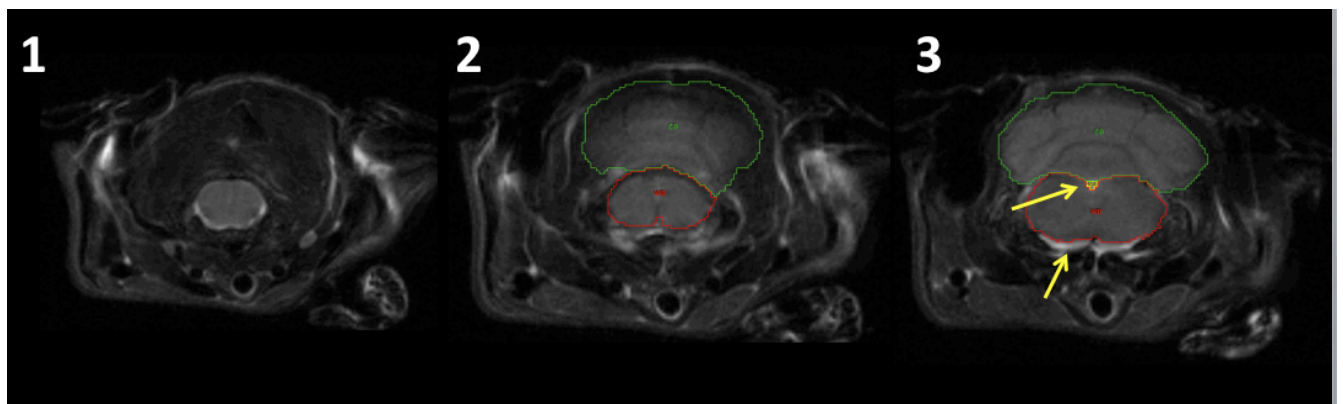
## Appendix A: Tracing Guide

This guide should be used as a reference for tracing structures in a mouse brain. Below are twenty-one contiguous slices, or images, of a male HET mouse brain on PND 35. Each image is labeled with a number and as the number increases, the images go from posterior (back) to anterior (front) of the brain. Notes on tracing appear underneath the images. Some regions may be difficult to trace due to lack of distinction or outline, thus it may be necessary to refer to a mouse brain atlas and/or use your best judgment. When tracing, the most important thing to remember is to be consistent in how you define a region.

Regions of interest were traced using the region of interest tool in Analyze 10.0, image analysis software. Each region is outlined by a different color and labeled with an abbreviation (Table AA-1)

**Table AA-1.** Abbreviation and outline color of brain regions and images in which the regions were traced.

<u>Brain Region</u>	<u>Abbreviation</u>	<u>Outline Color</u>	<u>Images with the Region</u>
Whole Brain	WB	Red	All
Cerebellum	CB	Green	2,3,4,5,6
Fourth Ventricle	4V	Yellow	3,4,5
Left Hippocampus	L-HP	Dark Blue	8,9,10,11
Right Hippocampus	R-HP	Bright Purple	8,9,10,11
Left Lateral Ventricle	L-LV	Teal	9,10,11,12,13,14
Right Lateral Ventricle	R-LV	White	9,10,11,12,13,14
Third Ventricle	3V	Peach	9,10,11,12,13



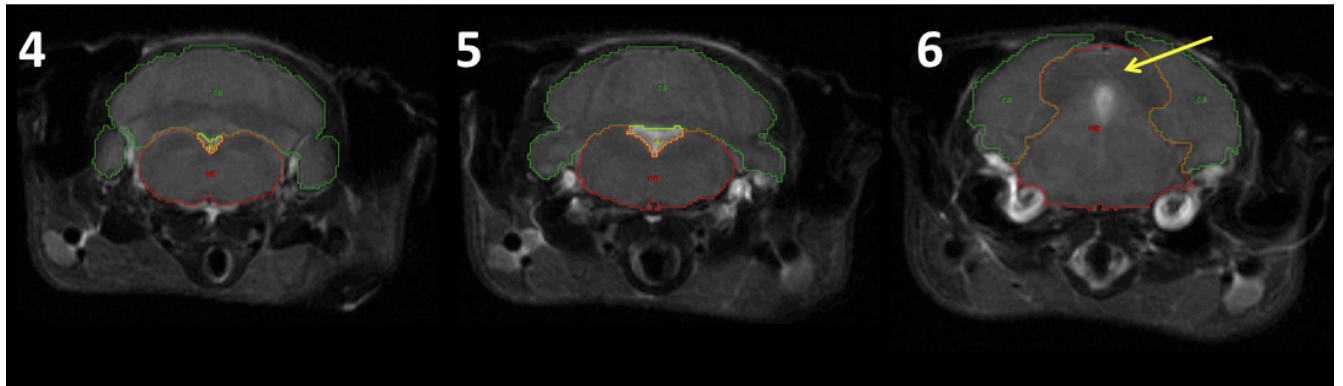
### Images 1-3

Tracing begins in the most posterior slice that the cerebellum can be seen (Image #2). The cerebellum is recognizable as it appears striated and rests on top of the brain stem. In slices with the cerebellum, the whole brain region is traced as all tissue excluding the cerebellum. While this may seem like the cerebellum isn't part of the whole brain, whole brain volume is



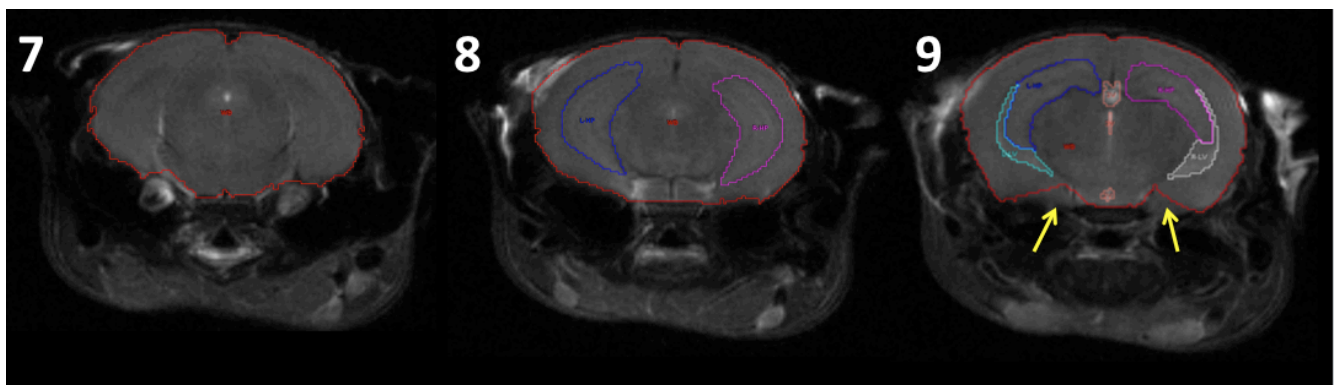
calculated as a summation of all regions traced during analysis. The fourth ventricle appears white and triangle-shaped (Image #3).

If there are smaller regions to be traced inside a larger region, such as the fourth ventricle within the whole brain in Image #3, then the larger region is traced first such that the smaller region is not “over-traced” (middle arrow, Image #3). Avoid tracing external areas that appear white as they are likely fat or connective tissue and not part of any brain region (bottom arrow, Image #3)



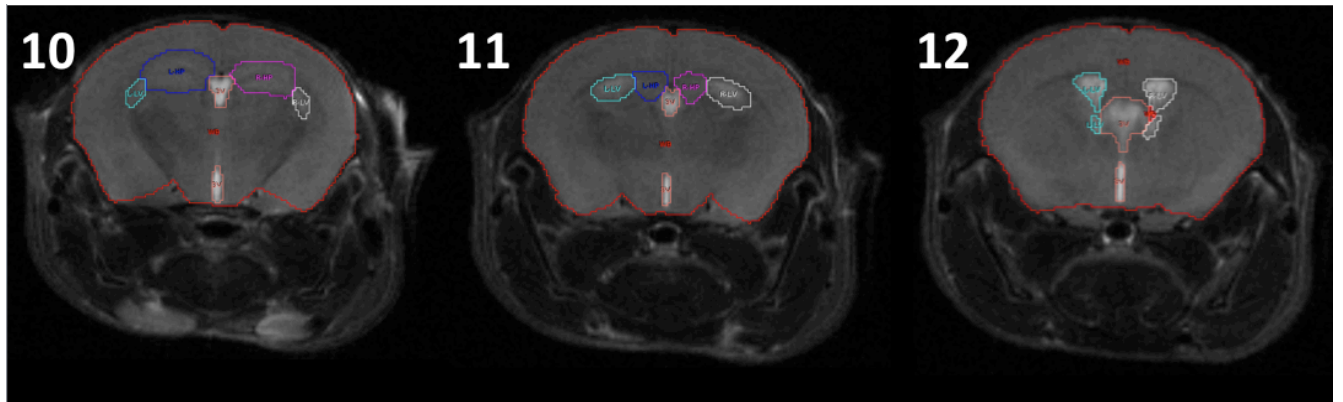
#### Images 4-6

The lobes of the cerebellum, or paraflocculi, appear in Image #4. Occasionally the paraflocculi will appear disconnected from the brain, but they should still be traced. In Image #6, the colliculi appear and should be traced as part of the whole brain (top arrow). The cerebellum is distinct from the whole brain in Image #6, as it is striated.



#### Images 7-9

The left and right hippocampi appear in Image #8. The left and right lateral ventricles appear white in Image #9 and are usually adjacent to the left and right hippocampi, respectively. Also in image #9 is the third ventricle down the center; the third ventricle may not appear connected. In image #9, the bottom arrows indicate connective tissues that should not be traced. The connective tissues are distinctly triangle-shaped.



### Images 10-12

Continue tracing the left and right hippocampi, left and right lateral ventricles, and third ventricle. Again, the connective tissues that appear triangle-shaped should not be traced. In Image #12, the lateral ventricles connect with the third ventricle. In our tracing we defined the lateral ventricles as outer edges right up until they curve inward.

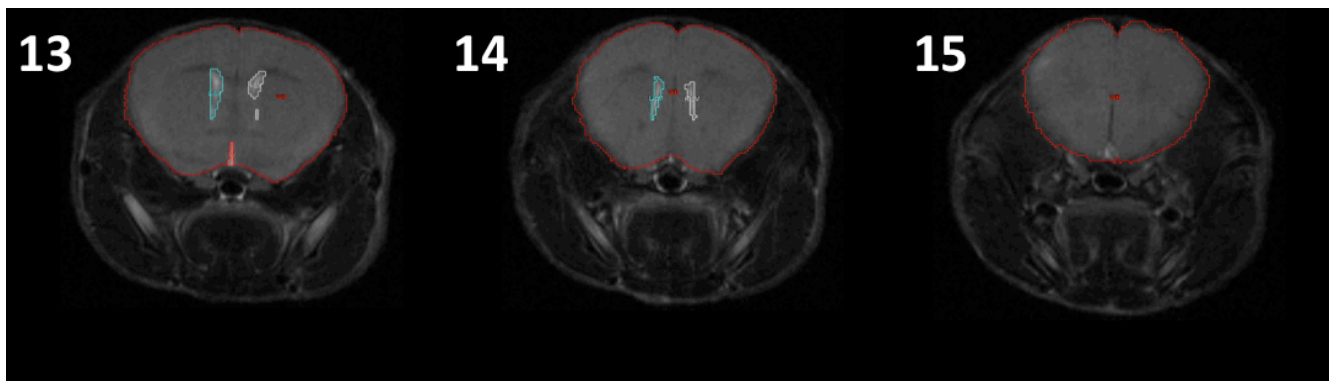
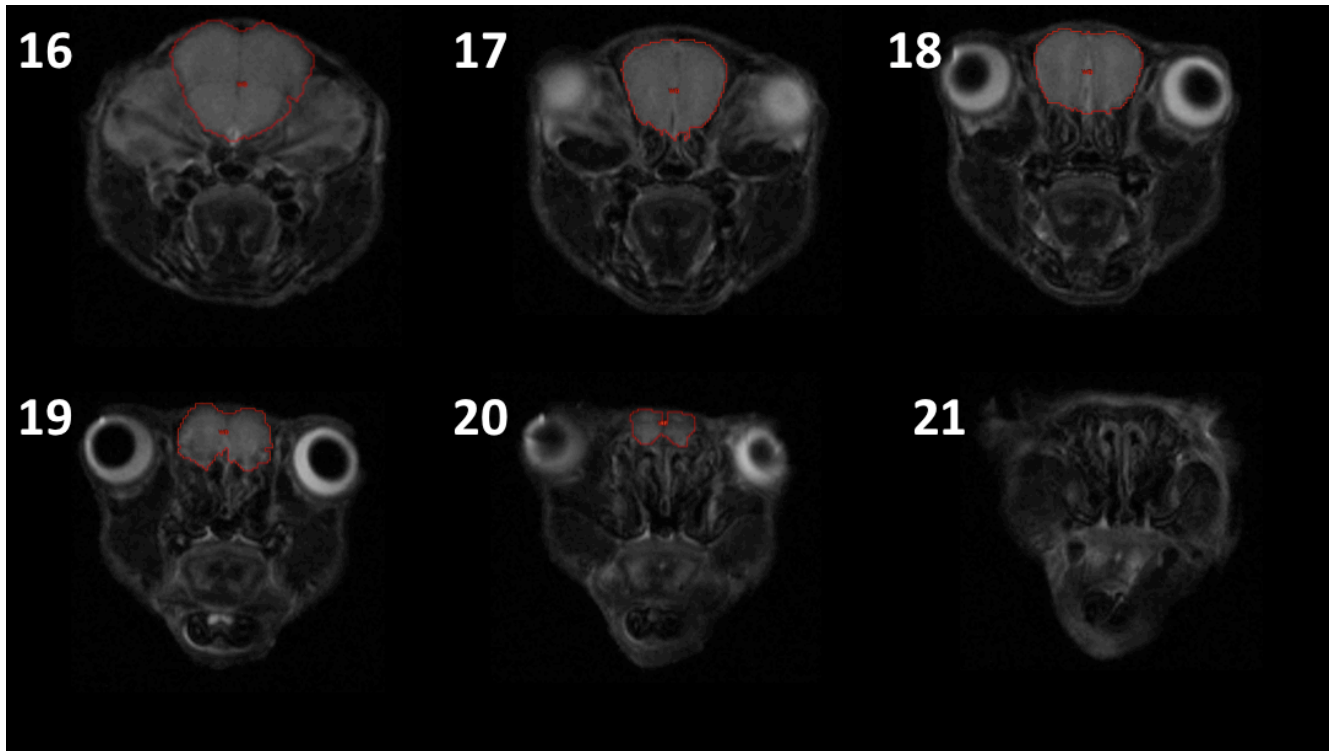


### Image 13-15

Continue tracing the left and right lateral ventricles, and third ventricle. Eventually, the third ventricle ends (Image #13) and the lateral ventricles continue (#14).

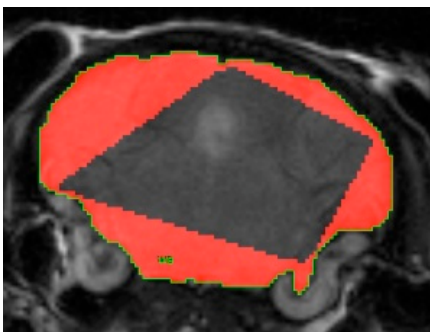


### Images 16-21

Continue tracing the whole brain until there is no more brain tissue to trace. Generally, there is no more to trace when the eyes are no longer visible (Image #21).

### Other important notes (Mu, 2011)

- When tracing, you will often not be able to finish tracing an entire region without lifting the pen. When adding to the region, use the edit tool; do NOT continue using the trace tool. Otherwise when the area is being calculated a chunk will be missing in the middle as shown below-



- The “undo” button is near the bottom of the window. Pressing Ctrl + Z does not work.
- The “delete button” is near the undo button, and is a picture of a trash can.

- Pressing “Esc” on the keyboard will force quit the ROI window, and deletes any unsaved work. Analyze will not save any work automatically. Save often and avoid that corner of the keyboard!

## **References**

Mu, W. (2011) Assessment of the Neuroanatomy and Neurochemistry GCPII<sup>+/-</sup> Mouse Model with Magnetic Resonance Imaging and Spectroscopy. Honors Thesis, Wellesley College, Wellesley, MA.

Paxinos, G., Franklin, G.B.J. (2004) The Mouse Brain in Stereotaxic Coordinates. Elsevier, San Diego.



## Appendix B: The R168X Mouse Model of Rett Syndrome and Viability

Rett syndrome (RTT) is a neurodevelopmental disorder that is the second leading cause of mental retardation in girls. RTT is primarily caused by a random mutation in the X-linked gene that encodes methyl-CpG-binding protein 2 (MeCP2; Rett Syndrome Fact Sheet, 2007). MeCP2 specifically binds to methylated DNA and regulates the transcription of other genes. If MeCP2 is mutated, insufficient or abnormal amounts of MeCP2 are produced which leads to irregular expression of these regulated genes (Chen, 2001). The effects of the mutation are severely debilitating; symptoms of RTT, such as breathing abnormalities, are often responsible for premature deaths. There is no cure for RTT and effective treatments are limited because early diagnosis is difficult.

Previous work in this lab attempted to establish early detection and monitoring methods for RTT treatment development by investigating, *in vivo*, the longitudinal brain morphology and neurochemical profile of MeCP2<sup>R168X</sup>, a mouse model of RTT (Huang, 2011). These mice are unique in that they have R168X, one of the most common mutations in patients with RTT, knocked into the *Mecp2* gene. The *Mecp2*<sup>R168X</sup> mouse model exhibits many features similar to RTT, such as hypoactivity, forelimb stereotypies, breathing irregularities, weight changes, hind limb atrophy, scoliosis, and a reduction in UBE3A RNA and protein products (Lawson-Yuen, 2007).

Through a longitudinal study on the MeCP2<sup>R168X</sup> mouse model, we hoped to better understand the developmental and neurochemical basis of RTT to identify, monitor, and treat RTT. We hypothesized that our findings on the MeCP2<sup>R168X</sup> mouse model would reflect studies conducted on RTT patients and other mouse models of RTT. However, breeding and breathing-related complications arose that prompted us to terminate this study.

The non-invasive techniques of Magnetic Resonance Imaging (MRI) and Spectroscopy (MRS) were used to examine male mutated (null) and normal (wild-type; WT) mice on postnatal days (PND) 21, 28, 35, and 49. In this study, only male mice were examined because null male mice exhibit more severe symptoms of RTT compared to the mutant, or heterozygous, female counterparts. MRI allowed us to visualize brain structures and quantify their volumes, which reflect neural development. With MRS, we determined neurometabolite concentrations, whose levels are known to be indicators of neuronal health. MRS data were collected from the hippocampus, a region in the brain known to function differently in RTT patients.

In early experiments, breathing abnormalities were observed- null mice exhibited shallow breathing or would cease breathing for brief intervals. Over time, breathing abnormalities in the new litters were more severe. Mice are normally sensitive to the isoflurane, where a slight decrease or increase in % isoflurane/O<sub>2</sub> gradually causes breaths per minute (bpm) to increase or decrease, respectively. However, null mice appeared to be hypersensitive to isoflurane increases, but resistant to decreases. For example, if isoflurane/O<sub>2</sub> levels were increased slightly, bpm would plummet, but when isoflurane/O<sub>2</sub> levels were decreased, bpm would remain constant or continue to fall. Null mice survived the two hour-long experiments, but ceased breathing post-anesthesia during recovery on a heating pad. When the mice were genotyped, it was determined

that all the mice that had died were null. The cause of death was likely related to breathing abnormalities from the MeCP2 mutation combined with stress and isoflurane exposure.

Plasma levels of epinephrine are known to increase in isoflurane-anesthetized in MeCP2<sup>1lox</sup> mice, a different MeCP2 deficient model, compared to controls (Ladas et al., 2009). Ladas et al. (2009) hypothesized that this hypersecretory phenotype may alter the sensitivity of MeCP2 null mice to stress. Our experiments found that null mice exhibited an exaggerated response to stress compared to control, which confirms these findings.

Upon consultation with the Wellesley College veterinarian, Dr. Lynn Jackson, it was determined that the R168X mutation was becoming more severe as the mice exhibited more genetic homogeneity. Backcrossed mice older than six generations began to exhibit almost exclusively homozygous or heterozygous characteristics (Figure AB-1). Our null mice were backcrossed for approximately six generations and were congenic to heterozygous mice at the loci of the R168X mutation.

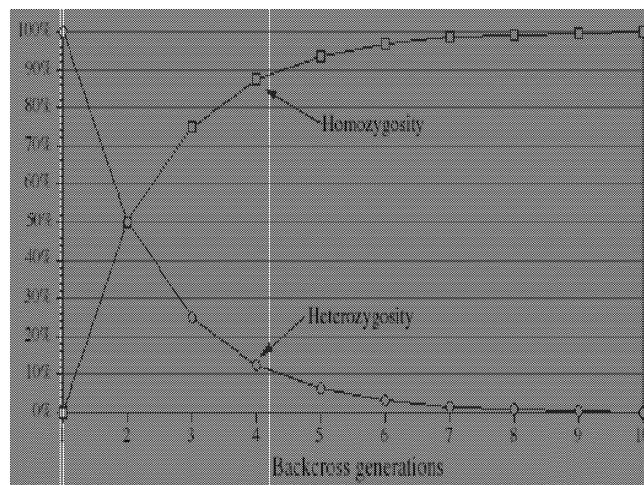


**Figure AB-1.** Genomic homogeneity and heterogeneity during the creation of a congenic strain. The reciprocal points on each line indicate the percentage of loci in the genome of each individual animal that will be homozygous for the inbred partner allele or heterozygous with the donor allele at each generation backcrossing. Adapted from Wellesley College Animal Care Facility Manual (2011).

Interestingly, a congenic strain is usually desirable, as homozygous and heterozygous mice would be 100% different at the loci of the R168X mutation and could be compared for phenotypic differences. However, as the loci became more homozygous in null mice, viability declined. Attempts to maintain loci percentage below 100% would have been ideal to maintain viability, but not feasible. Even if the homozygous mice were outbred to a different strain of WT mice to reduce percentage homozygous loci, the mice would have shortly returned to genetic homogeneity after several backcross generations.

Several measures were taken to prevent mouse death. The PND 21 imaging date was removed to limit the amount of stress experienced in one day, as mice were also weaned, or removed from the mother into a separate cage, on PND 21. Isoflurane levels were kept as low as possible so that bpm would not plummet, however bpm fell even with low levels of isoflurane. Resuscitation techniques were also attempted on mice that stopped breathing during recovery.

The plunger of a syringe was removed and the narrow end of the syringe was inserted into the mouse mouth. The large and open end of the syringe was used to blow small puffs of air into the mouse's mouth. This technique was not successful, as it was difficult to insert the syringe into the mouse's mouth. Further, even if the syringe was thoroughly inserted, there was no seal to direct the air into the mouse's lungs.

As the experiments continued, it also became apparent that MeCP2<sup>R168X</sup> litters produced few progeny and fewer males than females; there were approximately two males in every litter. The cause of these problems were unknown, but likely related to the more severe symptoms experienced by male null mice compared to heterozygous female mice. These breeding problems made it difficult to collect data with a sample size large enough for analysis.

The R168X mutation is one of the most common mutations found in human RTT patients and causes the most severe symptoms. These human symptoms relate to the breathing and breeding abnormalities issues found in the MeCP2<sup>R168X</sup> mouse model. The origins of these problems were thought to be associated to a hypersensitive stress response to isoflurane and null mice exhibiting genomic homogeneity. Attempts were made to reduce the stress-related breathing problems, but they were unsuccessful as the mice continued to die post-anesthesia. Given the inability to collect data due few male progeny and sudden post-anesthesia deaths, we determined that the MeCP2<sup>R168X</sup> mouse model of Rett syndrome is not viable.

## References

- Chen, R.Z., Akbarian, S., Tudor, M., Jaenisch, R. (2001) Deficiency of methyl-CpG binding protein-2 in CNS neurons results in a Rett-like phenotype in mice. *Nat Genet.* 27, 327-331.
- Huang, S. (2011) Magnetic Resonance Study of Neurochemistry of Rett Syndrome in a Mouse Model. Chem 350 Independent Study. Wellesley College, Wellesley, MA.
- Lawson-Yuen, A, Liu, D, Han, Liqun, Jiang, Z .I., Tsai, G .E., Basu, A .C., Picker, J., Feng, J., Coyle, J .T. (2007) Ube3a mRNA and protein expression are not decreased in Mecp2<sup>R168X</sup> mutant mice. *Brain Res.* 1180, 1-6.
- “Rett Syndrome Fact Sheet.” National Institute of Neurological Disorders and Stroke. 18 May 2012. National Institute of Health. 15 Dec. 2007 <[http://www.ninds.nih.gov/disorders/rett/detail\\_rett.htm](http://www.ninds.nih.gov/disorders/rett/detail_rett.htm)>.
- Wellesley College Animal Facility Manual (2011). Wellesley College, Wellesley, MA.





## Appendix C: Development of a “Green” MRI Phantom

A phantom is an object that can hold NMR tubes to assess the image intensity of solutions in MRI experiments. Traditionally, these phantoms were made by suspending three NMR tubes in a large conical tube using agarose, a gel-like material (Figure AC-1). The phantom was then wrapped with paper towels until wide enough to fit securely in the MRI probe. The agarose used for these phantoms was expensive and could not be removed or re-used, thus a new phantom had to be made for every experiment. A new “green” phantom was designed to eliminate the need to re-make phantoms. This is a guide on how the “green” phantom was developed and created.



**Figure AC-1.** Old MRI Phantom

### Phantom Design

The phantom had to meet the following criteria:

- Must be re-usable
- Must hold a several 3-mm or 5-mm NMR tubes
- Must incorporate a way to distinguish among NMR tubes in MR images

The first phantom design was made to be a single solid piece to be printed with a 3D printer (Figure AC-1). The phantom could hold four 5-mm NMR tubes. Hollow slits were positioned around the tube and could be filled with a contrast agent so that the solutions in each tube could be differentiated in an MR image.

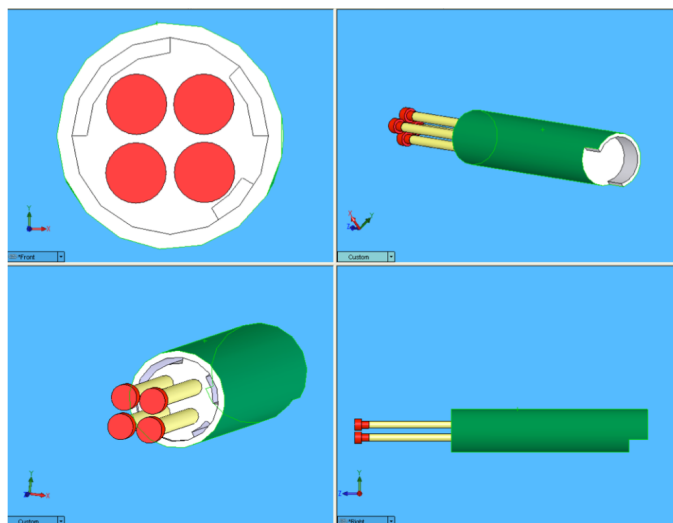


**Figure AC-2.** Original phantom design.

When the original phantom was created it was determined that the plastic material used in the 3D printer was porous and could not hold any liquid contrast agent (Figure AC-3). Further, the holes for the NMR tubes were too small to fit NMR tubes and the body of the phantom was too big to fit into the probe. This phantom taught us many lessons. We realized that measurements must be exact to the tenth of a millimeter and that a solid piece may not be the best option.

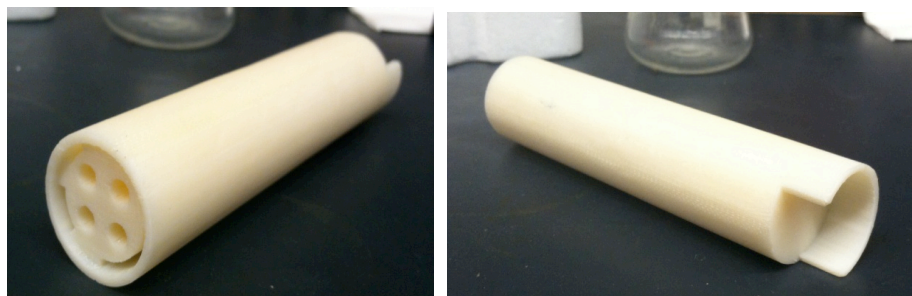


**Figure AC-3.** Front (left) and back (right) view of the original solid phantom.

The final phantom design incorporated pieces made from a 3D printer and laser cutter. Instead of being a solid piece, the phantom was made of a hollow outer-casing (Figure AC-4) and an NMR tube holder made of interchangeable pieces (Figure AC-5).

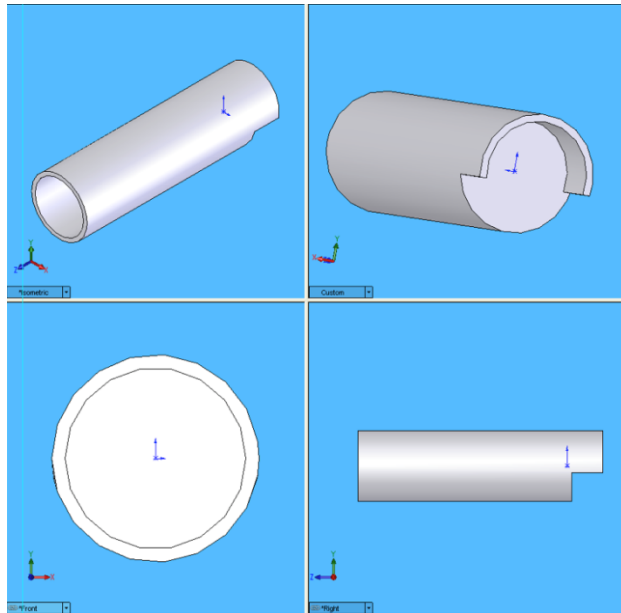


**Figure AC-4.** Outer-casing of phantom.

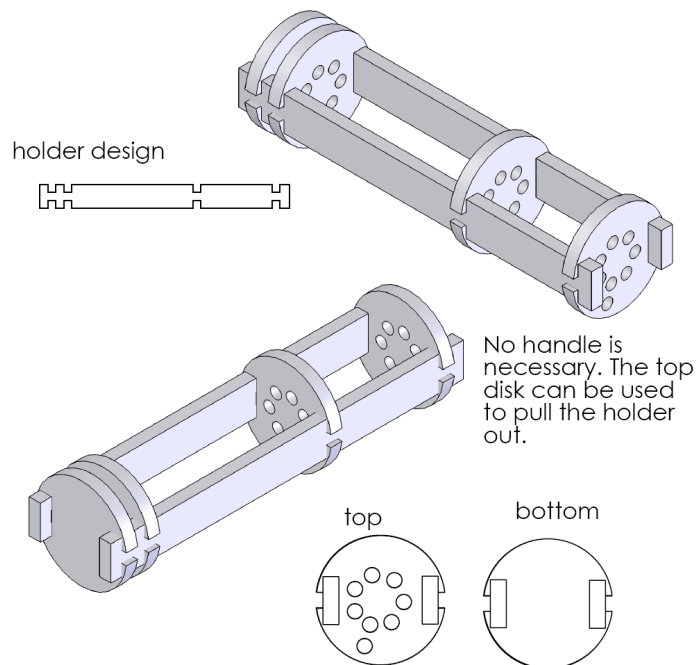


**Figure AC-5.** Assembled NMR tube holder displayed on SolidWorks

The outer-casing was designed by modifying the structure of the original phantom made. Several short (~3 cm) hollow rings of different sizes were then printed to ensure that the phantom would have the correct diameter to fit snugly into the MRI probe. Once a size was determined, the entire outer-casing was printed with the 3D printer.

The NMR tube holder shown in Figure AC-3 can hold eight 3-mm NMR tubes where one

tube can be placed outside of the ring and act as a marker. The inner pieces were designed such that the disks could be modified to hold a different number or type of NMR tubes. Again, pieces of different sizes had to be cut to determine which size allowed all the pieces to fit snugly together.

**Table AC-1.** Images of the final phantom:

Image	Description
	<p>Outer-casing (above) and NMR tube holder with a 3-mm NMR tube (below)</p>
	<p>Outer-casing (right) and NMR tube holder with a 3-mm NMR tube (left)</p>
	<p>NMR tube holder halfway inserted into outer-casing with a 3-mm NMR tube</p>
	<p>NMR tube holder completely inserted into outer-casing with a 3-mm NMR tube</p>

When imaged, the solutions inside the NMR tubes were all visible and the tube positioned outside of the ring of tubes served as a marker (Figure AB-6).

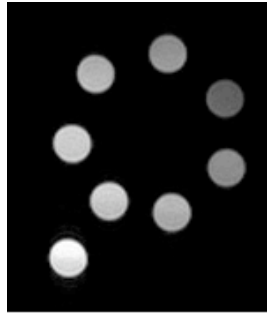


**Figure AC-6.** Magnetic resonance image of the final phantom holding seven NMR tubes that contain different concentrations of contrast agent

The design and creation of a “green” MRI phantom was successful. The new phantom is completely re-usable, can hold eight NMR tubes, and has a method to identify tubes inside an MR image.

## Methods

### Laser Cutter

A sheet of Delrin, a general-purpose thermoplastic, was selected based on desired thickness (1/8” Delrin was used for all phantom pieces). Phantom designs were made on SolidWorks, 3D CAD design software, and drawn as flat images. These images were then converted into .PDF format and transferred to a computer connected to the laser printer. On this computer, CorelDrawX3, a graphic design program, was used to make the outline of all the shapes red so that the laser printer could identify which regions to cut. The red image was then transferred to Trotec Job Control 7.4.9, a laser cutter program. The sheet of Delrin was placed into the Trotec Speedy 300™ laser cutter. After the laser was calibrated with the computer and laser-setting were selected (P:100%, f=10,000; V=1.0), the pieces were cut.

### 3D Printer

A Dimension 1200es 3D printer was used to create pieces of the phantom that could not be made with the laser cutter. These pieces were designed on SolidWorks and then transferred to Catalyst EX, a 3D printer program, which printed the design with ABS plastic.